An Investigation into The Nano Fluids Physiochemical Properties Due to Ultrasonic Perturbation for Near Wellbore Remediation

A thesis submitted to Auckland University of Technology in fulfilment of the requirements for the degree of

Doctor of Philosophy (PhD)

Author: **Vickneswaran M Veloo**

Primary Supervisor: Professor Ahmed Al-Jumaily

July 2021

Institute of Biomedical Technologies
School of Engineering
Faculty of Design & Creative Technology
Auckland University of Technology
Auckland, New Zealand

AUT INSTITUTE OF BIOMEDICAL TECHNOLOGIES

Abstract

Research on nanofluids has been conducted extensively. However, to the best of our knowledge the protocol to produce nanofluid which will enhance the physio-chemical properties using external perturbation such as ultrasound and their effect on mass transfer kinetics during near well remediation is not established for field implementation for the oil and gas industry. In this thesis, a comprehensive study has been conducted to investigate the effect of ultrasonic amplitude variation on nanofluids physio-chemical properties. The study includes nanofluids formulation, preparation, optimization, ultrasonication at various amplitude, physio-chemical properties characterization, mass transfer kinetics evaluation and theoretical simulation.

The physio-chemical properties characterization was carried out using various established scientific methods outlined in the thesis. The changes in the physio-chemical properties have significant effects on the mass transfer kinetics of near wellbore remediation process for hydrocarbon production improvement. Thus, laboratory experiments simulating the near wellbore remediation and enhance recovery process using the sonicated nanofluids at various amplitudes under isothermal and non-isothermal were carried out using filter cake dissolution and sand packed column flow tests. Filter cake is a layer formed by solid particles in drilling fluid against porous zones due to differential pressure between hydrostatic pressure and wellbore pressure. The mass transfer kinetics evaluation was established for the experimental work. The experiments indicated that the optimum mass transfer enhancement achieved for this study when the nanofluids sonicated at 60% amplitude under non-isothermal conditions. This condition enables us to produce nanofluids with lowest interfacial tension, viscosity, mean average particle size and contact angle properties.

The experimental results for the filter cake dissolution for the best-case scenario was compared with theoretical simulation using Ansys Fluent (version.15). The comparative plot of filter cake dissolution rate for both the experimental and Ansys Fluent simulation showed the best similar correlation trend achieved with the 60% amplitude under the non-isothermal condition. Thus, we could establish a general correlation between the key physio-chemical properties, ultrasonic amplitude, and the mass transfer kinetics during the near wellbore remediation process in the petroleum industry.

Acknowledgements

Firstly, I truly thankful to my supervisor Professor Ahmed Al-Jumaily from the Institute of Biomedical Technologies of Auckland University of Technology (AUT) for his support, guidance, and encouragement throughout the years of this research. He has been more than a mentor, working closely with me to ensure the success of the research.

I would like to express my gratitude to Nexuschem Engineering Sdn Bhd for providing funding and laboratory facility that enable me to complete my experiments timely.

I would like to acknowledge Dr Sudip Ray, Dr Cathy Li and Robert Otupiri from Auckland University for providing the access and supervision in the use of the optical tensiometer and Zetasizer equipment. Thanks to Yelena Dumanovic from Institute of Biomedical Technologies of Auckland University of Technology for organizing and managing the financial invoices.

In addition, I like to express my gratitude to Louise Burnett of AUT for providing advice and support on laboratory equipment's.

I would like to extend my love and gratitude to my beloved wife for providing me the moral support during this challenging time. I also want to take this opportunity to appreciate the help and kindness I received from my colleagues at IBTec.

Last but not the least, my greatest appreciation to my family, especially to my late father, M.Veloo for inspiring me to pursue my PhD.

Attestation of Authorship

I hereby declare that this submission is my own work and that, to the best of my knowledge and belief, it contains no material previously published or written by another person, nor material which to substantial extent has been accepted for the award of any other degree or diploma of a university or other institution of higher learning, except where due acknowledgement within this document.

Vickneswaran M Veloo

Signature

Date 27/07/2021

Table of Contents

List of Figures

List of Tables

Abbreviations

Abbreviation	Description
AMP	Amplitude
APG	Alkyl Polyglucoside
API	American Petroleum Institute
ASP	Alkaline Surfactant Flooding
AUT	Auckland University Of Technology
CDG	Colloidal Dispersion Gel
CFD	Computational Fluid Dynamic
CMC	Critical Micellar Concentration
CNT	Carbon Nanotube
CSM	Chemical Solution Method
CTAB	Cetyltrimethylammonium bromide
DLS	Dynamic Light Scattering
ELS	Electrophoretic Light Scattering
EOR	Enhance Oil Recovery
HTHP	High Temperature High Pressure
IFT	Interfacial Tension
LDV	Laser Doppler Velocimetry
LHPN	Lipophobic and Hydrophilic Polysilicon
NaSal	Sodium Salicylate
NNI	National Nano Technology Initiative
NP	Nano Particles

Abbreviation	Description
PDC	Polycrystalline Diamond Compact
RPM	Rotational Per Minute
SDS	Sodium Dodecyl Sulfate
SIMPLE	Semi-Implicit Method for Pressure Linked Equation
SOP	Standard Operating Procedure
TDS	Total Dissolved Solid
USBM	U.S. Bureau Of Mines
VES	Viscoelastic Surfactant
VOF	Volume OF Fluid

Nomenclature

Symbol	Definition
A	Total surface Area
A_{HH}	Interaction energy between surfactant head
A_{OO}	Interaction energy between oil molecules
A_{SO}	Interaction energy of surfactant and oil
A_{SW}	Interaction energy of surfactant and aqueous
A_{WW}	Interaction energy between water molecules
A_{TT}	Interaction energy between surfactant tail
c_i	Concentration of species i (mol m^{-3})
c_j	Concentration of species j (mol m^{-3})
C_I	Concentration at interface
D	Diffusion coefficient
D_s	Diffusion coefficient of oil into nanofluids
D_i	Diffusion coefficient of species i (m^2 s^{-1})
D_{ij}	Diffusion coefficient of multicomponent (m^2 s^{-1})
E	Enhance oil recovery efficiency
E_d	Microscopic efficiency
E_i	Vertical sweep efficiency
E_s	Areal sweep efficiency
E_v	Macroscopic efficiency
$f(ka)$	Henrys function

Symbol	Definition
F	Momentum Transfer factor
J*i*	Flux vector of species *i*
k	Mass transfer coefficient
k_B	Boltzmann constant
l	Liquid phase
L	Boundary thickness
*M*i	Initial filter cake weight with filter paper
*M*f	Final filter cake weight with filter paper
*M*fp	Weight of blank filter paper
m_s	Mass fraction of oil phase
m	Total dissolved mass
$\dot{m}_{ls}$	Mass flowrate into liquid from solid phase
$\dot{m}_{sl}$	Mass flowrate into solid from liquid phase
N_i	Molar flux of species *i* ($m^2\ s^{-1}$)
N_I	Flux at interface ($m^2\ s^{-1}$)
P	Pressure
R	Interaction energy of surfactant, oil and water
R	Radius
R_0	Radius of curvature
S	Solid phase

T	Oscillation period/Time
U	Velocity
UE	Electrophoretic mobility
T	Temperature
t	Time
α	Volume fraction
∇	Gradient/Vector differential operator
ρ	Density
η	Viscosity of dispersant
ɲ	Viscosity of Nanofluids
γ	Surface tension
γ_{AB}	Interfacial tension between liquid A and B
γ_{A}	Surface tension of liquid A
γ_{B}	Surface tension of liquid A
γ^{d}	Dispersion force to surface tension
γ_{lg}	Interfacial tension liquid-gas
γ_{sg}	Interfacial tension solid gas
γ_{sl}	Interfacial tension solid liquid
β	Shape factor
φ	Tangent angle
$\Delta G^{a}{}_{AB}$	Free energy of adhesion of phase A and B
$\Delta G^{c}{}_{A}$	Free energy of cohesion of phase A

$\Delta G^{c}{}_{B}$	Free energy of cohesion of phase B
Φ	Contant of Girifalco and Good equation
Θ	Contact angles
ε	Dielectric constant
$\Delta\rho$	Density difference
$\mathbf{g}$	Gravity
g	Gravitational constant
x_i	Mole fraction of species *i*
x_j	Mole fraction of species *j*
R	Cylindrical coordinates
s	Cylindrical coordinates
z	Arch length
Z	Zeta potential
τ_l	Liquid stress term
μ_l	Molecular viscosity
ζ	Bulk viscosity
I	Prandtl length

CHAPTER 1 Introduction

1.1 Research Background

Nanotechnology terms is derived from the prefix “nano” that describes the art and science of manipulating atoms and molecules from their bulk states to nano scale to produce new materials, systems and devices [1]. A nanometer is defined as one billion of a meter, a distance equal to two to twenty atoms laid next to each other [1]. The development of this technology is aimed at creating functional performances of the new system, devices or materials resulting from manipulation of structure or matter on dimension less than 100nm [2]. The advancement of research and development of nanotechnology in the past few decades have enabled many innovative breakthrough technologies in medicine, biotechnology, energy, electronics, food and agriculture. The studies on nanotechnology has been explored by Richard Feynman as early as 1950’s although development on knowledge of nanotechnology was established by Drexler Eric K in 1980s [1]. Many developed countries have spent billions of dollars in nanotechnology R&D in recent years [2],[3]. In the United States alone, the government has spent more than USD22 billion [4], since the inception of NNI (National Nanotechnology Initiative) in 2000.

Nanotechnology provides a platform for the improvement in solubility, dispersion, mass and heat transfer, reduction in energy and material requirements for physical and chemical transformation, reduction of equipment sizing and footprint, resulting in direct economic and environmental benefits [2]. Hypothetically, nanotechnology is also believed to improve mass transfer kinetics mechanism during remediation of near wellbore to improve oil and gas productivity. However, to the best of our knowledge the protocol to produce nanofluid which will enhance the physio-chemical properties using external perturbation such as ultrasound and their effect on mass transfer kinetics during near well remediation in the petroleum industry is not well established.

The technological advancement in this area still faces numerous challenges despite the enormous research and development that have been carried out. Particularly in health, safety and environmental of some nanomaterials [2],[4] . Scaling up of the laboratory findings to real life applications and the cost of implementation is a complicated problem.

1.2 Nanotechnology in Oil and Gas Industries.

Hydrocarbons are often found below the earth's surface that consist of crude oil and gas made up of thousands of molecules of hydrogen and carbon atoms of simple to complex structure originated from the decomposition of organic materials such as animals and plants that died during the Palaeozoic Era between 245 to 544 million years ago. The modern oil industry begun when the first underground oil was discovered in 1859 in Pennsylvania by Colonel Drake and set the stage for the new oil economy [5]. Since then, the world energy demand has been relying on oil and gas as a cheap and abundant source for many centuries. The process involved in finding the oil and extracting it out of the ground is challenging and exciting. The first stage is referred as upstream where the hydrocarbon reservoir is discovered, drilled and produced from the ground [5]. Fig. 1.1 describes the drilling and production process, and Fig. 1.2 is an example of a typical offshore drilling and production facility. The hydrocarbon is first produced through special tubing from the drilled well and sent to a second stage production facility where the hydrocarbon is separated from water before sending to storage terminal at shore or offshore floating facility via pipeline. The final stage 3 involves process of refining and treating the hydrocarbon to produce various products such as gasoline, kerosene, natural gas and bitumen to be marketed as petroleum products and it's called downstream.

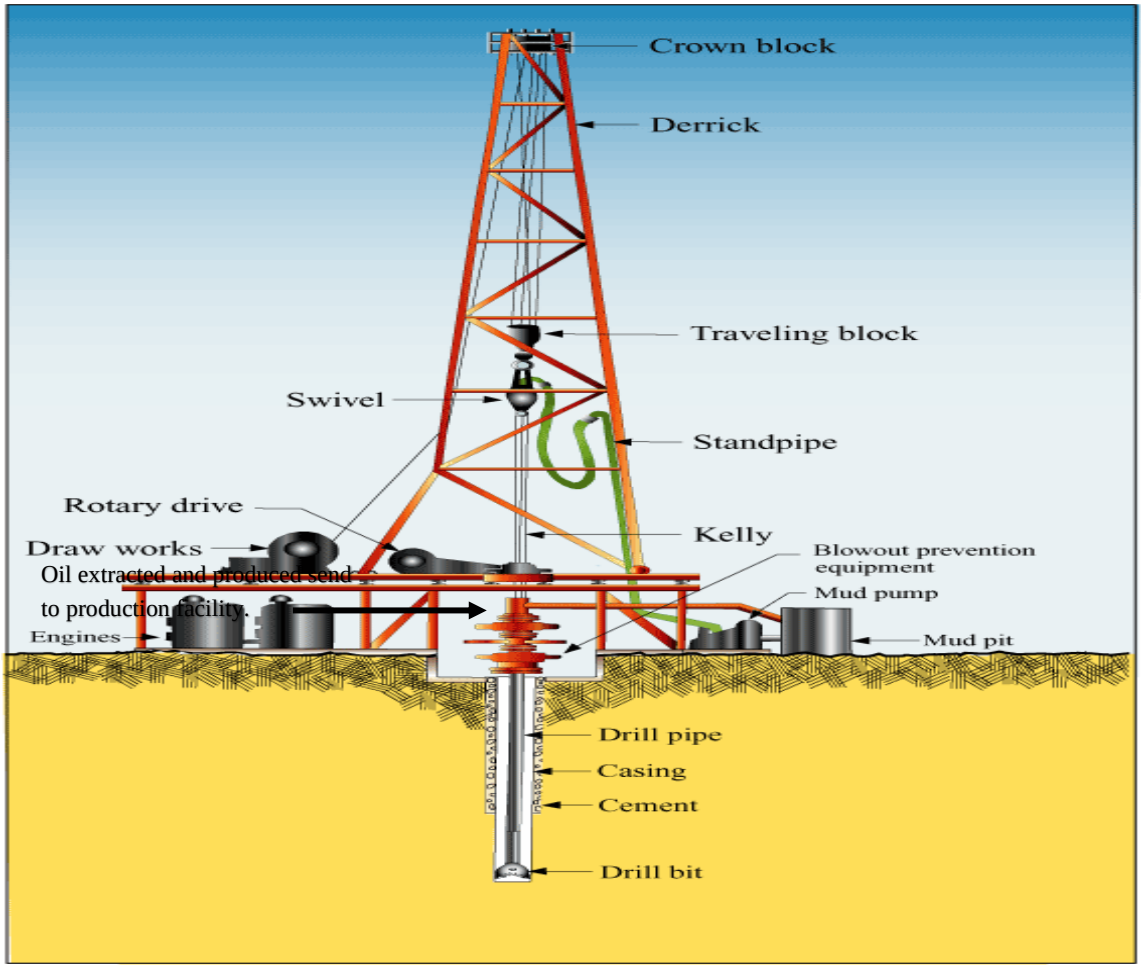

Figure 1.1: Drilling and Production of Hydrocarbon (source-http://getdrawings.com/drilling-rig-drawing#drilling-rig-drawing-59.gif)

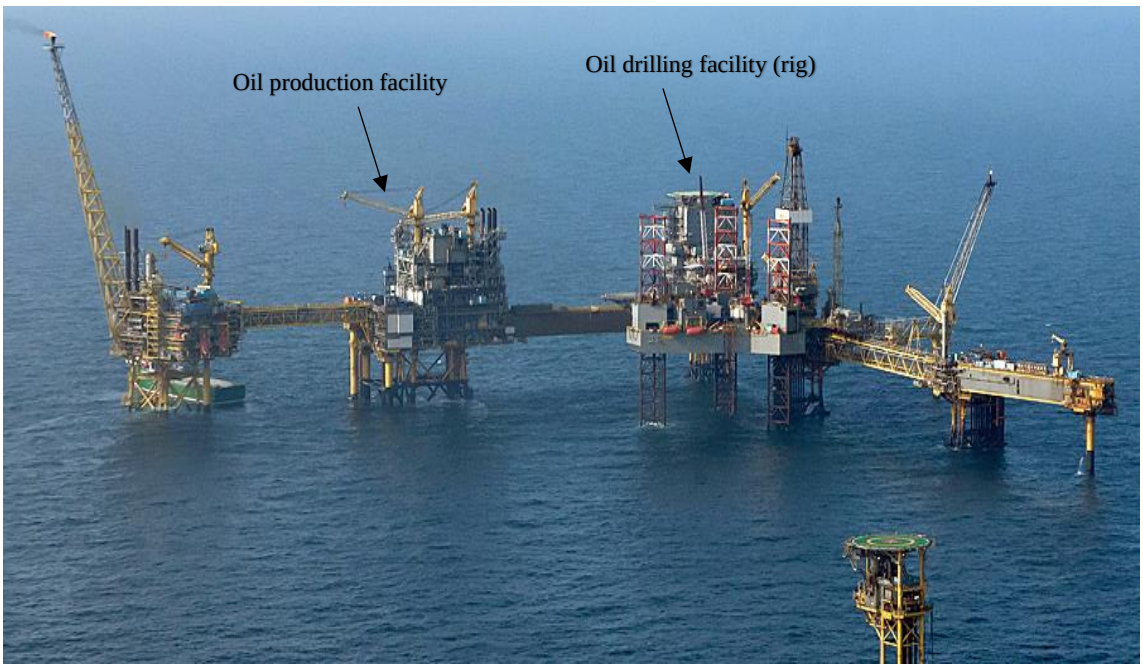

Figure 1.2: Typical set up of drilling and production facility (source-http://argoflares.com/wp-content/uploads/2012/01/Offshore-Complex.jpg)

Nanotechnology benefits from and contributes to many industries [6],[7]. Our focus is on the upstream oil and gas industry. The need for exploring the hydrocarbon reserves from adverse environments such as deep-water, remote location and extreme weather conditions provide the constant challenges to improve and stretch the limit of the system and equipment used in drilling and production phase. The era for easy hydrocarbon has been facing off slowly due to decline in reserves from the low temperature and pressure reservoirs. Oil companies facing challenges to design systems and equipment to suite the harsh condition reservoir that often led to extreme pressure and temperature that increases the failure rates of current technologies or rather limit the utilisation of such system and equipment at extreme conditions. Furthermore, the cost for operating in such environments is so high to a point that the project is no longer economically viable. The oil companies left with no choice, but to improve efficiency, reduce cost of material, system and reduce equipment failure rate. Nanotechnologies enable engineers and scientist explore the potential development of new materials that can be applied for fracturing fluids, flow assurance, drilling, completion, well stimulation and enhanced oil recovery [8]. Thus, nanotechnology has been identified as one of the ways forward for the industry need. Application of nanotechnology for enhanced oil recovery (EOR) seems to be in the top list of research area for the oil and gas industry. One such example is studies on injection of nanoparticles to improve the current conventional method of EOR [6]. The nanoparticles are utilised as part of the EOR nanofluids design that can change the physical properties of the reservoir such as wettability [9] and interfacial tension (IFT). These changes improve the reservoir fluids mobility ratio, control fine particles migration [6] and reduce adsorption.

Other benefits of nanoparticles in relation to EOR that have been discovered by scientist are reduction of oil viscosity, reduction of the capillary force within the pores and extension of polymer temperature stability. The latest trend that increasingly becoming popular is the use of ultrasonic tools as standalone or in combination with nanofluids for EOR and well stimulations [10],[11],[12],[13].

1.3 Problem Statement

The need for exploring the hydrocarbon reserves from adverse environments such as deep-water, remote location and extreme reservoir conditions provide constant challenges to improve and stretch the limit of the system and equipment used in drilling and production phase [14]. The era for easy hydrocarbon has been diminishing slowly due to

the decline in reserves from the low temperature and pressure reservoirs. The hydrocarbon flows out of the reservoir when the natural pressure in the reservoir is greater than the producing well. However, in many cases the full production capability of a well is not achieved due to reservoir and near wellbore damage induced during drilling and production phase [15].

Enhance oil recovery (EOR) techniques have provided an alternative for oil companies to increase production from their old reservoirs without the need to drill more wells in the extreme reservoir conditions. EOR success is largely dependent on removing near wellbore damage that occurred in both injection and production well. Previous research has focused on changing the reservoir properties to improve the fluids mobility [16],[17],[18],[19] and neglecting the importance of near wellbore damage removal prior to commence EOR. Various advance chemical treatments have been designed for near wellbore damage removal, but the industry is still facing low success rate. Conventional methods of improving oil production have given mixed results often lead to non-economical to produce due to the lack of a structured well stimulation or remediation program [20]. Chemical treatment for near wellbore remediation is purely dependent on mass transfer mechanism and its kinetics. Thus, chemical treatment alone has its limitation. Recent research and development of nanotechnology combination of chemical and external perturbation such as ultrasound treatment for enhance oil recovery [10] has shown some promising results despite the limitations of uniformity, penetration and wave propagation depth. However, such combination for near wellbore damage remediation is not well researched [11]. Furthermore, to the best of our knowledge the protocol to produce nanofluid which will enhance the physio-chemical properties using external perturbation such as ultrasound and their effect to mass transfer kinetics during near well remediation are not established. Further research is needed to understand the benefits of this nanotechnology and the mechanism involved in enhancing the near wellbore damage remediation as an alternative well stimulation method. The research gaps are summarised in bullet points as below.

1) Lack of proper protocol for nano fluids production and field implementation for oil well remediation.
2) Lack of studies on external perturbation effect on physio-chemical properties of remediation fluids and the mass transfer kinetics.
3) past relevant studies are scattered without interconnection.

4) Effect of Near well bore remediation in EOR process has not been studied.
5) There is no theoretical simulation study done on near wellbore remediation mass transfer kinetics.

1.4 Objectives and Significance of the Study

The use of nanofluids synthesized using external perturbation such as ultrasonic to remediate the near wellbore damage will provide a technology leap from the conventional method. Thus, this thesis is intended to provide an investigation on nanofluids physio-chemical properties for near wellbore remediation of an oil well focusing on optimizing the mass transfer mechanism as an effect of variable ultrasonic induction. The research is aimed at providing a better understanding of the correlation between various near wellbore damage mechanism and the mass transport kinetics during the near oil well remediation process. The objectives of this study being summarised as below.

1) Develop a protocol for stable nanofluids synthesis for field implementation.
2) Determine the limiting mass transfer mechanism for near wellbore damage media.
3) Determine the effect of various ultrasonic amplitude, under both conditions isothermal and non-isothermal on nanofluids physio-chemical properties and mass transfer kinetics during well remediation.
4) Develop correlation with ultrasonic amplitude %, nanofluids physio-chemical properties and mass transfer kinetics during well remediation.
5) Validate the effect of coupling near well remediation in EOR process.

Hence, the significance of this research is to reduce extensive trial and error laboratory hours and improve the well remediation success rate by providing an integrated and structured nanofluids synthesis guideline for near wellbore remediation.

1.5 Scope of The Study

To complete this study, a systematic approach will be developed to conduct the research. The research will cover the following scopes.

1. Experimental works that covers nanofluids sample preparation, formulation optimisation, nanofluids physio-chemical properties characterisation and mass transfer kinetics evaluation due to ultrasonic treatment under both isothermal and non-isothermal conditions.

2. Theoretical Simulation to represent the near wellbore remediation mass transfer mechanism with Ansys Fluent computational fluid dynamic Software.

1.6 Thesis Outline

The thesis has been organised with an outline to give readers the best flow of the thesis. The thesis has been broken down into various chapters to provide the flow. **Chapter 1** provide the background, problem statement, objective, and significance of the research work.

Chapter 2 provides details literature review relevant to this research that help us understand the past works and the knowledge gaps to design the methodology and scope of studies to meet this thesis objectives. In **chapter 3**, we will detail out the nanofluids formulation, basis of our formulation and how the concept of phase behavior studies used to optimise the formulation. Further, we will explain how ultrasonic equipment is used to synthesis the nanofluids and explain the basis of fixed 20 KHz ultrasonic frequency selection for the experiments. **Chapter 4** mainly will focus on nanofluids physio-chemical properties characterisation that are relevant for mass transfer kinetics during near wellbore remediation process. In this chapter, procedure for each characterisation procedures will be outlined. The physio-chemical properties characterisation of the nanofluids that were treated with ultrasonic at various amplitudes % under both isothermal and non-isothermal conditions will be compared for understanding the effect of ultrasonic amplitude on key physio-chemical properties that effect the mass transfer kinetics during near well remediation.

Following the experimental work in chapter 4, results, and observation from this will be used to perform mass transfer kinetics evaluation experiments. These evaluations will be covered in **Chapter 5** where dissolution of filter cake and sand packed column flow experiments will be used as a basis for mass transfer kinetics study for this thesis.

In **Chapter 6,** we will use results from chapter 5 to identify the best-case scenario, ie whether isothermal or non-isothermal condition favouring the mass transfer kinetics enhancement for carrying out mass transfer kinetics simulation with Ansys Fluent. The simulation will mimic the filter cake dissolution process in near wellbore remediation experiment that was carried out in earlier, chapter 5. This chapter will also cover all the details on, basis of model selection and assumption taken to conduct the simulations. The results of filter cake dissolution from experimental and simulation will be compared for

generalizing the correlation between the ultrasonic external perturbation and physio-chemical properties and their effect to mass transfer kinetics during wellbore remediation process.

Last but not least, **Chapter 7** will provide conclusions covering overall summary of the thesis, discussions and future work recommendations.

CHAPTER 2 Literature Review

2.1 Introduction

This research focus on to developing a protocol to produce nanofluid with enhanced physio-chemical properties to improve the near wellbore remediation using a new approach such as ultrasound. To achieve the objectives of the study, we need to review key fundamentals that provide background to this study. The main seven fundamentals area of the past research work review are as follow.

1. Enhance Oil Recovery & Well Stimulation
2. Nanoparticles and Nanofluids
3. Ultrasonic Tools
4. Physio-Chemical properties of fluids
5. Mass Transport Phenomena
6. Theoretical simulation
7. Experimental work

Section 2.2 covers introduction to enhance oil recovery and well stimulation concepts, limitation on current methods and challenges applying nanotechnology in the current methods. The review on the nanotechnology specifically proposed in this thesis will be covered in section 2.3 and 2.4, respectively. This will be followed by section 2.5 briefly discussed about the physio-chemical properties of the nanofluids that are important for this study. The various experimental methods for the fluid's characterisations will also be covered in this section. Section 2.6 will provide review on the fundamentals of mass transport phenomena useful for this study. The past theoretical simulation and experimental work relevant to this study will be reviewed in section 2.7 and 2.8 respectively. Finally, a summary of literature review will be discussed in section 2.9. For clarity, at the end of each section, the main contribution to each area by this thesis is underlined.

2.2 Enhance Oil Recovery and Well Stimulations

The following sections will provide review about the concept of Enhance oil recovery and well stimulation, the current issues, and limitations of these methods. The review will provide some background knowledge on how this study will improve the current methods mentioned earlier.

2.2.1 Enhance Oil Recovery

The enhance oil recovery method is deployed in a reservoir when the production of hydrocarbon is no longer can be accomplished using natural reservoir energy due to decline in the reservoir pressure over a period of time. The method refers to a process of repressurizing the reservoir with external fluids such as gas or liquids [21]. In general, only 30 to 40% of the initial oil in place from a reservoir is produced through the natural production. Thus, it is extremely attractive to recover the remaining oil utilizing EOR techniques. In current technology the remaining oil is recovered by pumping displacing fluid into an injection well and moving it through the reservoir as a bank of fluid that pushes oil a head towards a production well [21],[22]. Fig. 2.1 describes the mechanism of the fluids displacement or sweep method used in the enhanced oil recovery process. The type of displacing fluids is dependent on the reservoir conditions that have many variables such as pressure, temperature, crude oil type, nature of the formation, connate water characteristic and the saturation history [21]. The most common EOR processes are water flooding, chemical flooding, and water alternate gas (WAG) flooding. Table 1 summarizes a typical guideline for selection of the suitable EOR techniques for various reservoir conditions [21].

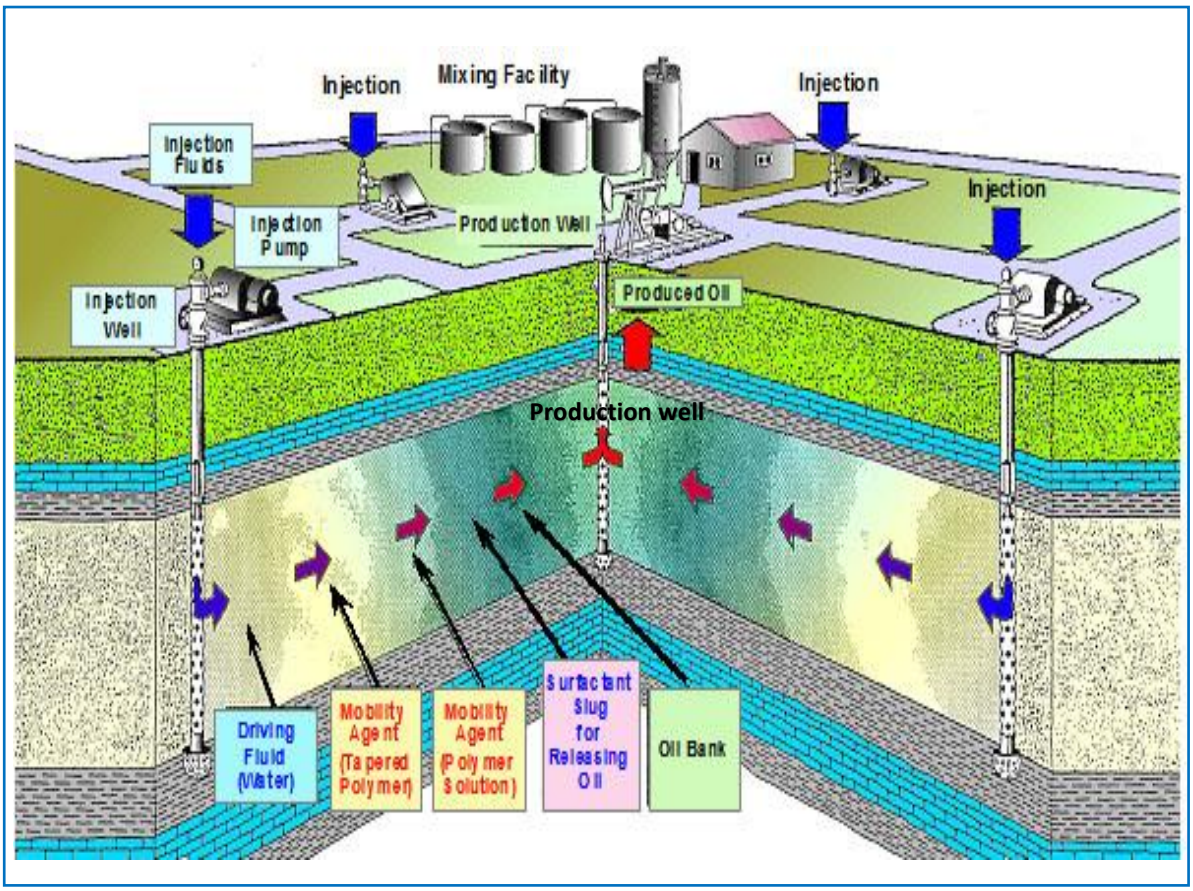

Figure 2.1: EOR system (source-ugmsc.wordpress.com) describing the series of fluids pumped as injection or displacing and sweep fluids to push the oil from the reservoir into the production well.

Table 2.1- Screening Criteria for Enhanced Oil Recovery Techniques [21].

Process	Oil gravity (°API)	Oil viscosity (cP)	Oil saturation (%)	Formation type	Net thickness (ft)	Average permeability (mD)	Depth (ft)	Temp (°F)
Miscible								
Hydrocarbon	>35	<10	>30	Sandstone or carbonate	15–25	—[a]	>4500	—[a]
Carbon dioxide	>25	<12	>30	Sandstone or carbonate	15–25	—[a]	>2000	—[a]
Nitrogen	>35	<10	>30	Sandstone or carbonate	15–25	—[a]	>4500	—[a]
Chemical								
Polymer	>25	5–125	—[b]	Sandstone preferred	—[a]	>20	<9000	<200
Surfactant–polymer	>15	20–30	>30	Sandstone preferred	>10	>20	<9000	<200
Alkaline	13–35	<200	—[b]	Sandstone preferred	—[a]	>20	<9000	<200
Thermal								
Steamflooding	>10	>20	>40–50	Sand or sandstone with high porosity	>10	>50	500–5000	—[a]
Combustion	10–40	<1000	>40–50	Sand or sandstone with high porosity	>10	>50	>500	—[a]

[a] Not critical but should be compatible.
[b] Ten percent mobile oil above waterflood residual oil.

To assess this process, the oil recovery efficiency E, is used. The oil recovery efficiency E of the EOR process with any type of fluids is governed by the macroscopic and microscopic efficiency, ie E_v and E_d respectively [9] [21],[22]:

$$E = E_v E_d \tag{2.1}$$

Where E_v is made of the areal E_s and vertical E_i sweep efficiencies.

E_s is the areal sweep efficiencies and E_i is vertical sweep efficiencies; thus,

$$E_v = E_s E_i \tag{2.2}$$

Macroscopic displacement efficiency measures the effectiveness of the displacing fluid in contact with oil- bearing parts of the reservoir while the microscopic displacement efficiency measures the effectiveness of displacing fluids mobilizes the residual oil upon contact. It is also very important to understand the parameters that are affecting the efficiency of both displacements. In general, factors such as surface tension forces, wettability, capillary pressure and relative permeability influence the microscopic displacement whereas heterogeneities and anisotropy of the rock, mobility ratio of displacing fluids against displaced fluids, actual placement between injection and production well and type of formation influence the macroscopic displacement [21],[22],[23].

While many research works have been continuously conducted in improving the microscopic and macroscopic displacement efficiencies, heterogeneities of the rock matrix remain the biggest factor for low oil recovery efficiency due to the present of faults, fractures and high permeability streaks. The fluids flow in such a reservoir condition is difficult to be engineered and controlled from the surface for a maximum displacement efficiency. This often leads to issue of bypassing of residual oil by the displacing fluids, early breakthrough of water phase channelling into often referred as “fingering effect” [21]. Another major contributor for EOR failure is the formation damage caused by fine particles, hydrocarbon residue, polymer and drilling fluids particles plugging the near wellbores of injection and production wells. Thus, it is very important for the reservoir engineers to plan the EOR project and put great emphasises on near wellbore clean-up of both the injection and production wells to establish the injectivity factor prior executing the large scale EOR. This process is often referred to as near well stimulations or remediations.

2.2.2 Well Stimulations

The other important areas where nanotechnology have been explored are for well stimulation techniques for improving oil production. In general, there are few conventional well stimulation methods that have been used extensively:1) Hydraulic or acid fracturing, 2) acid cleaning and 3) acid stimulation [15]. The illustrations of those method presented in Fig. 2.2.

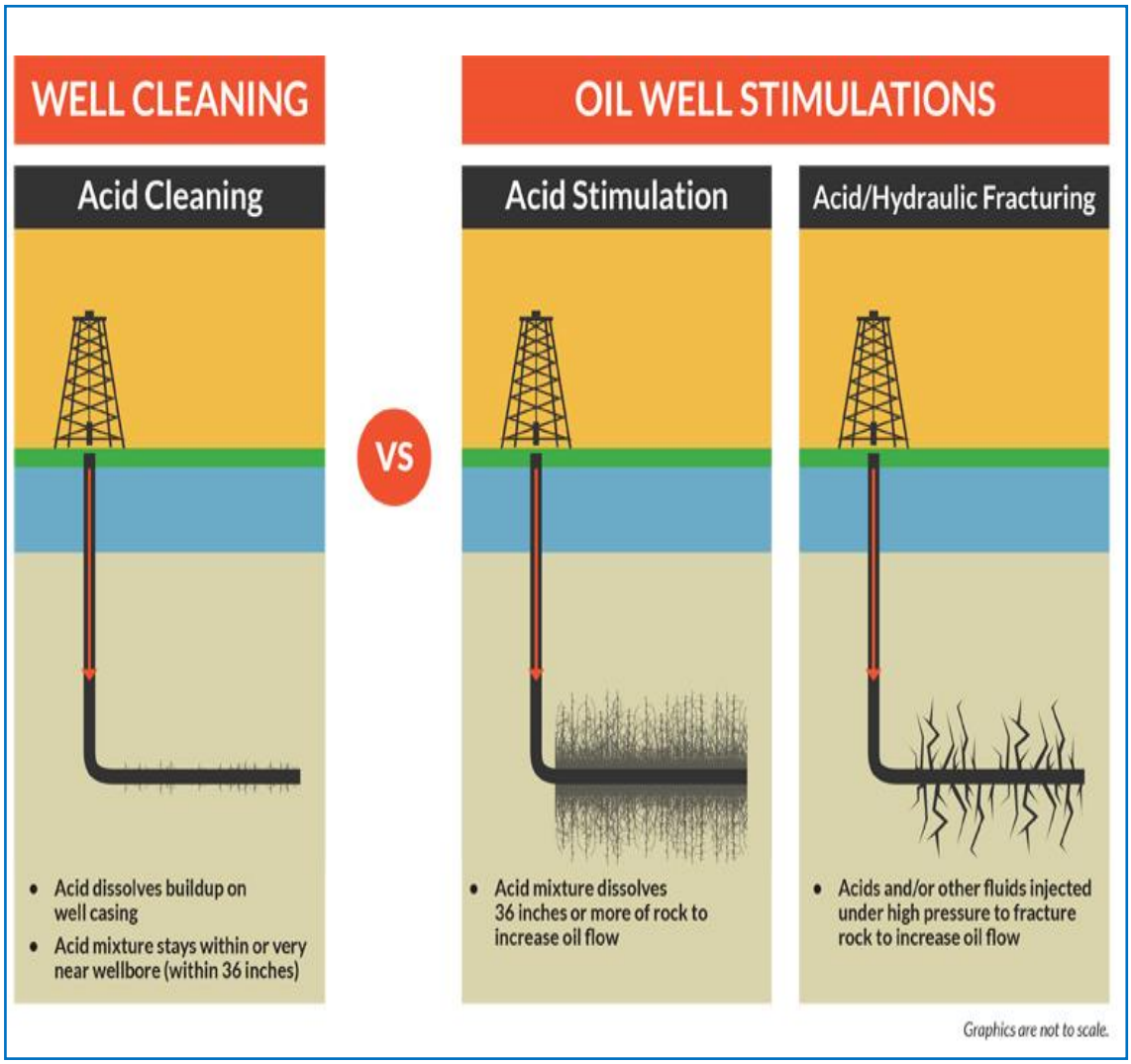

Figure 2.2: Illustration of various well stimulations. (source- The Conservancy of Southwest Florida website- https://www.conservancy.org/our-work/policy/oil/hydraulic-fracturing-acidizing)

The definition of well stimulation refers to a process of increasing hydrocarbon production rate by means of increasing the permeability of the media where the hydrocarbon flows to the producing wells. Generally, well stimulation techniques are applied when a well is plugged by a damage mechanism from drilling and production

activities. Thus, stimulation can be applied for a newly drilled well or remediation of an old producing well. The near wellbore damage mechanism is usually caused by the chemical interaction between the reservoir fluids and the drilling fluids such as emulsion and mud particles plugging. Other form of damages includes the natural mineral precipitation that creates scale, hydrocarbon residue deposits and fine particles migration that occur due to crushing and compaction of rocks during perforation operation [15].

In some cases of unconventional production, stimulation techniques are applied on undisturbed formation, and it is often referred to as reservoir stimulation. It is a technique to enhance natural permeability of the reservoir. The conventional well stimulations method described above have great deal of limitations. In hydraulic fracturing [24], fluids that carries proppant made of a solid material, typically sand, treated sand or man-made ceramic material is pumped in the wellbore to generate fractures in the rock for the hydrocarbon to flow from the reservoir. The success of this technique largely depends on the ability of the proppant to form a matrix structure that hold the opening of the fluid flow path. The second and third type of stimulation treatment are acidizing performed by pumping acid into the well to dissolve carbonate formation such as limestone, dolomite and calcite of the reservoir rocks [25],[26]. This process enlarges the pores of the reservoir and remove mud plugging particles that reduce the permeability of the formation. However, this acidizing method often lead to pinhole and non-uniform treatment of wellbore as the acid reaction to the rock is rapid [26]. Acid treatment often accelerates fine particle migration and promote emulsion formation. A typical onsite set up of well stimulation operation is shown in Fig. 2.3. Such set up is costly and require large footprint at rig site. The operation involves high pressure pumping of the stimulation fluid consist of proppant and gel. The fluid is pumped into the wellbore to fracture the formation and create flow path for the hydrocarbon to flow.

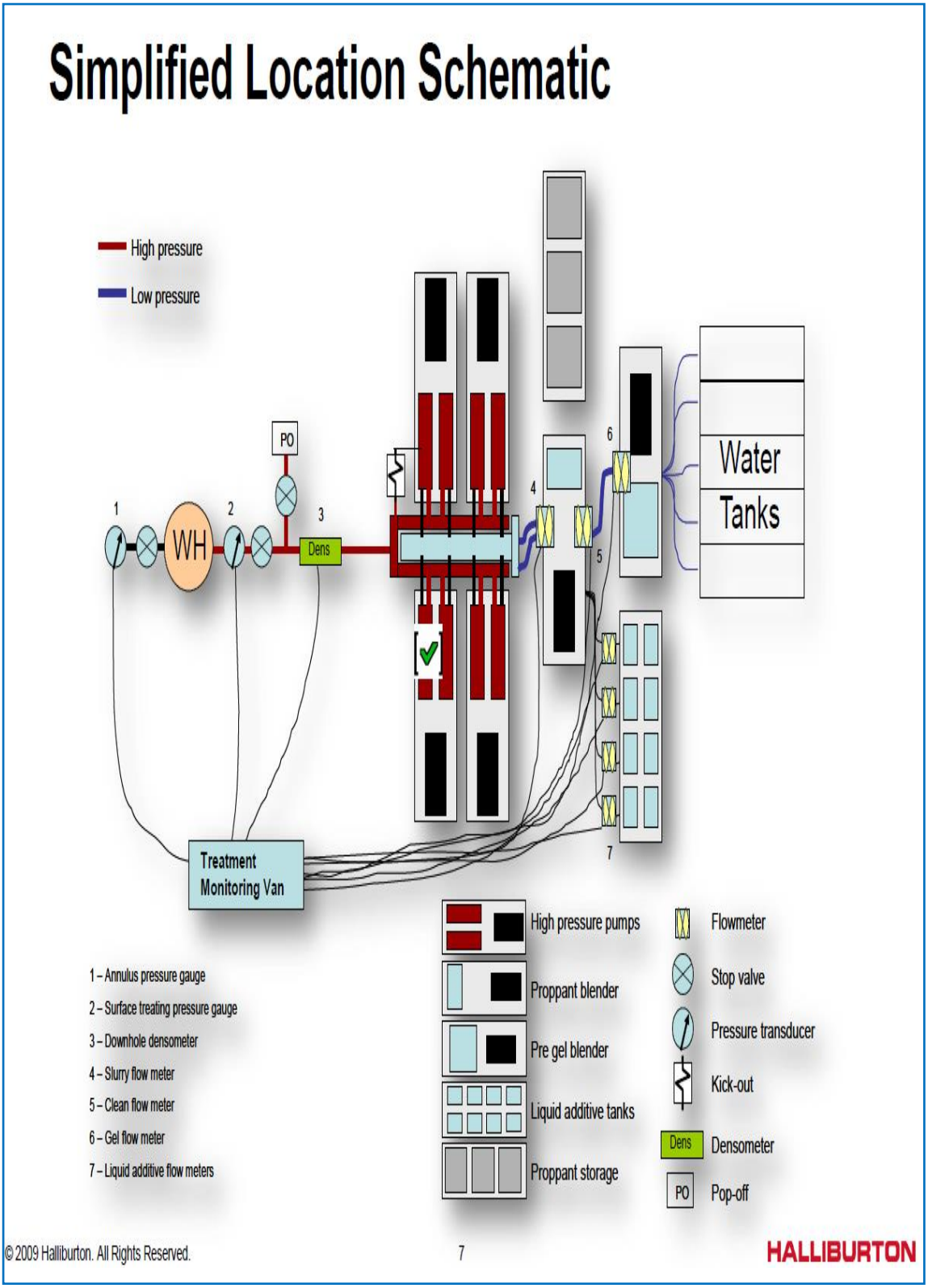

Figure 2.3: Simplified location schematic -Well stimulation equipment operation set up (source: https://www.epa.gov/sites/production/files/documents/fracturedesignandstimulationmonitoring.pdf)

The efficiency of hydrocarbon production improvement using the conventional EOR and well stimulation methods described above are not satisfactory due to the fact that these methods are energy intensive with high investment cost and environmentally not safe. The techniques produce tremendous amount of waste that are detrimental for the environment if they are not managed or contained properly.

Cost and clean environment remain as the main driving mechanism for new and improved technique. Exploring nanotechnology advancement has attracted a great attention in improving oil production. Extensive research on nanofluids termed as "smart fluids" has become more popular in oil and gas industry in recent years [27]. The development of nanofluids for the oil and gas production improvement has a great practical importance. The nanofluids is generated by incorporating nanoparticles to fluids for enhancement of their properties at low concentration. It is also reported that by incorporating certain type of surfactant, the interfacial properties between liquid/liquid system can be altered [27]. The use of nanofluids to remediate the near wellbore damage for well stimulation operation provides a technology leap from conventional method. However, the effective use of such method is still being explored especially on the interface interaction mechanism between the nanofluids and the damage media consist of multiple deposit of scale, mud particles and hydrocarbon that embedded together in the form of solid or semi-solid is not well researched. Thus, detail studies and understanding of the mass transfer kinetics correlation with the governing nanofluids physio-chemical properties for the effective near wellbore damage remediation will address this shortfall. This will be covered in detail in **chapter 5** of the thesis.

2.3 Nanoparticles and Nanofluids

The following sections will provide brief review on nanoparticles and nanofluids and how they are used in oil and gas industry for well production enhancement. We also will discuss the issue with the current method of nanofluids production.

2.3.1 Nanoparticles

Nanoparticles refer to the simplest form of nano materials that have been explored in recent decades as the way forward for resolving challenges in technology development in key areas of oil and gas engineering. The application of certain type of nano particles for a specific use is very much dependent on the physiochemical properties that it exhibits as a result of functionalizing with bulk materials [27],[28].In general, nanoparticles are

classified as metal oxides, organic and inorganic [6]. Table 2.2 summarizes various nanoparticles applied in oil and gas applications. Metal oxide nanoparticles have been reported as the most common nanoparticles used for EOR due to their structures, physio-chemical properties and compositions. Table 2.3 classifies the various nanoparticles dominant mechanism in respect to the physio-chemical properties that relevant for EOR and well stimulation enhancement [6].

Table 2.2: various nanomaterial applications in the oil and gas industry [9]

Processes	Material Type	Applications	Comments
Drilling and Completion			
Drilling Bits	Carbon nanomaterial - nano-diamond polycrystalline diamond compact (PDC) Technology	* Suitable for functionalization of PDC cutters for drill bits. * Effective for manufacture of advanced drill bits that has good resistance to abrasion and corrosion upon nano-coating	This application has reached mature level and PDC bits a re used widely in the industry for its performance
Logging while drilling (LWD)	Nanostructured glass -ceramics	* effective neutron detectors-Li-6 scintillation nanostructured glass ceramics shows better efficiency than ordinary Li-6 scintillation materials	
Cementing	Carbon nanotube (CNT)	* Suitable as reinforcement materials for cement instead of conventional fibers.	This applicationa still under research stage
Drilling fluids	Nanoparticles (NP)	* Control of fluid loss and wellbore stability * Design of drilling fluids suitable for harsh reservoir conditions. * Nanoparticle based drilling fluids can be effective for elimination or reduction of drilling problems such as pipe sticking, equipment wear and tear, rig instability and poor hole cleaning issues.	Many drilling fluids company have been actively involved in research however , dispersion and stability still key hinderance for commercialisation
Exploration			
Imaging tool	NP	* Hyperpolarized silicon NP deliver innovative tools for measurement and imaging oil exploration	
Production			
Hydrate Recovery	NP	* Nickel-iron NP can be used dissociation of hydrates	
Viscoelastic surfactant stimulation fluid (VES)	NP	* NP accociates with VES micelles for stabilization of fluid viscosity	some field trial has been done with mixed results due to lack of understanding on the mecahnism

Table 2.3: Various Nanoparticles with dominant mechanism functionality [6].

Nanomaterial Functionality as dominant mechanism	Material Type
Viscosity Reduction	* Aluminum Oxide, (Al_2O_3)
	* Copper (II) Oxide, (CUO)
	* Iron Oxide, (Fe_2O_3/Fe_3O_4)
	* Nickel Oxide, (Ni_2O_3)
	* ethanol and magnesium oxide
	* Polymer Coated Nano Particles
Interfacial Tension (IFT) reduction	* SiO_2 nanoparticles
	* HLP (Hydrophobic and lipophilic polysilicon)
	* Ployacrylamide Micro-gel Nano spheres
	* Polymer Coated Nano Particles
	* Ferrofluid
Wettability Alteration	* Tin Oxide (SnO_2)
	* SiO_2 nanoparticles
	* Alumina Coated Silica Nanoparticles
	* Hydrophobic Silicon Oxide (SiO_2)
	* Spherical Fumed Silica Nanoparticles
	* NWP (Naturally wet polysilicon)
	* LHPN (Lipophobic and Hydrophilic Polysilicon Nanoparticles)
	* Polymer Coated Nano Particles
Efficient in sweep & displacement	* Nano-Sized Colloidal Dispersion Gels (CDG)
	* Polymer Nano Particles
	* Polymer Coated Nano Particles

The nanoparticles that are able to change the physio-chemical properties mentioned above are mainly due to the fact that they multiply the surface area to volume ratio to a million times over the conventional bulk materials. This phenomenon generates very high surface energy that leads to structural transitioning [6]. Thus, studying the structure of nanofluids produced from incorporating nanoparticles become an important element for understanding its effect onto mass transfer coefficient in any fluid transport behaviour. However, the biggest challenge is to keep the nanoparticles suspended in the fluids for longer period. Thus, the constant search for improve method of generating stable nanofluids is the key for field application in the oil and gas industry.

2.3.2 Nanofluids

The initial study of nanofluids started in 1981 by D.B Tuckerman who introduced the microchannel technology [29]. Nanofluids are new type of fluids often referred as “smart fluids” that created by addition of nanoparticles to fluids by means of dispersion. This methodology and term were proposed by Choi in the early 90s’ for improving thermal conductivity of base fluids [30]. In 1998, the US department of energy funded the

research work on both fundamentals and applications of nanofluids. Wiley published the first book on nanofluids titled, "Nanofluids:Science and Technology" in 2007 [29]. The book summarizes the evolution of nanofluids from its conceptual to practical through research and development. Till now, researchers constantly attempting to prove their findings on effectiveness of nanofluids as what they have predicted before to apply in large scale [31],[32].

Microemulsion studies have been reported as flowback aids for enhance oil recovery by Amir Mahmoudkhani and his team [33]. The paper was published in Society of Petroleum Engineers journal in 2015. In this literature, a special attention was given on testing various formulation of microemulsion generated spontaneous, requiring no physical energy input on its performance to improve regain permeability for fracturing flowback aids. Microemulsion is defined as thermodynamically stable isotropic liquid [34], means its properties are uniform in all directions. Unlike microemulsion, nano emulsion does not form spontaneously, and it required external energy to generate it [35]. Hence, it is defined as kinetically stable emulsion [36],[37]. In summary the distinct differences between microemulsion and nano emulsion are summarised in Fig. 2.4 [34], [38],[39]. Chengwen Wang and his team published the very initial work on nano emulsion used as mud filter cake breaker in 2016 [40]. However, his work was very limited and does not study the effect of ultrasonic parameters such as amplitude % on nanofluids physio-chemical properties. Nano emulsion provides great advantages compared to microemulsion as it has more tolerances to external factors such as pressure, temperature, and pH [35],[41],[42]. This characteristic will enable engineers and scientists in oil and gas to minimise the complexity of fluids design for reservoir application. However, the correlation between the energy input from the external perturbation such as ultrasound induction and the resulting properties of nano emulsion that is kinetically stable is not well understood. This understanding holds a key aspect of nanofluids design for near wellbore remediation application. Hence, one of the aims of this research is to establish the fundamental of external energy input from ultrasound in transforming the thermodynamically stable to kinetically stable fluids and how it will benefit the near wellbore stimulation process.

Parameters	Emulsion[1-5]	Microemulsion[6-15]	Nano emulsion[35-42]
Appearance (Figure 6)	Turbid	Clear	Clear

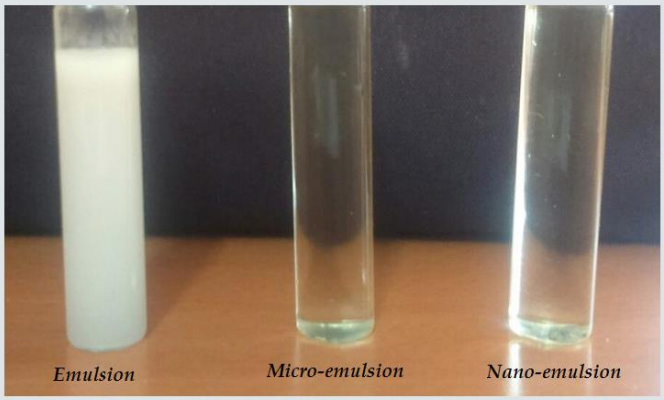

Figure 6: Appearance comparison between emulsion, micro emulsion and nano emulsion.

Particle size	1 to 20 mm	1 and 100 nm	1 and 100 nm
Formation	Mechanical shear	Self assembly	Mechanical shear
Stability	Thermodynamically unstable, Kinetically Stable	Thermodynamically Stable Long shelf life	Kinetically stable/ metastable, thermodynamically unstable
Phases	Biphasic	Monophasic	Monophasic
Viscosity	High	Low	Low (about 1 cP at room temperature)
Preparation cost	Higher cost	Lower cost	Higher cost
Interfacial Tension	High	Ultra Low	Ultra low (less than 10 dyn cm^{-1})
Optical isotropy	Anisotropic	Isotropic	Isotropic
Light scattering	Less scattering	Strong multiple scattering of visible light hence white	Strong multiple scattering of visible light hence white

Figure 2.4 : Example of differences between macro, micro and nano emulsion [34].

Various type of nanoparticles is dispersed in the base fluids to create nanofluids as described in Table 2.2. Each of these particles has its unique challenges in dispersing uniformly in base fluids [43] that makes up the nano scale colloidal. Some of the most critical aspect in achieving the desired properties and structures in nanofluids are uniform dispersion and stable suspension [30],[44]. Engineers and scientist have discovered many one step and two steps method to synthesis nanofluids either by physical or chemical processes. In the one-step process, the nanoparticle synthesis and dispersion happen simultaneously [30],[44]. The two steps method involve process of producing dry nanoparticles first and then dispersed it in base fluids using the aid of mechanical homogenizer. However, many researchers still facing problems to keep the particles from agglomeration over time. In industry such as oil and gas where the nanofluids need to be stored or transported for longer duration due to remote operation, pose a big challenge to scale up the technology from laboratory development. However, the recent advancement of ultrasonic tools enables engineers to discover new method for producing stable and uniform nanofluids [45].

Thus, to address this issue, researchers have further extended the concept of nanofluids by exploring dispersion of liquids and gas bubbles to generate nanofluids. A new methodology of synthesising nanofluids by means of Chemical Solution Method has been discovered to provide stable and uniform generation of particles structures of the nanofluids. This method enables engineers to manipulate and control the structures by varying variables such as temperature, pH and also the external energy input such as ultrasonic irradiation [46]. Fig. 2.5 describes a typical schematic of Chemical Solution Method of producing nanofluids using external perturbation such as ultrasonic tool.

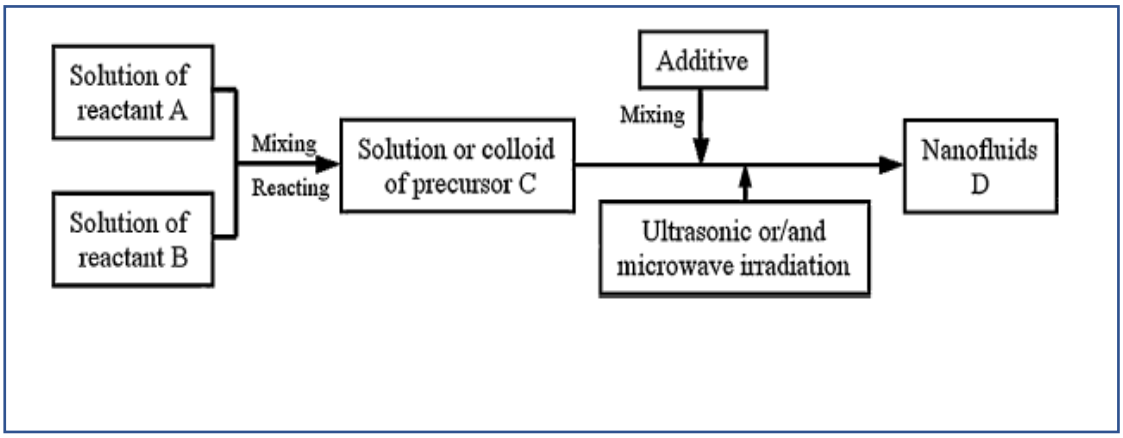

Figure 2.5 : Example of Chemical solution method (CMS) process flow schematic for synthesizing nanofluids [46].

2.4 Introduction to Ultrasonic

The term ultrasonic is derived from the latin root ultra and sonic. Ultra means beyond and sonic is sound. Ultrasonic waves are sound waves having frequencies above the audible range of 20 KHz and it is not part of electromagnetic wave such as light and heat. These waves are classified as high frequency waves and travel in different velocity depending on the media, for instance in liquid and solid the travel speed ranges from 1500m/s to 5000m/s [47]. Ultrasonic wave travel in straight line through homogeneous medium without changes in velocity, however it undergoes reflection and refraction in heterogenous media. It is often used for imaging, detection, and navigation. Industry such as medical and military have used these technologies widely as it does not radiate harmful wave unlike electromagnetic waves [47]. Hence, it appears to be a popular alternative to electromagnetic waves. In recent development, scientists have explored its potential in material processing for improving the physical and chemical reaction in various industries. In this research, we will explore the use of ultrasonic tools to create nano micellar

structures [45],[48] as an alternative method to produce stable nanofluids with the ability to control physio-chemical properties of the fluids designed for effective near wellbore damage removal. Thus, improve oil production.

2.4.1 Ultrasonic used in Enhance Oil Recovery and Well Stimulation

The idea of using wave treatment for enhance oil recovery and well stimulation is originated from the natural incident of earthquake that caused a kick in oil production [49]. Since then, the very first study in this area was reported in 1965 to the best of our knowledge by Duhon and Campbell [10]. They conducted waterflooding test on cores under ultrasonic energy with varies frequencies with results showing oil recovery improvement utilizing ultrasonic energy. However, their study also pointed out increasing frequency and cavitation to certain point decrease the recovery. This has left a gap in understanding the true mechanism of ultrasound effect to the reservoir. The next three decades, attention was devoted to elastic wave stimulation on oil recovery by seismic waves with lower frequencies than ultrasound waves. Beresnev and Johnson compiled and well documented all these efforts in 1994 [50].

Recent work by Aarts and Ooms [51] showed that the mechanism of peristaltic transport works only at ultrasonic frequencies and the intensity of the ultrasonic field should be more than a specific amount and the effect will occur only near wellbore due to high attenuation of ultrasound. Graham and Higdon numerically studied the motion of fluid droplets in harmonically forced capillary tubes and observed a significant enhancement in mobility for large droplets with diameters greater than diameter of the capillary [52]. Wong et al. [53],[54] designed a special “Linear Cell” setup in which a cylindrical core sample was placed. They used this setup to see the fine damages and mud cake removal in the wellbore by acoustic waves. They observed that higher frequency results in better well cleaning, but causes more attenuation, ie the wave penetration into rocks decreases. Thus, the optimum frequency must be chosen to balance the cleaning efficiency and wave attenuation. The very recent investigation on applying ultrasonic for generation of nanofluids was conducted by Nor Saadah and Muthupandian in 2014 reveal that by varying the power and frequency of ultrasonic on structural transformation of micelles of CTABr/NaSal fluids, provides the knowledge useful for controlling micelle’s structure that influence the physio-chemical properties [48]. Thus, our aim is to design nanofluids using the ultrasonic energy input to control the suitable physio-chemical properties

behaviour shown by respective micellar structure to enhance near wellbore damage removal in oil and gas application.

2.5 Physio-Chemical Properties of Nanofluids

Many of the previous works have focused on the effect of nanoparticles on physio-chemical properties of nanofluids in relation to conventional method of EOR and well stimulation [9],[17],[32], very minimal studies have been devoted in understanding the physio-chemical properties of nanofluids that influence the effectiveness of near wellbore remediation. The physio-chemical properties for the near wellbore remediation are different from the EOR as the mechanism involved in near wellbore remediation is largely dependent on mass transfer or diffusion process between the contacting media. The mechanism for EOR is based on displacement of fluids from reservoir, thus fluids properties that increase mobility ratio between the displacing and displaced fluids are the key driver. However, certain properties such as interfacial tension (IFT) [23] and wettability [55] are important for both processes. Exploiting the mechanism of external perturbation such as ultrasound induction on smart fluids to control the physiochemical properties [56] have potential for improvement in penetration depth, effective remediation of formation damage and improving permeability to unlock the trapped hydrocarbon in fine pore of reservoir rock. However, to our knowledge, no literature has addressed all these parameters in one study, making it difficult to correctly model and solve the near wellbore damage problem in the reservoir. This research will also be focusing on characterization [57] of nanofluids in terms of its phase behaviour, particle size distribution, morphological studies of the controlled micellar structure and its effect to interfacial tension, solubility, surface and interfacial tension, fluids rheological properties and their correlation for effective mass transfer kinetics.

2.5.1 Surface and Interfacial Tension

We deal with surface and interfacial tension phenomena almost in everything we do in our daily life right from washing dishes, laundry, and shower. These phenomena occur at interface of two phases, including solid-liquid, solid-gas and liquid-gas [58]. Surface tension term is typically used only when the liquid surface is in contact with gas such as the air. If the surface is between two liquids such as water and oil or between solid and liquid, it is called interfacial tension. Surface and interfacial tension has the dimension of force per unit length, or of energy per unit area [23]. The two are

equivalent, but when referring to energy per unit of area, it is common to use the term surface energy. The SI unit of surface and interfacial tension is millinewton per meter (mN/m) which is equivalent to often used cgs unit, dynes per centimetre (dynes/cm) [59]. Two forces that influence surface and interfacial tension are cohesion and adhesion. Cohesion exists when molecules of same substance are attracted to each other and resist separation. Adhesion is the attraction between different molecules that are holding to each other [60]. Fig. 2.6 explains the effect of cohesion and adhesion as water forms nearly spherical droplets due to cohesion and adhesion keeps the drops in place.

Figure 2.6: Image of cohesion and adhesion effect on water drop
(source:https://static.diffen.com/uploadz/2/2e/Adhesion-Dew-drops.jpg)

The development of mathematical equation to measure the interfacial tension has gone through few corrections since Antonoff's introduced the rule predicts that the interfacial tension between two liquids A and B will be equal to the difference between the respective surface tensions which represented by the equation (2.3) [61].

$$\gamma_{AB} = |\gamma_A - \gamma_B| \tag{2.3}$$

Where,

γ_{AB} = interfacial tension between liquid A and B

γ_A = surface of tension of liquid A

γ_B = surface of tension of liquid B

However, this equation does not hold for many liquids. Thus, Girifalco and Good introduced the effects of the free energies of cohesion of the two phases and the free energy of adhesion on interfacial tension in 1957 [61]. This is represented by equation (2.4).

$$\gamma_{AB} = \gamma_A + \gamma_B - 2\Phi\sqrt{\gamma_A\gamma_B} \tag{2.4}$$

where Φ is a constant, which is defined as,

$$\Phi = \frac{\Delta G^a{}_{AB}}{\sqrt{\Delta G^c{}_A - \Delta G^c{}_B}} \tag{2.5}$$

where $\Delta G^a{}_{AB}$ is the free energy of adhesion for the interface between the phases A and B, $\Delta G^c{}_A$ is the free energy of cohesion for phase A, and $\Delta G^c B$ is the free energy of cohesion for phase B [61].

Further improvement to Girifalco and Good correlation, Fowkes assumed that the interaction between the immiscible liquid phases A and B involve only dispersion forces. The interfacial tension is than given by the following equation [61].

$$\gamma_{AB} = \gamma_A + \gamma_B - 2\sqrt{\gamma^d{}_A\gamma^d{}_B} \tag{2.6}$$

γ^d is the contribution from dispersion forces to the surface tension of the pure liquid and for a nonpolar liquid, $\gamma^d = \gamma$. Therefore, this provides a method to determine the unknown γ^d [61]. Thus, for Fowkes' equation to be applicable we have to exclude all interaction between the phases except dispersion forces [23]. It is believed that the best estimation for interfacial tension for liquids are based on experimental and scientists have developed few methods such as Du Noüy ring, Wilhelmy plate and Spinning-drop method. The spinning pendant drop method uses optical tensiometer technique and classified as one of the most widely used method in oil and gas industry.

It is reported in various literature that by decreasing interfacial tension, will facilitate easier oil droplets movement through porous media. This mechanism also applicable for the near wellbore remediation when the damage media is covered or deposited with oily hydrocarbon residue. However, how low the interfacial tension between the two media

for enhance mass diffusion is not well understood. In this study we intent to conduct experimental work on the effect of the ultrasonic tools on the nanofluids size and structure and their effect to the interfacial tension properties of the nanofluids and its correlation to interface mass diffusion coefficient.

2.5.2 Wettability

Wettability referred to the wetting forces and it is a measurement of the contact angles between a liquid droplet on a solid surface. It is the tendency of a solid to be in contact with one fluid than the other [23]. The preferred fluids are called wetting fluids and the other fluids as non-wetting. In general, maximum wetting condition is achieved when the wetting fluid spread out completely on a solid surface to maximize contact approaching zero contact angle. Maximum non-wetting condition on the other hand is achieved when non-wetting fluid minimize contact and try to create a spherical bead [23] approaching maximum contact angle. Reference to Fig.2.7, the contact angle explains the correlation between the interfacial tensions acting upon their respective interface in a system with a solid, gas and liquid drop [23], Thomas Young in 1805 derived an equation to calculate the contact angle θ of a liquid drop on an ideal solid surface under thermodynamics equilibrium of the of three interfacial tensions known as Young's equations [61],[62],[63] presented as the following equation.

$$\gamma_{sg} = \gamma_{sl} + \gamma_{lg} \cos\theta \tag{2.7}$$

Thus,

$$\cos\theta = \frac{\gamma_{sg} - \gamma_{sl}}{\gamma_{lg}} \tag{2.8}$$

Where, γ_{lg}, γ_{sg} and γ_{sl} are the interfacial tension of liquid-gas, solid-gas and solid-liquid interfaces respectively described in Fig. 2.8.

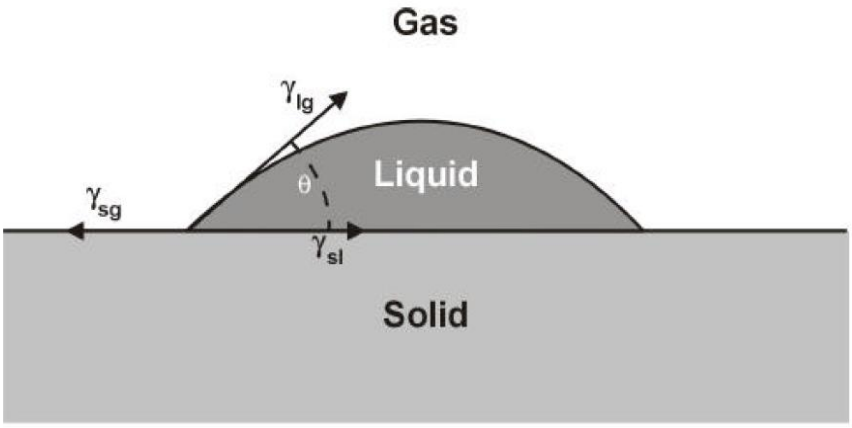

Figure 2.7: Diagram of Liquid-Solid-Gas interfacial tension at equilibrium describing the contact angles, θ between the liquid and solid phase [62].

Wettability of a rock or solid to various fluids can be determined using various method such as Microscopic observation, Amott wettability measurements, NMR longitudinal relaxation and Wilhelmy plate. Table 2.4 summarizes the various methods used to measure contact angels.

Table 4: Example of contact angle Measurement Techniques [62]

Measurement Technique	Physical Observation
Amott and Amott-Harvey	Amounts of oil and water imbibed by a sample spontaneously and by force.
U.S. Bureau of Mines (USBM)	Work required to imbibe oil and water.
Microscopic examination	Microscopic examination of the interaction between the fluids and the rock matrix.
Nuclear Magnetic Resonance	Changes in longitudinal relaxation time.
Flotation method	The distribution of grains at water/oil or air/water interfaces.
Glass slide method	Displacement of the non-wetting fluid from a glass slide.
Relative permeability method	Shape and magnitudes of K_{ro} and K_{rw} curves.
Reservoir logs	Resistivity logs before and after injection of a reverse wetting agent.
Dye adsorption	Adsorption of a dye in an aqueous solvent.

Modern digital instrument uses drop profile along with numerical integration of the Young–Laplace equation to generate the best-fit curve. This method referred as sessile drop method. It is one of the most reliable and accurate technique for measuring the contact angle [61].This method is commonly preferred and used in oil and gas industry.

Understanding reservoir wettability has been a key aspect for enhance oil recovery and failure to understand the wettability condition of certain reservoir could lead to

irreversible formation damage [55]. Thus, the properties of wettability are one of key parameters for EOR and well stimulation fluids design. Many research works have been conducted to prove altering the reservoir wettability improve oil production. Lezorgia Nekabari in his recent study [9] has proved that altering wettability with nanoparticles for EOR on limestone reservoir improve oil recovery. It has also been reported in few technical papers on microemulsion fluids that changing the wettability of damage media present in near wellbore from oil wet to water wet improve the remediation of the near wellbore damage [64],[65],[66]. However, to the best of our knowledge, there are no studies reported on the effect of ultrasonic on the wettability propensities of the nanofluids and its correlation to the changes of size, structural and critical micellar concentration (CMC) yet to be discovered.

2.5.3 Particle size and Structure of Micellar

It was discovered after 40 years of early discovery of micelles in 1913 that viscoelasticity was observed at low micelle concentration by incorporating additive such as benzoic acid [48].This behaviour leads to manipulation of surfactant and additive formulation for preferred micelle structural changes under external induction of energy such as ultrasonic or pulsating device. Micelles are known to form various nanostructures due to the molecular rearrangement between different micelle structures based on the area occupied by the hydrophilic and hydrophobic groups of surfactants [67] and from external stimuli [48]. The ratio of the hydrophobic group area to the hydrophilic head area referred as surfactant packing parameter determined the shape and the size of the micellar aggregate [34],[54]. Fig.2.8 describes some of the micellar structure as function of surfactant packing parameter.

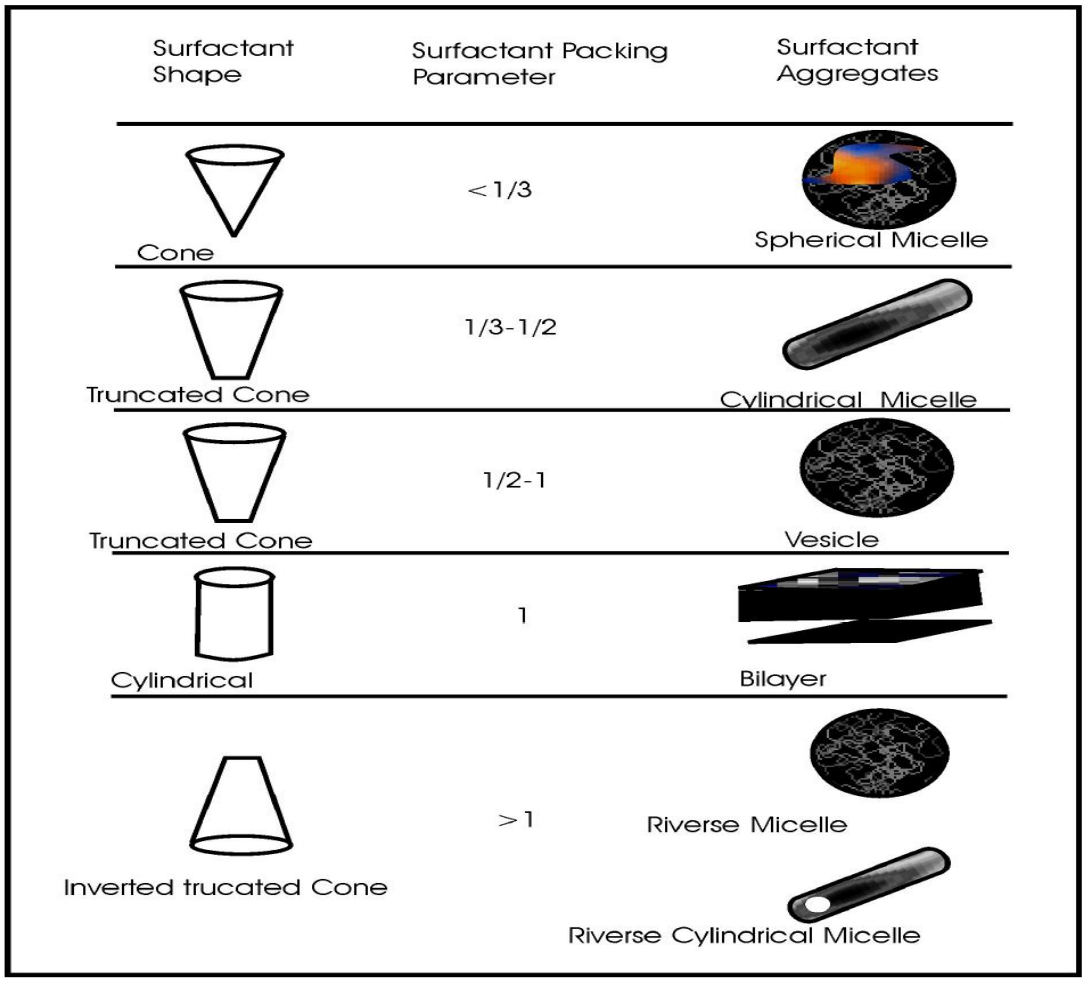

Figure 2.8: Micellar structure as function of surfactant packing parameter and shape [67]**.**

Nor Saadah and Muthupandian in their publication has reported that wormlike micelles, threadlike micelles and tubular micelles ranging from 2nm to 30 nm can be generated with ultrasound induction [45]. They have noted that by transforming the micelles structure, the nanofluids temperature stability can be extended without using additional hazardous chemicals and expensive processes. This will benefit the oil and gas industry to extend the nanofluids applications for higher temperature conditions [48],[68].

In this research, we intend to understand the effect of ultrasound to control micellar structures and size by varying the ultrasonic amplitude under both isothermal and non-isothermal condition to study the effect of such structure shift on nanofluids physio-chemical properties and their correlation to interface mass transfer mechanism during the near wellbore stimulation or remediation process.

2.5.4 Critical Micellar Concentration

Critical micelle concentration (CMC) is an important characteristic of surfactant in colloidal and surface chemistry. It is defined as the concentration of surfactants at which the molecules form micelles [67]. It indicates the point at which a monolayer absorption is complete, and the surface-active properties are at peak. The concentrations of monomers above CMC are nearly constant. As a result, there are no significant changes in the surfactant properties of the solution [67]. Critical micelle concentration of a surfactant is a function of temperature, pressure and presence of co-surfactant and electrolytes. Micelles only form above critical micelle temperature referred as Krafft temperature. The CMC concept was explored by Lindman in 1980 [67] and reported that there is an abrupt change in physio-chemical properties at a particular concentration of a surfactant system. There are several methods to determine CMC as reported by Mukherjee in 1971 varying in reliability and accuracy. The most common physical methods are measuring viscosity, conductivity, solubility, surface tension and light scattering.

2.5.5 Solubility and Dissolution

Solubility and dissolution are different concept, but they are interrelated. Solubility is a chemical property used to describe or quantify the ability for a given substance that may be dissolved in another [69]. However, it is not the same as the ability of a substance to dissolve another due to a chemical reaction. It is the maximum amount of solute that may be dissolved in solution at equilibrium, which produces a saturated solution [70]. Miscibility term is used when substances can dissolve in all proportions in a solution such as ethanol in water. Under certain conditions, additional solute may be dissolved beyond the equilibrium solubility point resulting in a supersaturated solution which is metastable [70]. This special condition holds for nanoemulsion where we could engineer the fluids for extending the solubility beyond its equilibrium. Solubility is expressed as unit of concentration include molarity, molality, mass per volume, mole ratio, mole fraction, and so on. The process of dissolving is termed as dissolution which can be expressed with Noyes–Whitney equation [71]. These properties play a key role in our review to understand phase behavior and transport phenomena which will be covered briefly in the subsequent sections.

2.5.6 Phase Behavior

The interaction of the different molecules in a mixture causes behavior that distinctly difference from what is observed in pure fluids. It is represented in phase diagram that describe the volumetric behavior of mixtures referred as phase behavior. The phase behavior is very important in designing microemulsion fluids as reported by Lirio Quintero [65] in her published papers in oil and gas conference. Phase behavior study is needed to optimize formulation of surfactant, oil and aqueous phase in condition where nanoemulsion is prepared by phase inversion temperature method and self-emulsification method [72]. The phase characterization is performed to determine the phase of nanoemulsion and dispersibility. This is done by placing the different ingredients of nanoemulsion by varying the concentration in glass ampules and thoroughly homogenized at a certain temperature for a time until equilibrium is reached. In summary, phase behaviour is very important for formulating microemulsion as it is thermodynamically stable but kinetically unstable [38]. External disturbance can easily influence the state of the phase of microemulsion. Nanofluids produced using high energy method are less sensitive to this external disturbance, thus are kinetically stable [39].

2.6 Transport Phenomena

Mass transfer and diffusion are two important terms used to explain the concept of transport phenomena. Mass transfer is a general term, and diffusion is a form of mass transfer [73]. Mass transfer is the transport of mass from one place to another either in single phase or over phase boundaries in multiphase system [74]. Diffusion is the even distribution of solutes throughout the system. The main difference between mass transfer and diffusion is that mass transfer may or may not occur across a concentration gradient whereas diffusion occurs across a concentration gradient [75]. The rate of mass transport of a solute through any fluid over a space is governed by the molecular diffusivity or the diffusion coefficient of the solute in the fluid or solution. Adolf Fick in the 19th century introduce the simplest description of diffusion and referred it as Fick's laws, which is written as first law in a modern mathematical form.

$$N_i = -D_i \nabla c_i \tag{2.9}$$

where for species *i*;

N_i is the molar flux (mol m^{-2} s^{-1}), D_i is the diffusion coefficient (m^2 s^{-1}), ∇ is the gradient operator for two or more dimension and c_i is the concentration (mol m^{-3}). From the mass continuity equation:

$$\frac{\partial c_i}{\partial t} + \nabla . \mathrm{N}_i = 0 \tag{2.10}$$

We can derive Fick's second law directly:

$$\frac{\partial c_i}{\partial t} = - D_i \nabla^2 c_i \tag{2.11}$$

This equation is based on the following assumptions:

1. The molar flux due to diffusion is proportional to the concentration gradient.
2. The rate of change of concentration at a point in space is proportional to the second derivative of concentration with space.
3. Diffusion in unsteady state without chemical reaction.
4. D_i is a constant, which is only true for dilute solutions.

Fick's second law of diffusion is a linear equation with the dependent variable being the concentration of each chemical species where diffusion occurs independently. Hence, simplify the theoretical simulation of diffusion coefficient. Initial assumption that all diffusion coefficients of each chemical species are equal and independent of temperature, pressure, etc is often a good idea to begin with till the behavior of a system with all equal diffusion coefficients is well understood [76].

Further modification to Fick's law has been developed for concentrated solutions or fluid mixtures where multi chemical species is present in significant mass fractions. In such case the diffusion coefficient cannot be treated as a constant or composition independent as the inter-molecular dependencies become relevant. Thus, we need to relate the mass flux of one chemical species to the concentration gradients of all chemical species present for modelling the diffusion coefficient. This condition is represented as Maxwell-Stefan equation where the diffusive mass flux of each species is expressed based on the gradients of the mole or mass fractions, using multi-component diffusion coefficients D_{ij} and Ji is the flux vector of species i relative to the velocity of the mixture and c is the

total concentration of all species in a mixture where activity of a species *i* and *j* are given by its mole fraction, denoted as x_i and x_j [75],[77],[78].

$$x_i \nabla \ln a_i = \sum_{j \neq 1}^{N} \frac{C_i J_j - C_j J_i}{c^2 D_{ij}} \tag{2.12}$$

In this thesis we will be interested to study the mass transfer from an interface into a well-mixed nano solution. We assume that the amount of mass transferred is proportional to the concentration difference and the interfacial area and this can be represented as the following.

$$\begin{pmatrix}\text{rate of mass} \\ \text{transfered}\end{pmatrix} = k \begin{pmatrix}\text{interfacial} \\ \text{area}\end{pmatrix} \begin{pmatrix}\text{concentration} \\ \text{difference}\end{pmatrix} \tag{2.13}$$

The proportionality is summarized by *k*, called a mass transfer coefficient [75]. Dividing the above equation with area on both sides will yield something similar to Fick's first law.

$$N_I = k(C_{Ii} - C_I) \tag{2.14}$$

Where, N_I is the flux at the interface and C_{Ii} and C_I are the concentrations at the interface and in the bulk solution, respectively. The flux N_I includes both diffusion and convection. This describes the relation between diffusion coefficient and mass transfer coefficient at interface. The flux equation 2.13 describes that if the concentration difference is doubled, the flux will double. It also suggests that if the area is doubled, the total amount of mass transferred will double, however the flux per area will not change ie the mass transfer coefficient is a constant [75]. In this thesis our aim is to study the bulk mass transfer and diffusion mechanism at interface between the nanofluids and solid or semi-solid of the damage mechanism during the near wellbore remediation. We also aim to understand the influence of certain physio-chemical properties affecting the mass transfer kinetics that will provide an integrated structured guidance in designing enhanced nanofluids for damage remediation of various well conditions. These objectives can be achieved by conducting relevant experimental work and theoretical simulation. The next two section will review on some of the relevant work done in the past to guide the experiment and theoretical simulation works carried out for this thesis that are covered in Chapter 5 and 6 later.

2.7 Theoretical Simulation

Theoretical Simulation using computer aided modeling has recently become a major analytical tool to understand system dynamic in a wide range of disciplines including oil and gas. A substantial work in oil and gas industry problems are analysed using this formal methodology as an alternative to the traditional analytical methods that unable to provide satisfactory solution for analysing complex dynamics of a systems [79]. Many advanced reliable commercial software's have been developed for reservoir fluids flow modelling in petroleum industry. Examples are GEM, STARS and ECLIPSED that able to derive the reservoir system's dynamic characteristics and prediction that are limited in their ability with mathematical analysis [18],[80]. One example of simulation work using ECLIPSED for an alkaline surfactant polymer (ASP) flooding was presented by Farid Abadli in his thesis evaluating the effectiveness of various combination of surfactant, polymer and alkaline flooding [81]. Prabir Daripa in one of his paper have presented the issues and challenges in simulation modelling for chemical enhance oil recovery using commercial software STARS [82]. Jocelyn Veilleux in his research work has conducted mass diffusivity numerical modelling to understand the hydrodynamics of mass diffusion enhancement in nanofluids designed with Al2O3 nanoparticles and deionized water and how the solute buoyancy effect the process. He reported that nanofluids has 10-fold incremental in mass diffusion compared to its base [83].

Hence, theoretical simulation has been used extensively in the oil and gas industry to analyse many engineering issues. However, to best of our knowledge there has been no theoretical simulation work conducted to optimize interface mass transfer kinetics between the well stimulation fluids and the near wellbore damage media under the effect of external perturbation such as ultrasound.

2.8 Experimental Work

Experimental work is an integral scope of any research to investigate and validate the results from theoretical simulation. In some scenario, we need to conduct certain laboratory work prior to theoretical simulation to provide the input value for computer aided simulation when the required data is not available in literature or to validate the mathematical model. Experimental research in the area of enhance oil recovery and well stimulation using nano particles has been published widely [6], [9]. Most of the findings iterated that significant improvement of oil recovery observed during core flooding

experiment [9],[27]. Engineers also demonstrated by experiment that ultrasonic tool used in down hole could improve the oil production [16],[84] by altering reservoir properties. Many fluids formulation experimental works have been conducted by researchers especially on microemulsion and its application for near well remediation [33],[66]. However, these are limited to study on asphaltene dissolution rate, acid reaction rate on carbonates, oil solubility, detergency, wettability, interfacial tension, fluids compatibility and mud filter cake clean-up tests [66],[85],[86] as part of the fluids design process. These studies were depending on chemicals to modify the fluids physio-chemical properties. Chemically modified treatment has limitation on the kinetics that involve during near well remediation. This study will combine the effect of chemical and external perturbation such as ultrasound to modify the nanofluids physio-chemical properties to extend the limitation. To the best of our knowledge, no experimental work ever been carried to establish the correlation between the external perturbation such as ultrasonic variables, nanofluids physio-chemical properties and the mass transfer kinetics during near wellbore remediation as an integrated approach. We will conduct relevant experimental work to establish these correlations to complete the thesis objective of developing a structured guideline for nanofluids design for an effective near wellbore remediation treatment.

2.9 Chapter Summary

In summary, the detail literature review of all the key areas enabled us to identify what has been done in the respective area in the pass and what are the gaps for us to spell out the research objectives and the significance of this research. The broad area of literature review enables us to connect the studies done and how this study will be able to add value to bridge the knowledge gaps. Those gaps are summarized in bullet points as below.

1) Lack of protocol for nano fluids production and field implementation for oil well remediation.
2) Effect of Near well bore remediation in EOR process has not been studied.
3) Lack of studies on ultrasonic amplitude variation effect on physio-chemical properties of remediation fluids and how it affects the mass transfer kinetics.
4) Past relevant studies are scattered without interconnection.
5) There is no theoretical simulation study done on near wellbore remediation mass transfer kinetics and its correlation to ultrasonic amplitude variations.

Thus, in this thesis we will address these gaps by carrying out the scope of the studies briefly outline in section 1.5 earlier. The detail of the scope of the studies are covered in chapter 3, chapter 4 , Chapter 5 and Chapter 6.

CHAPTER 3 Nanofluid Preparation and Optimisation

3.1 Introduction

Nanofluids are new type of fluids often referred as “smart fluids” that are created by addition of nanoparticles to fluids by means of dispersion. Some of the most challenging aspect in achieving the desired properties and structures of nanofluids for well remediation are uniform dispersion, stable suspension, and optimum formulation. In this chapter we will address these issues using a new methodology of synthesising nanofluids by combining the use of Chemical Solution Method (CSM) of surface functionalization using non-ionic surfactant and mechanical dispersion method (ultrasonication). This method able to provide stable and uniform generation of particles structures of the nanofluids [42]. The phase behaviour method then will be used to optimise the nanofluid formulation. This chapter will cover the experimental procedures and methods adopted to investigate the nanofluid preparation and optimisation protocol. The following are the experiments outlined.

1. Nanofluids preparation
2. Nanofluid formulation optimisation

3.2 Nano Fluids Preparation

Ultrasound sonication of a liquid medium is known to generate acoustic cavitation which is the growth of existing bubble nuclei, followed by the violent implosion of these microbubbles. Extreme thermal conditions and strong physical forces are generated upon bubble implosion. Stimuli-responsive micelles are known to form nanostructures that have scientific importance in biomedical and industrial applications with their ability to flexibly reform over external stimuli such as ultrasonic. Such transformation of surfactant in aqueous solution to micelle structure is shown in Fig. 3.1 [45]. This procedure produces sufficiently well dispersed, homogenised, and stable nano fluids.

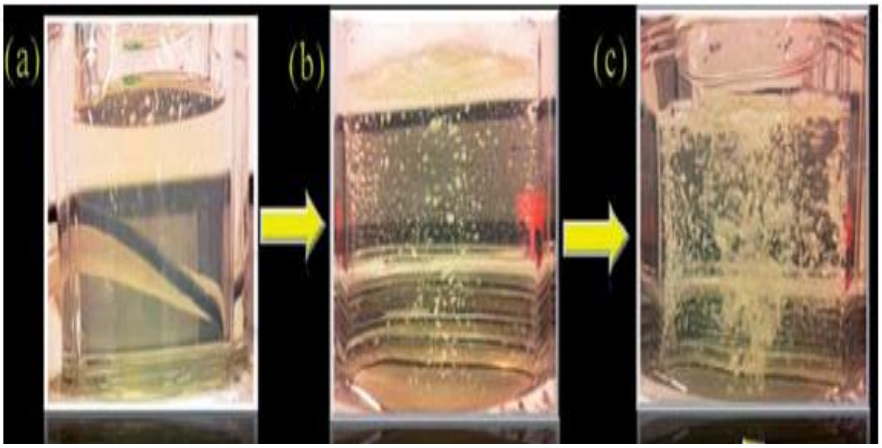

Figure 3.1: Experimental images for sonication of CTAB/NaSal: the images of an aqueous micelle solution: (a) before sonication, (b) instantly after sonication starts, (c) 5 minutes after sonication [45].

Nano emulsion formulations for near well remediation need to have high oil solubilization and ultra-low interfacial tension, which typically achieved with relatively high concentration of surfactants. Efficient single phase nano emulsion systems with lower surfactant concentrations are desired to optimize the cost of nano emulsion technology for near well remediation. The reduction of surfactant concentration and cost could be achieved by introducing linker additives in the formulations. The addition of linker molecules enhances the solubilization property of nano emulsions, which increases the hydrophilicity and/or the lipophilicity behavior of surfactants. Previous research studies prove that addition of a proper linker molecule could significantly increase the solubilization of the oil. The lipophilic linker molecules such as long chain amines, acids, alcohols and phenols increase the interactions between the surfactant and oil, although with some disorder to avoid formation of highly organized structures and to decrease the viscosity [87].

The section below details the materials, equipment and procedures used to prepare the nanofluids.

3.2.1 Materials

The following materials are used to investigate the nanofluid preparation.

a) Alkyl Poly Glucoside (APG) TRITON CG-425 non-ionic surfactant sourced from Dow Chemical Company

b) Organic acetic acid sourced from Sigma Aldrich.

c) Sodium Chloride (NaCl) salt sourced from NexusChem Engineering

d) N-Butanol solvent sourced from Thermo Fisher

e) Deionized water

3.2.2 Equipment

The following equipment are used to investigate the nanofluid preparation

a) VCX 500 lab scale ultrasonic liquid processor with a titanium alloy micro tip of 13 mm diameter

b) Magnetic Stirrer with 220V/50 Hz.

c) 500 ml Beakar

d) 10 ml cylinder

e) 3 ml pipet

f) Digital weighing balance

3.2.3 Procedures

Nanofluids were prepared by the following procedures and the experiment set up is illustrated in Fig. 3.2.

1) Base fluid was prepared in quantities of 350 ml at laboratory scale by directly mixing 1.0 % of non-ionic surfactant, 2.5% N-Butanol, 1.5% organic acid by volume, 5% sodium choride salt by weight and +/-328 ml deionised water under magnetic stirrer. The volume of 350 ml was used based on American Petroleum Institute standard for one barrel volume equivalent to laboratory scale . The nanofluids are then generated by placing the mixture under ultrasonic treatment at 0 % amplitude with fixed frequency of 20 KHz and 500 watts power input for a duration of 30 minutes at 25^0C room temperature. The controlled sample was observed for stability for a minimum period of 24 hours. The fixed 20kh frequency was chosen as its in the sonic range and based on the reference, ultrasonic device for fluids homegenizing and particle dispersion , its best to operate at low frequenzy and high power set up [88],[89].

2) The procedure above were repeated to prepare various formulation of laboratory scale nanofluids with variable concentration of surfactants (TRITON CG-425) starting from 1.5 % by volume to maximum of 20% and fixed NaCl salt concentration of 5 % by wt, 2.5% by volume of N-butanol ,1.5% by volume of acetic acid [87],[90],[91],[92] as per table 3.1 based on common oil field service companies labroratory formulations and works that been applied in the industry.

Figure 3.2: Picture of Nanofluids Preparation in laboratory (Image taken from SONICS & MATERIALS; INC ultrasonic VCX-500 liquid processor manual)

Table 3.1: Various formulation of nanofluids with changes in surfactant concentration and fixed other additives concentration

Variable surfactant concentration (APG Surfactant % vol/vol)	**Fixed concentration of additive**
1.0	Sodium Chloride 5 % by weight N- Butanol 2.5 % by volume Acetic acid 1.5% by volume
1.5	
2.5	
5	
10	
15	
20	

3.3 Nano Fluids Formulation Optimisation

The Critical Micellar Concentration (CMC) for alkyl polyglucoside (APG) Triton CG-425 surfactant was determined from literature to be 61 ppm and was used as the guiding minimum concentration to generate the desired base nanostructures [45],[90],[91],[92]. Formulation of an optimum nanofluids for near well remediation requires good understanding of phase behaviour of its brine-surfactant(s)-oil systems and their properties after the effect of oil solubilization into nano fluids, producing nano emulsion of a single phase. Nano emulsion are fluids containing oil and water stabilized by an amphiphile that contains both hydrophobic and hydrophilic parts in its molecular structure such as surfactant and co-surfactant. Nano emulsion has unique properties such as kinetically stable, ultra-low interfacial tension, large interfacial area, and capacity to solubilize both aqueous and oil soluble compounds. The phase behaviour technique was used to achieve the optimal nanofluids formulation using four component mixture studies to determine the formation of single-phase oil in water nano emulsion in excess water system often referred as Winsor type IV. The concept of ratio of interaction energies (R) between the surfactant, oil and water which determine the convexity of the interface and the resulting phase behavior, the formation of single phase, two phase or three phase emulsion or bicontinuous emulsion was introduced by Winsor in 1968 and represented in equation below [87].

$$R = (A_{SO} - A_{OO} - A_{TT}) / (A_{SW} - A_{WW} - A_{HH}) \quad (3.1)$$

The term A_{SO} represents the interaction energy between the surfactant and the oil. A_{SW} is the interaction energy between the surfactant and the aqueous phase, A_{OO} is the interaction energy between oil molecules, A_{WW} is the interaction energy between water molecules, A_{TT} is the interaction energy between the tails of the surfactant molecules, and A_{HH} is the interaction energy between the surfactant heads [87]. An example of Winsor phase behavior of a brine-surfactant-oil system with the ratio of interactions changes from R<1 to R>1 when a variable such as salinity is systematically changed is shown in Fig. 3.3.

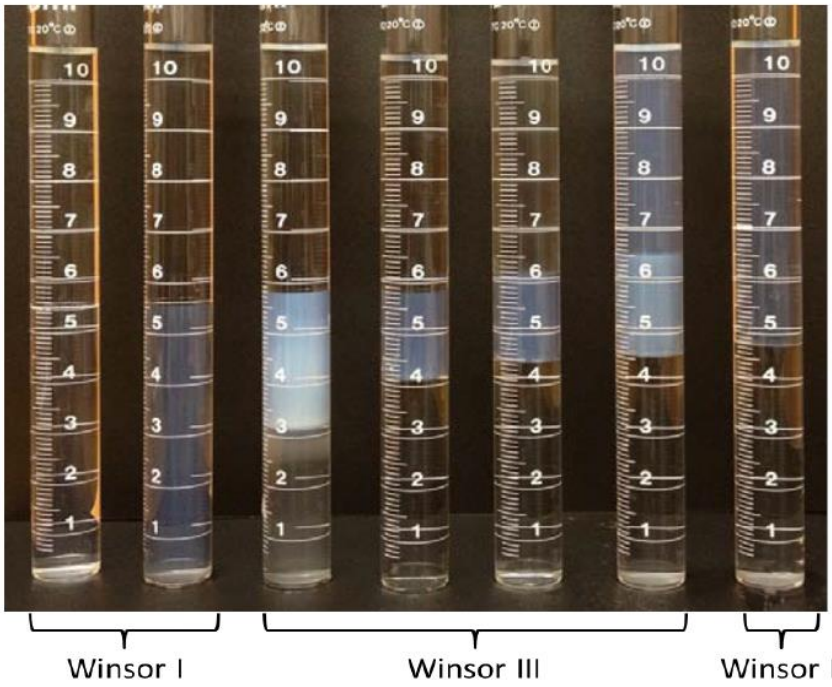

Figure 3.3: Phase behavior obtained by varying salinity in a water-surfactant-oil system [87].

In this research, different formulation with varied surfactant concentrations and fixed concentration of the other three compounds were carried out to obtain the desired single phase. A three-phase triangle in the pseudo quaternary system brine-oil-surfactant-alcohol phase behavior diagram, Fig 3.4 is adopted to achieve the desired formulation.

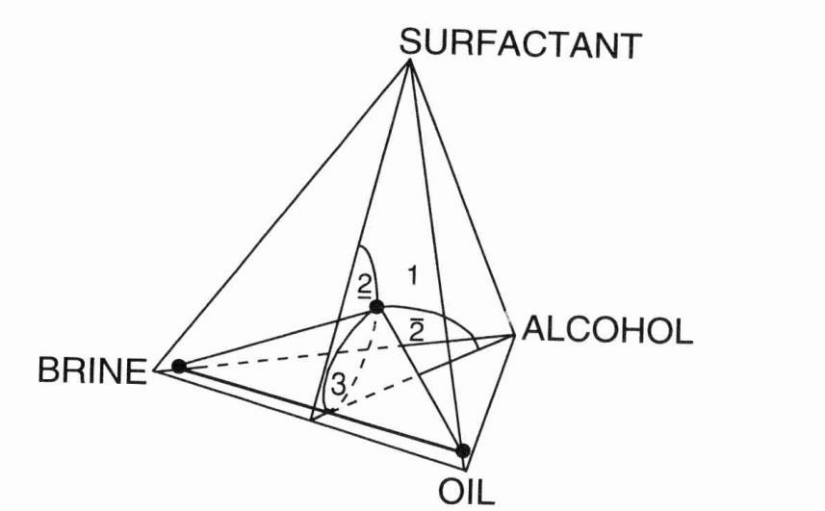

Figure 3.4: Schematic representation of a three-phase triangle in the pseudo quaternary system brine-oil-surfactant-alcohol [93].

The section below detailed out materials, equipment's and procedure used to optimize nano fluids formulation.

3.3.1 Materials and Equipment

The following materials and equipment are used for nanofluid formulation optimization

a) Nanofluids sample with various APG surfactant concentration

b) 50 ml Vial Tube

c) Kerosene Mineral Oil

3.3.2 Procedures

The following procedures are used for nanofluid formulation optimization

1) The phase behavior of water-surfactant-oil systems is typically studied by preparing a series of vials in which only one variable, the concentration of surfactant is progressively changed. The concentrations of brine (salt and water), oil and alcohol were fixed as per the table 3.2. This will allow us to determine the optimum surfactant concentration that will provide the desired single phase.

2) The Vial tubes are checked for cleanliness and scratch. Only new or clean vial to be used.

3) 2.5 ml of kerosene mineral oil were added to each 42.5ml of nanofluids produced from different concentration of surfactant (APG) into the 45ml vial tubes as per the table 3.2. and the mixtures were left overnight, 24 hours for phase changes observation at 25 ^{0}C room temperature as per the industry laboratory practice.

4) The formation of each phase was observed, and photographs were taken.

Table 3.2 : Phase behavior test series with various surfactant concentration and fixed concentration of other components.

Variable surfactant concentration (APG Surfactant % vol/vol)	Fixed concentration of additive	Fixed concentration of oil to study the type of phase formation
1.0	Sodium Chloride 5 % by weight N- Butanol 2.5 % by volume Acetic acid 1.5% by volume	Kerosene oil 5% by volume
1.5		
2.5		
5		
10		
15		
20		

3.4 Observation and Remarks

Preliminary basic comparison on the effect of ultrasonication on the colloidal dispersion of surfactant, co-surfactant, salt, and water nanofluids system was measured based on qualitative fluids turbidity. Turbidity is the measure of relative clarity or cloudiness of a liquid. It is an optical characteristic of liquid and is a measurement of the amount of light that is scattered by particle in the liquid when a light is shined through the liquid sample. The turbidity of the mixture was observed and compared on both the sample before sonication and after sonication as shown in Fig. 3.5. The sample before sonication has higher turbidity compared to the sample after sonication supporting the theory that ultrasound induction provides well dispersed, uniform, and stable nanofluids. The sonicated nanofluids stayed in homogeneous phase for more than 24 hours. Unlike the non-treated nanofluid has slight cloudy phase separation after 24 hours.

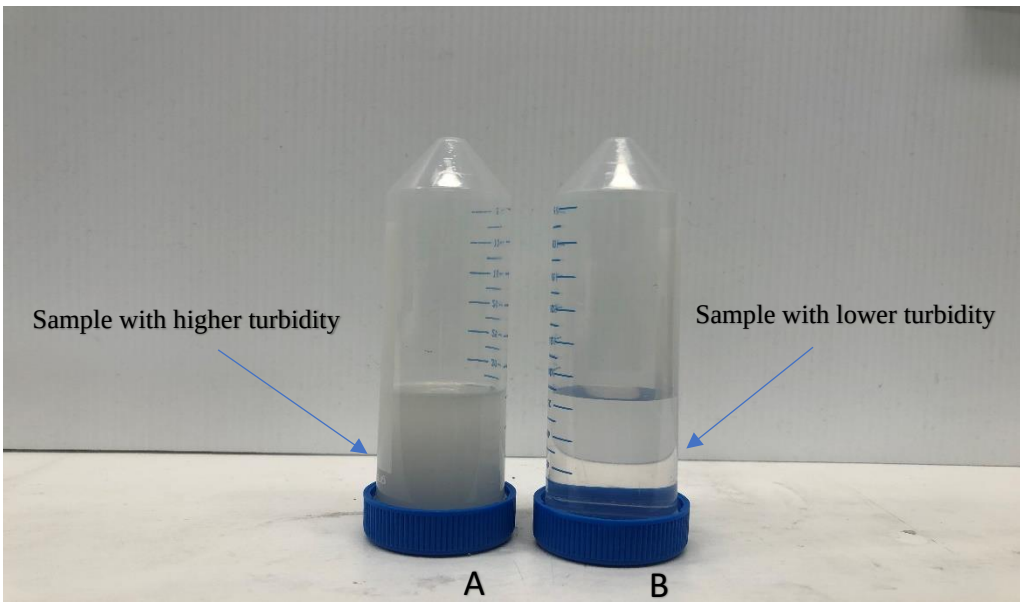

Figure 3.5: Sample A before sonication and Sample B after ultrasound induction.

The phase behavior studies were performed under specific conditions of surfactant concentrations, alcohol, salinity, oil/water ratio and temperature [87]. Each data point in the ternary phase behavior diagram represents a test tube under unique conditions at the specified 25 ^{0}C room temperature. The test tubes contain different surfactant concentrations; however, the salinity, oil/water ratio and alcohol remain constant. The test tubes were prepared, mixed, and placed at the specified room temperature until they reached equilibrium for 24 hours period. The actual number of components for the system that formulated in this research work are five; oil, brine (salt and water), non-ionic surfactant, cosurfactant (alcohol) and acetic acid. Complete phase diagrams would be multidimensional and hard to draw or describe. Therefore, its common to reduce the number of components by combining water and salt, alcohol, and acetic acid into one quasi-component, brine and alcohol [93] as described earlier in Fig. 3.3. The results of the phase behavior of these tests are represented in Fig. 3.6 and summarised in table 3.3. At low surfactant concentrations 1 and 1.5 %, two phase 0/W nano emulsions are found in equilibrium with excess water. Upon further increase the surfactant concentration between 2.5 to 5 %, one phase nano emulsion O/W are found in equilibrium with excess water. At higher concentration of surfactant between at 10% concentration the O/W nano emulsion shift to two phase. Further increase in surfactant concentration between 15 to 20%, three phase in equilibrium (oil+ nano emulsion + water) are formed as described schematically in Fig. 3.7 where o represents oil phase, o/w represents oil in water phase, w represents water phase and n represents nano emulsion phase.

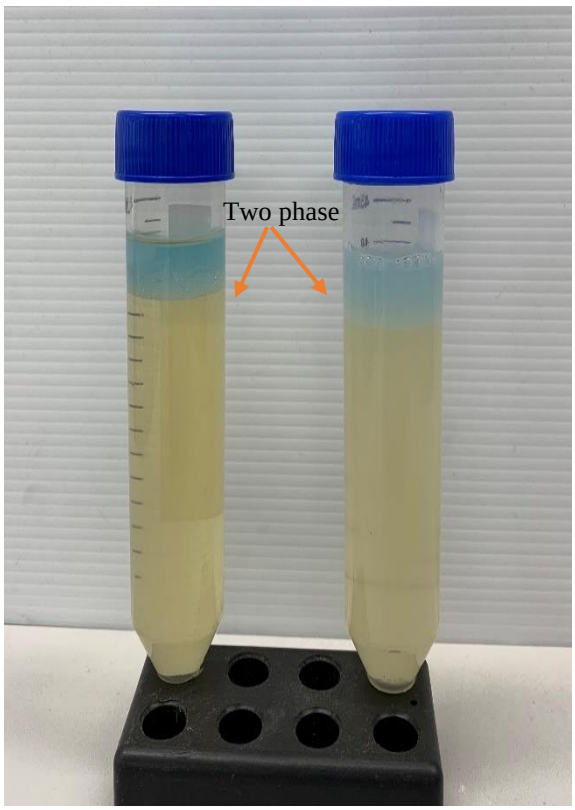

A) 1.0% and 1.5% formed two phase

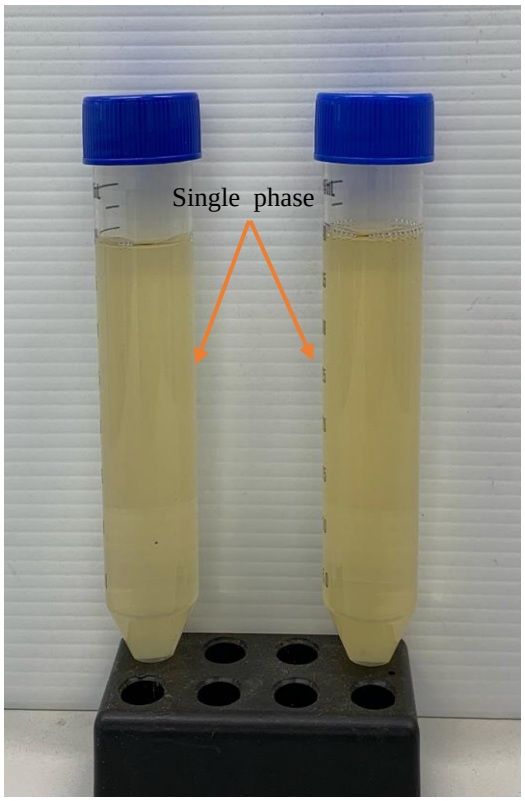

B) 2.5% and 5% formed single phase

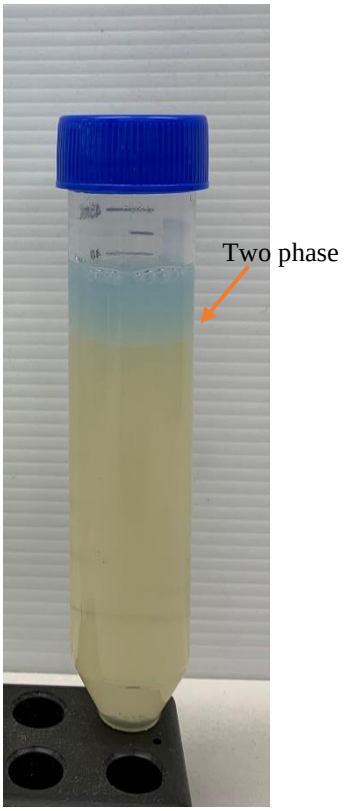

C) 10% formed two phase

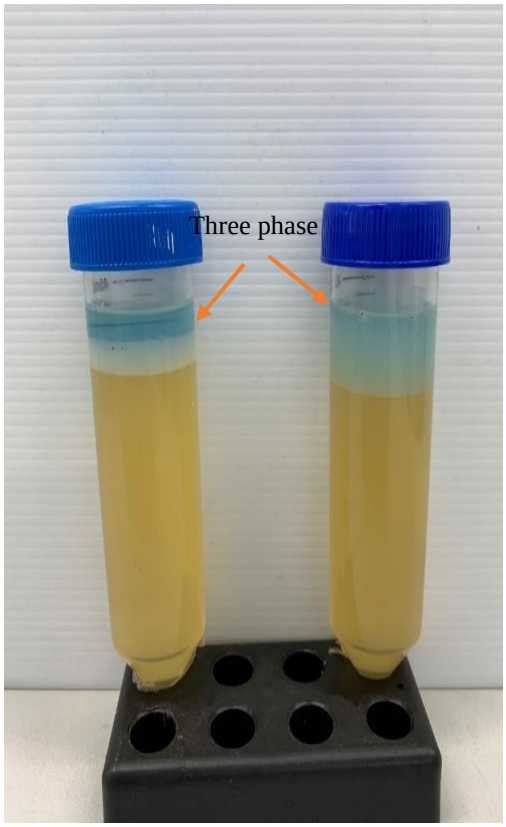

D) 15% and 20% formed three phase

Figure 3.6 : A) images of samples formed two phase emulsion, B) images of samples formed single phase nano emulsion, C) image of two phase emulsion, D) images of samples formed three phase emulsion.

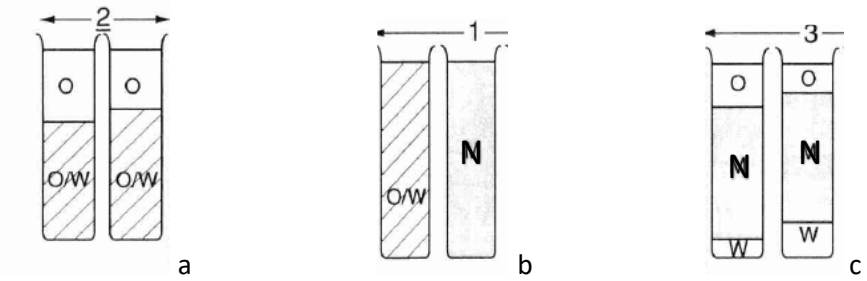

Figure 3.7 : a) two phase , b) single phase , c) three phase state of nanofluids [93].

Table 3.3 : Result of phase behavior test for the various surfactant concentration and other variables as constant.

APG Surfactant % vol/vol	N-Butanol % vol/vol	Acetic Acid % vol/vol	Nacl % wt/wt	Emulsion Phase
1.0	2.5	1.5	5	two
1.5	2.5	1.5	5	two
2.5	2.5	1.5	5	single
5	2.5	1.5	5	single
10	2.5	1.5	5	two
15	2.5	1.5	5	three
20	2.5	1.5	5	three

3.5 Closure

This chapter presents an overview of the new method of nanofluids preparation for its stability and formulation optimisation for its potential application in near well remediation for mass transfer kinetics enhancement. The observation from the conducted experiments indicates that a stable nanofluids was able to be synthesised using the combination of sonication and chemical solution method. The optimum formulation of 2.5 % of surfactant provide the desired single phase nano emulsion from the results of the phase behavior experiments conducted [94], [95].

Nanofluids have displayed enormous potential, however there is a lack of experimental agreement between different researchers that hinder commercialization of nanofluids for mass application [96]. Further research is required to identify main factors influencing the mass transfer kinetics performance of the nanofluids. The detailed physio-chemical characterisation of the nanofluids under various induction parameter such as amplitude % of ultrasonication may be the key to unlock the potential and close the gap of such discrepancy. The detail nanofluids characterisation treated under various amplitude % will be carried out in the next chapter, **Chapter 4.**

CHAPTER 4 Ultrasonication and Characterisation

4.1 Introduction

It is believed that ultrasound process parameters have effects on nanofluids physio-chemical properties such as density, conductivity, pH, viscosity, particle size etc. The temperature increases as a results of wave propagation throughout the nanofluids medium from the effect of cavitation that generates thousands of implosions of bubbles. The rapid formation and collapse of bubbles leading to extreme temperature and pressure build at sub molecular level of the fluids medium, estimated around 5000 K and 1000 atm [97]. Cavitation efficiency depends on ultrasonic parameters such as frequency, intensity, and power [56]. Research works have indicated that cavitation effectiveness for manipulation of physio-chemical properties is greater at low ultrasonic frequency, high amplitude which is related to energy contents often referred as intensity, and power [97],[98]. Most of the works have been conducted by varying power and frequency of the ultrasonic treatment [56],[97]. In this thesis we will focus on ultrasonic induction on nanofluids at fixed frequency of 20 kHz and time 30 min and varying the amplitude from 0 to 100% at both isothermal and non-isothermal conditions. The 20 kHz frequency was chosen as it is the lowest frequency for ultrasonic and 30 min time was chosen as a minimum exposure required for nanofluids structural changes based on pass researcher works [97]. Various physio-chemical properties characterisation experiments will be conducted to study the effects of amplitudes at both conditions.

This chapter will cover the experimental procedures and methods adopted to complete part of the thesis scopes. The following are the experiments outlined in this chapter.

1. Nanofluids ultrasonic induction at various amplitudes for both isothermal and non-isothermal conditions
2. Nanofluids physio-chemical characterisation at various amplitude for both Isothermal and non-isothermal conditions.

The equipment's used to conduct the experiments carried out in this chapter will be explained in detail in subsequent parts of this chapter for a better understanding of methodology adopted for each of the experiment carried out.

4.2 Nanofluids Ultrasonic Induction

The section below details out the materials, equipment's and procedure used for ultrasonic induction on nanofluids. Fig. 4.1 describes the design of sonication chamber with double wall glass with inlet and out of colling and heating water system for temperature control. Fig. 4.2 details out the equipment set up to carried out the nanofluids ultrasonic induction at various amplitude under both isothermal and non- isothermal conditions. Each equipment listed below are labelled for reference in Fig.4.2.

4.2.1 Materials and Equipment

The following materials and equipment are used to investigate the nanofluids ultrasonic induction.

a) Nanofluid samples with optimized 2.5% surfactant (APG) concentration.

b) VCX 500 lab scale ultrasonic liquid processor with a titanium alloy micro tip of 13 mm diameter.

c) Digital Thermometer and probe

d) 250 ml Double walled cylindrical glass cell with embedded spiral coil connected to inlet and outlet for cooling and heating water sourced from Buchiglas.

e) Iced water bath

f) mini circulation pump

g) PVC hoses and lab fitting valves

4.2.2 Procedures

The following procedures are used to investigate the nanofluids ultrasonic induction.

1) 200 ml of optimized base nanofluids formulation sonicated at 0% amplitude was placed in double walled glass cylinder cell as described in Fig. 4.1.

2) The Sonic VCX-500 ultrasonic processor with a titanium alloy micro tip of 13 mm diameter, fixed low frequency of 20 kHZ and 500 watts was used to sonicate the

nanofluids. The probe was immersed to the centre of sample. The sample was sonicated at amplitude of 20% at fixed interval time of 30 min.

3) For the Isothermal condition, cooling water from the iced water bath was circulated to keep the sample temperature constant at 30 deg C during the sonication process as per the experimental set up shown in Fig. 4.2.

4) The sample was labelled and kept for physio-chemical properties characterization.

5) Procedure 1 to 4 were repeated for 4 more samples by varying the amplitude 40 %, 60% ,80% and 100% respectively.

6) For non-isothermal condition, procedure 1 to 5 repeated for 5 more samples with exception on procedure 3, the cooling water circulation was stopped for the temperature of the samples to rise due to sonication , and sample temperature was recorded at end of 30 min sonication process for each sample.

7) Total of eleven samples were labelled as per table 4.1, including the base sample at 0 % amplitude for physio-chemical properties characterization.

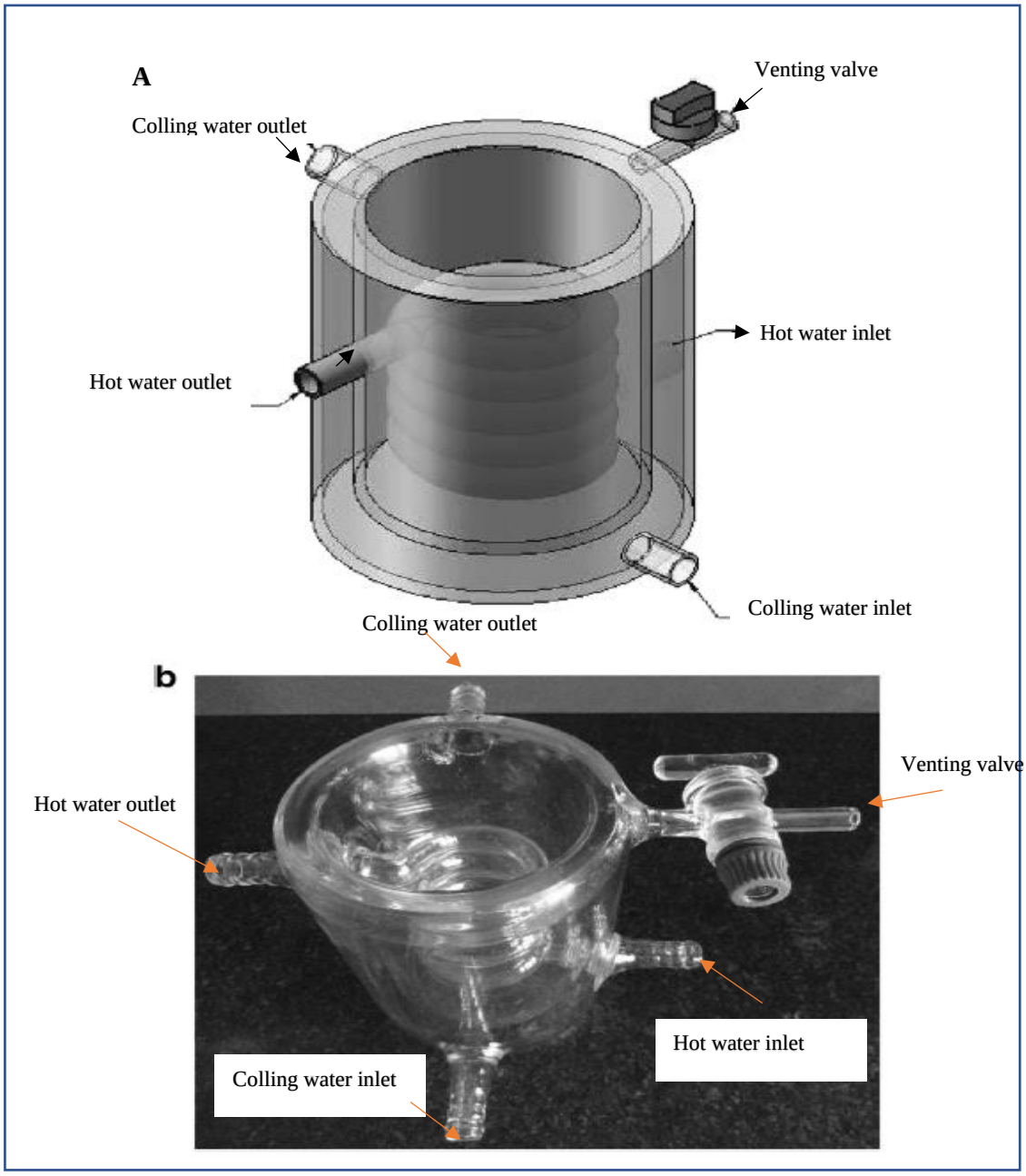

Figure 4.1: a) Illustration of a schematic and b) real design of ultrasonication chamber with cooling and heating circulation system for temperature control [99].

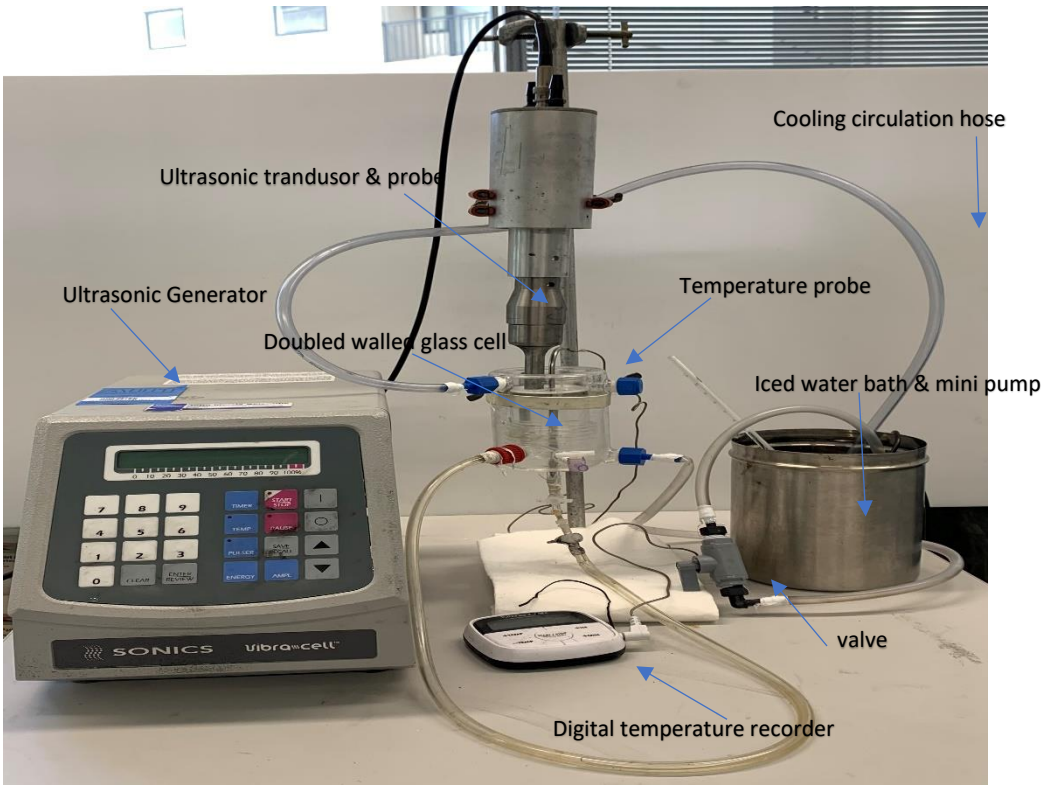

Figure 4.2: Nanofluids sonication experiment set up with cooling loops.

Table 4.1: Nanofluids samples sonicated at various amplitude% for isothermal and non-isothermal conditions

Sample Label	Amplitude %	Conditions
1	0	base
2	20	isothermal
3	40	isothermal
4	60	isothermal
5	80	isothermal
6	100	isothermal
7	20	Non-isothermal
8	40	Non-isothermal
9	60	Non-isothermal
10	80	Non-isothermal
11	100	Non-isothermal

4.3 Nanofluids physio-chemical characterisation.

This section details the different types of characterization methods and equipment used for analysing density, viscosity, surface tension, interfacial tension, contact angles, particle size, zeta potential, electrical conductivity, and morphological structure of the nanofluid samples induced with ultrasonic at various amplitude for both isothermal and non-isothermal conditions as tabulated in table 4.1. The changes in the properties were benchmarked against the base sample. Characterizations of each sample were done three times; an average reading was taken for each sample so that results should be repeatable and meet the statistical analysis requirement. Characterization techniques used here are briefly described below.

4.3.1 Density

Density of the nano fluid samples that induced with ultrasonic at various amplitude for both condition isothermal and non-Isothermal were measured using Mettler Toledo DE 40-density meter at 30 deg C room temperature. These compact density meters perfectly combine simple, easy-to-understand operation with a high level of measuring accuracy and outstanding reliability. The density meter was operated as standalone as per the user guide.

Measurement Principle

The density measurement of the DE40 is based on the electromagnetically induced oscillation of a glass U-tube. A hollow glass tube vibrates at a certain frequency. This frequency changes when the tube is filled with the sample. The higher the mass of the sample, the lower the frequency, which means the period of oscillation T increases. The frequency measurement is converted into density. A built-in Peltier thermostat controls the temperature precisely of the benchtops instrument, no water bath is required. A magnet is fixed to the measurement tube in the DE40 which is made to oscillate by a transmitter. A sensor measures the period of oscillation T as shown in Fig 4.3. The measuring principle of an oscillation-type density meter is based on the correlation between the density ρ of a fluid filled and the corresponding oscillation period T, in other words, 1 divided by frequency of oscillation f. According to the equation below, the density of a sample ρ can be calculated using the instrument constants A, B and the measured oscillation period T, (source: operation manual Mettler Toledo DE40).

$$\rho = AT^2 + B \tag{4.1}$$

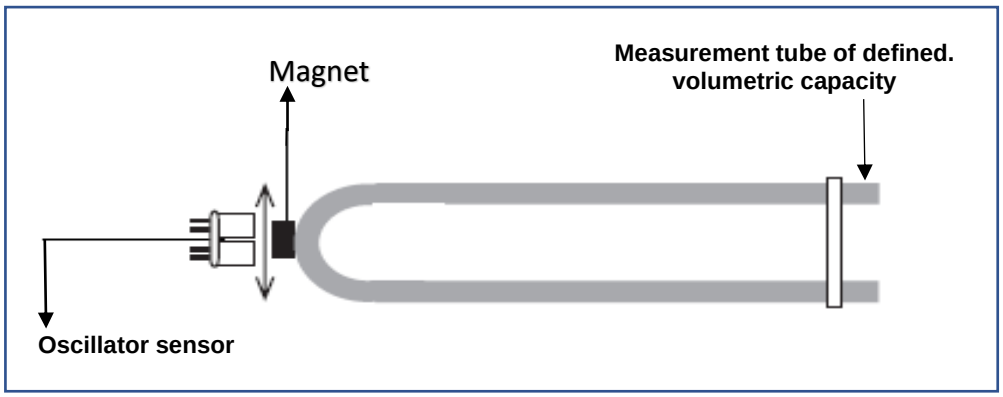

Figure 4.3: Density meter principle based on oscillation of a glass U tube.

(source:https://www.manualslib.com/manual/2028920/Mettler-Toledo-De40.html)

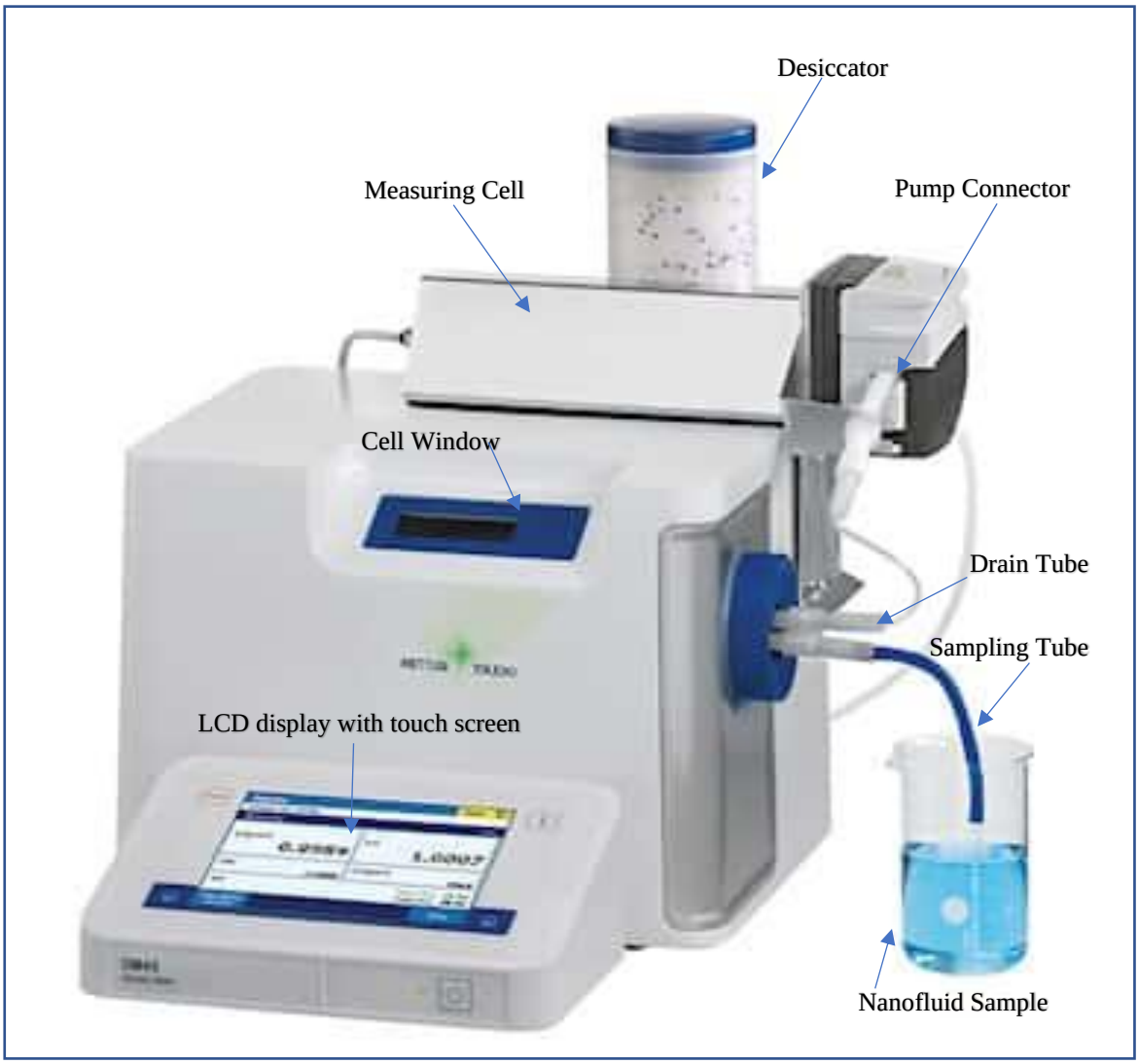

Figure 4.4: Density meter Metler Toledo DE 40.

(source:https://www.manualslib.com/manual/2028920/Mettler-Toledo-De40.html)

Procedure

1) Fill the sampling tube with approximately 3 mL of nanofluid sample by dipping the tube into sample beaker as shown in Fig 4.4. and press MEASURE key. The sampling will be completed once the measuring cell is fully filled.

2) During the sampling, watch carefully that no air bubbles enter the measuring cell.

3) Set the measuring temperature at 30 degrees Celsius and press the MEASURE key on the LCD screen as shown in Fig.4.4. Record the displayed density value.

4) Repeat the measurement for 3 readings for statistical consistency and record the average reading as final.

5) Insert the sampling tube into water to purge and clean the measuring cell.

4.3.2 pH

pH measurements were performed on the nano fluid samples that were treated with ultrasonic at various amplitude for both isothermal and non-isothermal conditions using Ohaus ST10 ph meter shown in Fig 4.5. A pH meter is a scientific instrument that measures the hydrogen-ion activity in water-based solutions, indicating its acidity or alkalinity expressed as pH [100]. The measurements were repeated for 3 readings and average readings was taken for each sample for statistical assurance.

Measurement Principle

The pH meter measures the difference in electrical potential between a pH electrode and a reference electrode, and so the pH meter is sometimes referred to as a "potentiometric pH meter". The difference in electrical potential relates to the acidity or pH of the solution. Potentiometric pH meters measure the voltage between two electrodes and display the result converted into the corresponding pH value. They comprise a simple electronic amplifier and a pair of electrodes, or alternatively a combination electrode, and some form of display calibrated in pH units. It usually has a glass electrode and a reference

electrode, or a combination electrode. The electrodes, or probes, are inserted into the solution for measuring the pH [101].

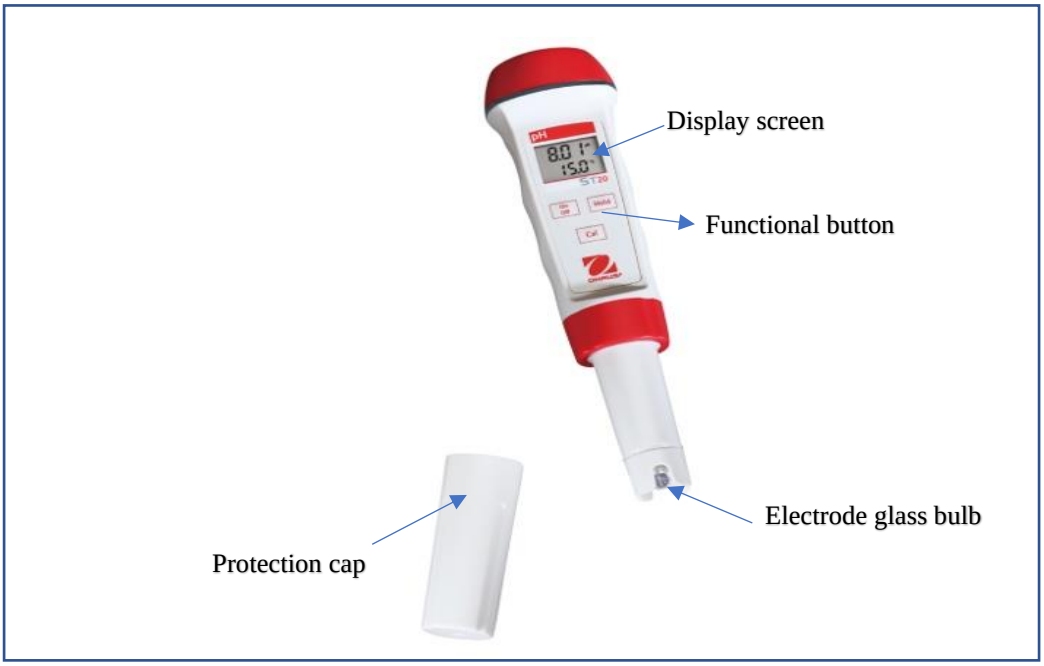

Figure 4.5: Ohaus ST 10 digital ph meter with glass electrode

Procedure

1) Remove the protection cap, rinse the pH electrode glass bulb with pure water (distilled water), and wipe clean. (Glass bulb is fragile, be careful, do not scratch it.)

2) Press button-On/Off turn on the meter and dip the electrode about 2 to 3cm into the test solution (at least 20ml).

3) Stir and wait until the reading stabilized. Clean the electrode with pure water after each measurement.

4) Repeat the measurement for 3 readings for consistency and record the average reading as final.

4.3.3 Viscosity

Viscosity of the nanofluids induced at various amplitude for both condition, isothermal and non-isothermal were measured using the digital rotary viscometer model NDJ8-S from WeighingInstru Corporation as shown in Fig.4.6. This viscometer adopts advanced mechanical design technology, manufacturing process and microcomputer control technology. This enables the data acquisition more precise with the display adopts blue LCD backlight and high brightness for clearer data display. The equipment can be used to measure liquid viscosity as low as 0.1mPas to maximum range of 2 x106 mPas. The guidelines for rotor selection for the range of viscocity tabulated in table 4.2. The measurements were carried out at 30 Degree Celsius temperature using rotor 0# as the fluids viscosity measured below 15 mPas.

Figure 4.6: Digital rotary viscometer model NDJ8-S

Table 4.2 : Viscosity range, rotor and RPM selection guide. (source: https://silo.tips/download/operation-manual-for-ndj-8s-digital-rotary-viscometer)

ROTOR TYPE	0	1	2	3	4
Velocity(RPM)		Viscosity Measurement Range (mPas)			
0.3	/	2 X10^4	10 X10^4	40 X10^4	200 X10^4
0.6	/	1 X10^4	5 X10^4	20 X10^4	100 X10^4
1.5	/	4 X10^3	2 X10^4	8 X10^4	40 X10^4
3	/	2 X10^3	1 X10^3	4 X10^4	20 X10^4
6	100	1 X10^3	5 X10^3	2 X10^4	10 X10^4
12	50	500	2.5 X10^3	1 X10^4	5 X10^4
30	20	200	1 X10^3	4 X10^3	2 X10^4
60	10	100	500	2 X10^3	1 X10^4

Measurement Principle

The viscometer model NDJ8-S uses the principle of 'rotational viscometry' [102], i.e., their measurement of sample viscosity is based upon immersing a specifically selected spindle within a sample of the fluid followed by measurement of the torque required to rotate the spindle at a set speed whilst immersed within the fluid sample. As the torque required will be proportional to the quantity of viscous drag upon the rotor, the torque moment will be measured by the sensors and processed into the viscosity and shown on the display. This therefore provides an assessment of the sample viscosity, reported in unit mPas.

Procedure

1) Prepare the liquid to be measured and put it into a glass beaker or a right-angle container with the diameter not smaller than 70 mm and the height not less than 125mm.
2) Maintain the liquid temperature at 30 degrees Celsius simulating the room temperature of laboratory at field site.

3) Adjust the lifting screw and put the rotor into the measured liquid till the level mark on the rotor reach the liquid surface and ensure the instrument is level.

4) Select the rotate speed, the instrument has eight rotate speeds: 0.3 rpm, 0.6rpm, 1.5 rpm, 3 rpm, 6 rpm,12 rpm, 30 rpm, 60 rpm and auto mode. After setting rotor and rotate speed, press OK, the rotor begins to rotate, and the instrument begins to measure automatically, search appropriate speed gradually. Finally, display the measured result.

5) Repeat the measurement for 3 readings for statistical consistency and record the average reading as final.

4.3.4 Electrical Conductivity

Electrical conductivity of the nanofluids induced at various amplitude for both conditions, isothermal and non-isothermal were measured using the digital conductivity meter, LabCHEM-C from TPS Pty Ltd as shown in Fig.4.7. This 3 in 1 meter feature an advanced yet simple user interface that does not require manuals or training to operate. LabCHEM-C meter connect three separates smart intellical electrodes for measuring electrical conductivity, total dissolved solids, and temperature. It automatically recognizes the testing parameter, calibration history, and method settings to minimise errors and setup time. The guidelines for electrode sensor selection for the conductivity measuring range is as per table 4.3.

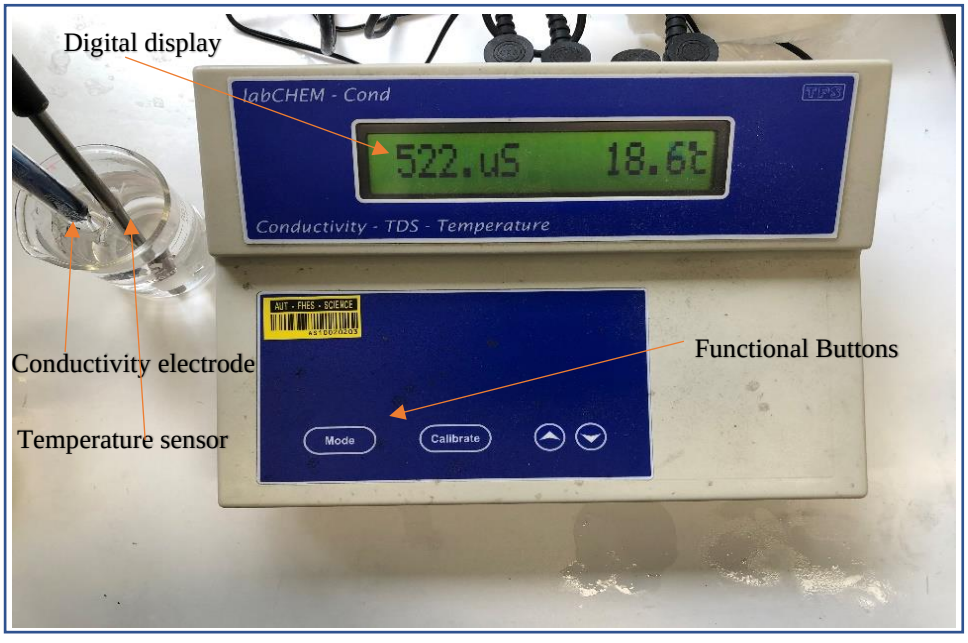

Figure 4.7: LabCHEM-C conductivity/TDS meter.

Table 4.3: Sensor selection guide and measuring range of conductivity in unit µs/cm or ms/cm (source: https://tps.com.au/assets/userfiles/files/content/handbook/lchemcv1_02.pdf)

	Ranges		Resolution	Accuracy
Conductivity	**K=0.1 sensor**			+/- 5 % of full scale of selected range at 25 deg C
	0 to 2.00	µs/cm	0.001 µs/cm	
	0 to 20.00	µs/cm	0.01 µs/cm	
	0 to 200.00	µs/cm	0.1 µs/cm	
	0 to 2000.00	µs/cm	1.0 µs/cm	
	K=1.0 sensor			
	0 to 20.00	µs/cm	0.01 µs/cm	
	0 to 200.00	µs/cm	0.1 µs/cm	
	0 to 2000.00	µs/cm	1.0 µs/cm	
	0 to 20.00	ms/cm	0.01 ms/cm	
	K=10.0 sensor			
	0 to 200.00	µs/cm	0.1 µs/cm	
	0 to 2000.00	µs/cm	1.0 µs/cm	
	0 to 20.00	ms/cm	0.01 ms/cm	
	0 to 200.00	ms/cm	0.1 ms/cm	

Measurement Principle

Conductivity is a measure of how well a solution or material conducts electricity, or in another word, ability to allow electricity to flow through the media and often measured in unit's micro or mili Siemen per cm. To carry a current, a solution must contain charged particles, or ions. Conductivity measurements are mostly made in aqueous solutions, and the ions responsible for the conductivity derived from the electrolytes dissolved in the water or aqueous solution [103]. This LabCHEM-C benchtop laboratory conductivity meters employ a potentiometric method and two electrodes sensors and contacting measurement technique. There are two types of conductivity measurement, contacting and inductive [103],[104]. The choice of which to use depends on the conductivity measurement range, the sample liquid corrosiveness, and the amount of total suspended solids. Generally, the inductive method is adopted when the conductivity is high, suspended solids are present and the liquid sample are corrosive [104],[105]. The contacting conductivity measurements are restricted to applications where the conductivity is low. Four-electrode sensors have a higher end operating range, insensitivity to interfering resistances due to long connecting cables, contaminants, or due to polarization compared to the two electrode sensors. The measuring cells of four

electrode sensors contain two pairs of electrodes. One pair measures the current, the other measures the voltage applied across the measured solution as shown in Fig. 4.8.

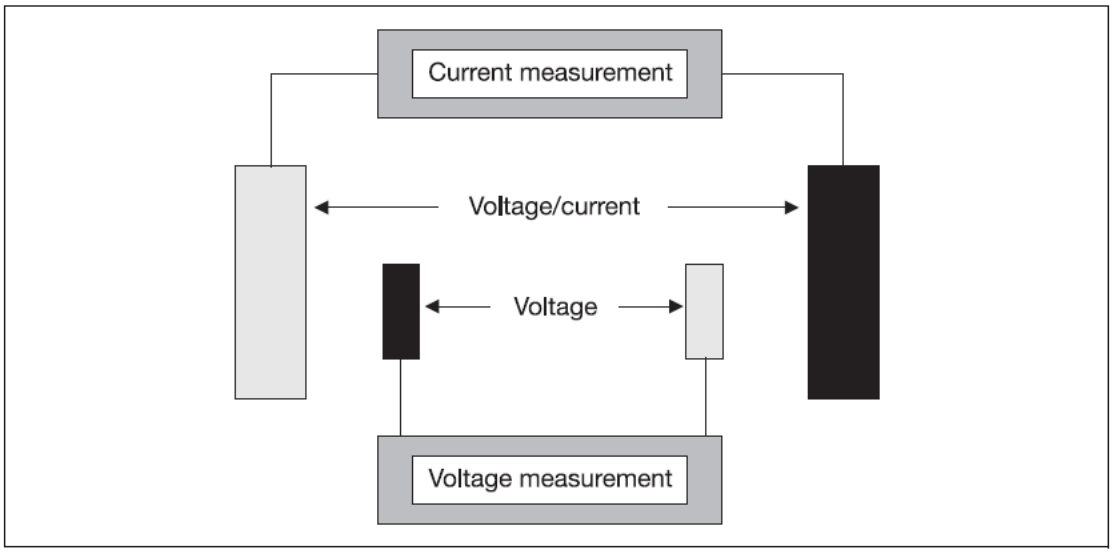

Figure 4.8: Diagram of a four-electrode sensors conductivity measuring cell (http://www.manoraz.com/_Uploads/dbsAttachedFiles/FAS624gb_Conductivity.pdf).

The two sensors electrode conductivity meters generally contains metal electrodes, usually stainless steel, or titanium in contact with electrolytes solution [103]. The model we used has platinum electrodes. The movement of ions due to the electric field generated from the analyser conduct ionic current through the solution that happens at the interface of the solution and the metal electrode as shown in Fig. 4.9.

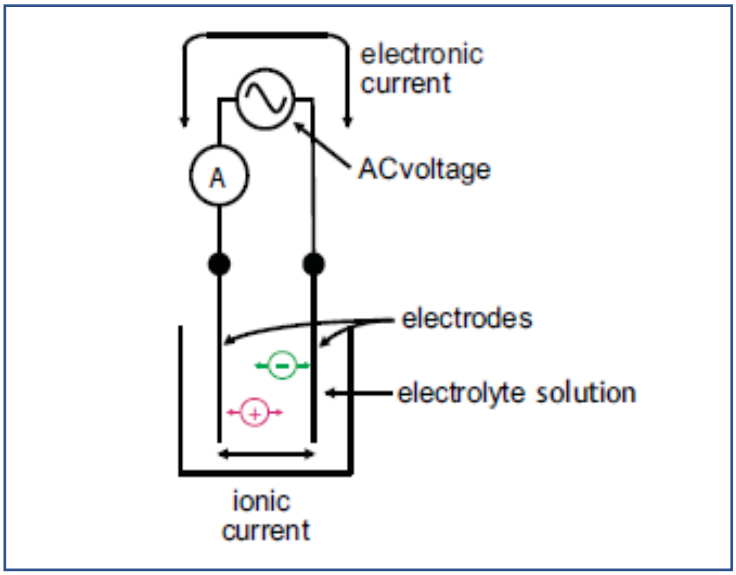

Figure 4.9: Diagram of two electrode sensors measurement of conductivity [103].

The basic principle of conductivity measurement is the same with all methods, the instrument generates an electric voltage across the measured solution. An electric current flows whose value depends on the conductivity. Depending on the method or application, the instrument either maintains the voltage signal constant and records the change in electric current or maintains the current value constant and evaluates the voltage change. Both measurement principles are based on Ohm´s law as per equation below [104]. The analyser measures the current and uses Ohm's law to calculate the resistance of the solution (resistance = voltage/current). The conductance of the solution is the reciprocal of the resistance [103].

$$R = \frac{U}{I} \tag{4.2}$$

And,

$$R = \frac{I}{G} \tag{4.3}$$

Where;
R: electrical resistance
I: electrical current
U: electrical voltage, or rearranged for the conductance
G: conductivity

Procedure

1) Rinse the electrode with de-ionized water before use to remove any impurities. Gently shake excess water droplets.

2) Dip the probe into the sample beyond the upper steel band (utilize the fill line on the outside of the probe guard for reference).

3) Allow time for the reading to stabilize. Note the reading on the display. Repeat the readings for 3 measurements for statistical assurance and take average as final.

4) Once you have completed the use of the conductivity meter, ensure you have thoroughly cleaned the electrodes by rinsing with deionized water. Place the electrode in deionised water solution.

4.3.5 Particle Size

Particle size of the nanofluids induced at various amplitude for both condition, isothermal and non-isothermal were measured using the Zetasizer Nano ZS ZEN3600 model from Malvern Instrument shown in Fig. 4.10. Particle size analysis is used to characterise the size distribution of particles in each sample. Particle size analysis can be applied to solid materials, suspensions, emulsions and even aerosols. There are many different methods employed to measure particle size. Some particle sizing methods can be used for a wide range of samples, but some can only be used for specific applications. It is quite important to select the most suitable method for different samples as different methods can produce quite different results for the same material. The Zetasizer Nano ZS series uses dynamic light scattering (DLS) technique for measuring the size and size distribution, typically in the submicron range, of molecules and particles which are dispersed, suspended, or dissolved in a liquid [14],[106].

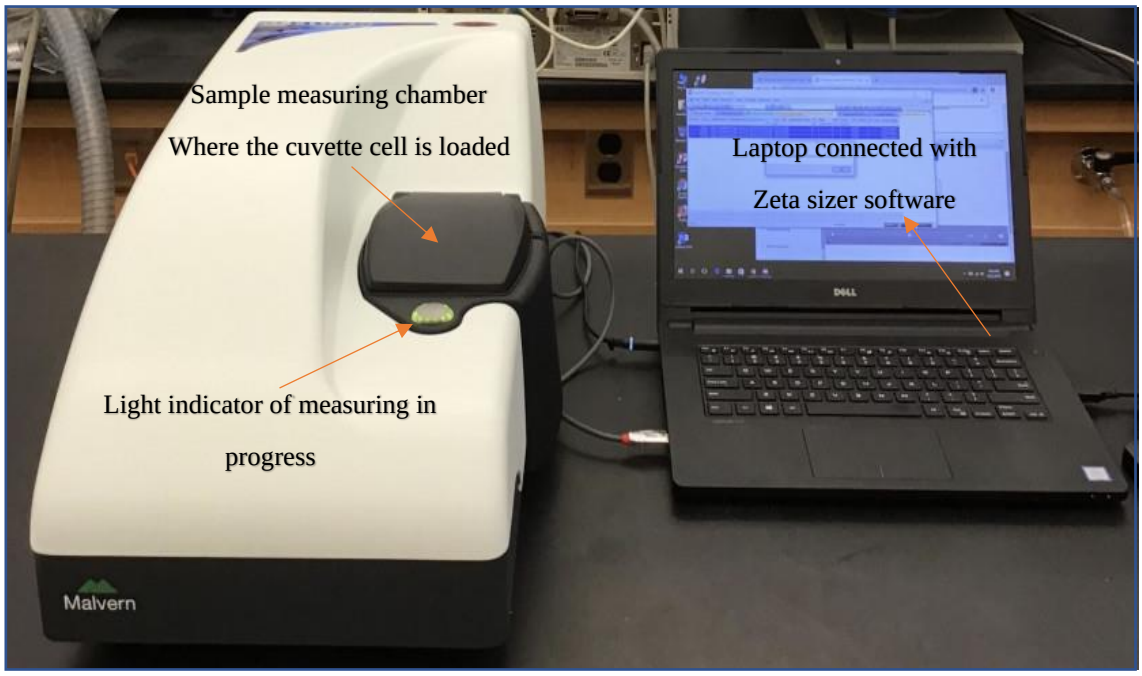

Figure 4.10: Zetasizer Nano ZS ZEN 3600 model used for nanofluids particle sizing and zeta potential measurement. (source: https://www.ursinus.edu/academics/chemistry/facilities-and-laboratories/instrument-instructions/malvern-zetasizer-nano-zs-zen-3600/)

Measurement Principle

For submicron particle measurement, dynamic light scattering (DLS) [107] has now become an industry standard technique. This method analyzes the fluctuations of scattered light by particles in suspension when illuminated with a laser to determine the velocity of the Brownian motion, which can then be used to obtain the hydrodynamic size of particles using the Stokes-Einstein relationship [108]. The basic principle is simple, the sample is illuminated by a laser beam and the fluctuations of the scattered light are detected at a known scattering angle θ by a fast photon detector as shown in Fig 4.11. From a microscopic point of view, the particles scatter the light and thereby imprint information about their motion. Analysis of the fluctuation of the scattered light thus yields information about the particles. Experimentally one characterizes intensity fluctuations by computing the intensity correlation function , whose analysis provides the diffusion coefficient of the particles (also known as diffusion constant). The diffusion coefficient D is then related to the radius R of the particles by means of the Stokes-Einstein Equation as below [108],[109].

$$D = k_{\mathrm{B}} \frac{T}{6\pi\eta R} \tag{4.3}$$

Where k_{B} is Boltzmann-constant, T is temperature and η is viscosity of the dispersant.

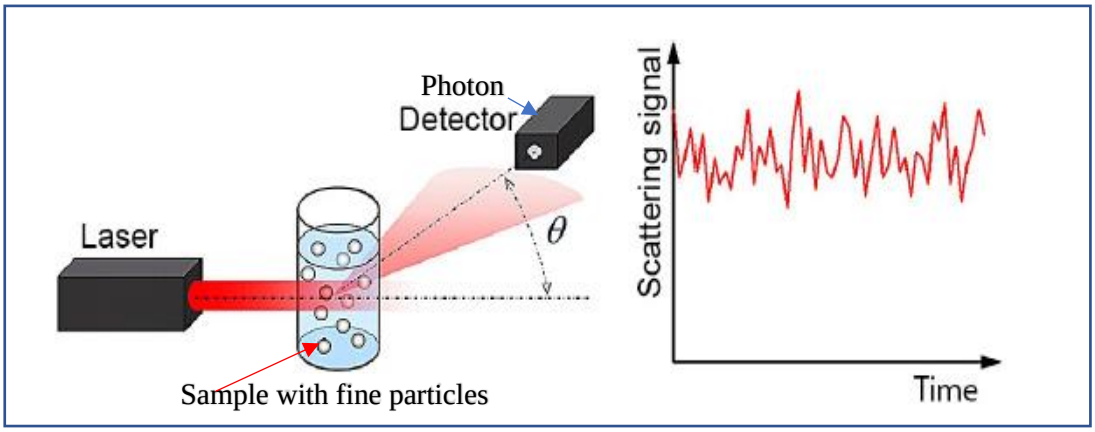

Figure 4.11: Principle of DLS: light scattered by a fine particle illuminated with a laser is measured with high time resolution under a defined angle θ; the fluctuation of the scattering signal reflects the dynamics of microstructural processes such as the particles' Brownian motion [110].

Procedure

1) Zetasizer system shown in Fig. 4.10 comprises the Zetasizer instrument and a computer with the Zetasizer software installed. A 12 mm disposable polystyrene cuvette cell is filled with the sample with 1 ml syringe and loaded into the cell area on the top of the instrument.

2) The software is used to control the measurement of the sample, there are two basic ways to make a measurement.

    - **SOP** measurements. A Standard Operating Procedure (SOP) is like a template that pre-defines all the measurement settings.
    - Manual Measurement. A manual measurement is where all the measurement parameters are set immediately before the measurement is performed.

3) Select the **SOP** measurement settings and edit the parameters appropriate for the sample being analysed.

4) The windows will show the sample is ready for measurement. Press the start button and the windows screen will display as shown in Fig 4.12 once the reading is stabilised. We will choose 3 readings setting for each sample for statistical assurance. Save the measurements into a selected file.

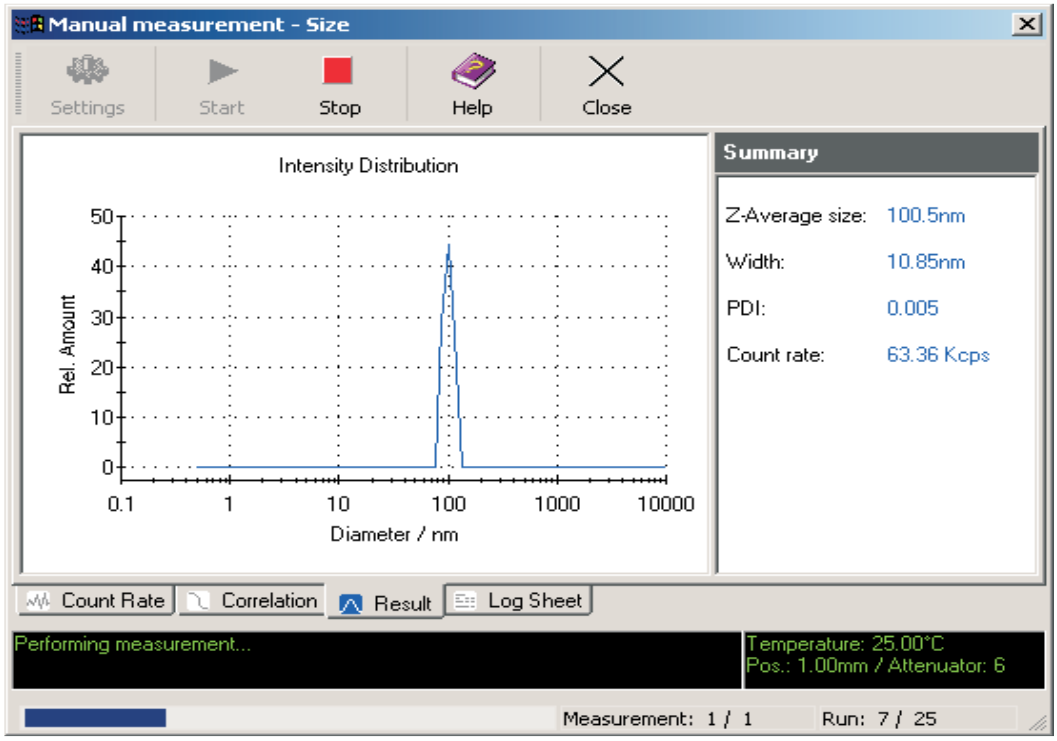

Figure 4.12: Example of particle size average measurement and display. (source: https://physics.nyu.edu/grierlab/manuals/ZetasizerNanoUserManual.pdf)

4.3.6 Zeta Potential

Zeta Potential of the nanofluids induced at various amplitude for both condition, isothermal and non-isothermal were measured using the Zetasizer Nano ZS ZEN3600 model from Malvern Instrument shown in Fig 4.10. The zeta potential is used to determine the stability of particles dispersion, suspension, or emulsion in a liquid [111]. If all the particles in suspension have a large negative or positive zeta potential, then they will tend to repel each other and there is no tendency to flocculate. However, if the particles have low zeta potential values, then there is no force to prevent the particles coming together and flocculating [112]. Particles with zeta potentials more positive than +30mV or more negative than -30mV are normally considered stable [113]. The Zetasizer Nano ZS series uses Electrophoretic Light Scattering (ELS) technique for measuring the zeta potential.

Measurement Principle

Electrophoretic Light Scattering measures the electrophoretic mobility of particles in dispersion or molecules in solution. This mobility is often converted to zeta potential. The electrophoretic mobility is obtained by performing an electrophoresis experiment on the

sample and measuring the velocity of the particles using Laser Doppler Velocimetry (LDV) [114]. The essence of a classical micro-electrophoresis system is a cell with electrodes at either end to which a potential is applied as described in Fig.4.13. Particles move towards the electrode of opposite charge, their velocity is measured and expressed in unit field strength as their mobility. When an electric field is applied across an electrolyte, charged particles suspended in the electrolyte are attracted towards the electrode of opposite charge. Viscous forces acting on the particles tend to oppose this movement. When equilibrium is reached between these two opposing forces, the particles move with constant velocity.

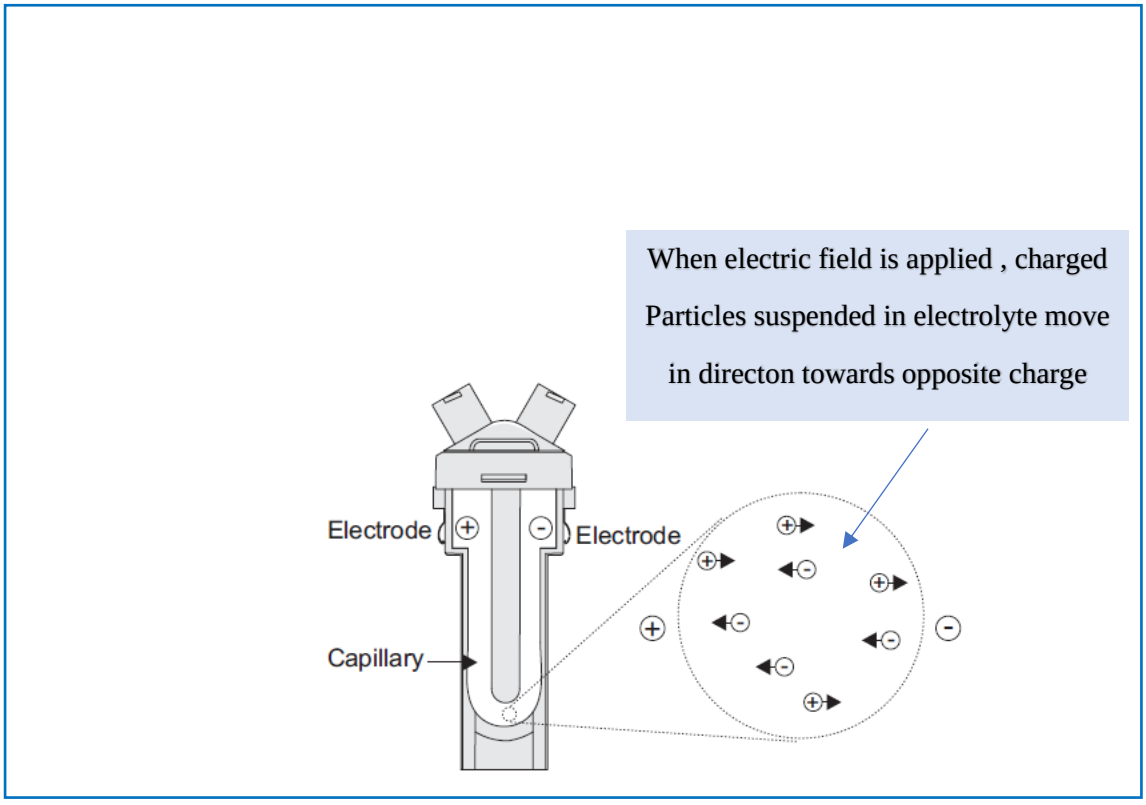

Figure 4.13: Schematic of double folded electrode cell used to measure Zeta Potential. (source: https://physics.nyu.edu/grierlab/manuals/ZetasizerNanoUserManual.pdf).

The velocity of the particle depends on the following factors:

- Strength of electric field or voltage gradient.
- The Dielectric constant of the medium.
- The Viscosity of the medium.
- The Zeta potential.

The velocity of a particle in an electric field is commonly referred to as its electrophoretic mobility. With this knowledge we can obtain the zeta potential of the particle by application of the Henry equation as below [114].

$$\mathrm{UE} = \frac{2\varepsilon Z f(ka)}{3\eta} \qquad (4.4)$$

Where;

- z : Zeta potential.
- UE : Electrophoretic mobility.
- ε :Dielectric constant.
- ɲ :Viscosity.
- $f(ka)$: Henrys function

Procedure

1) Close the lid and turn on the instrument and wait 30 minutes for the laser to stabilise.

2) Start the Zetasizer software.

3) Prepare the sample following the sample preparation guidelines.

4) Fill the double folded glass cell with the prepared sample.

5) Make an **SOP** measurement. If necessary open or create a new measurement file.

6) Select **Measure-Start SOP** from the Zetasizer software. Select the **SOP** required and select **Open** and follow any onscreen instructions that appear.

7) The Measurement display will now be shown. When requested, insert the cell into the measuring chamber of the instrument and wait for the temperature to stabilise.

8) Click **Start button**. The measurement will be made, and the results displayed and saved to the open measurement file. The settings for measurement will take 3 readings for statistical assurance and average value will be used as final.

4.3.7 Surface tension, Interfacial tension, and Contact angles.

Optical tensiometers also known as goniometers are utilized to measure surface tension, interfacial tension, and contact angles. The main components of the optical tensiometer are a camera, dispenser to dispense a drop, sample stage, and the light source to illuminate the drop on the sample stage. Optical tensiometers range from completely manual systems to fully automated instruments. The experiments were conducted using Theta Lite optical tensiometer shown in Fig. 4.14. Theta Lite comes with the OneAttension software which provides superior drop shape analysis, live measurement as well as a logic and pleasant user interface.

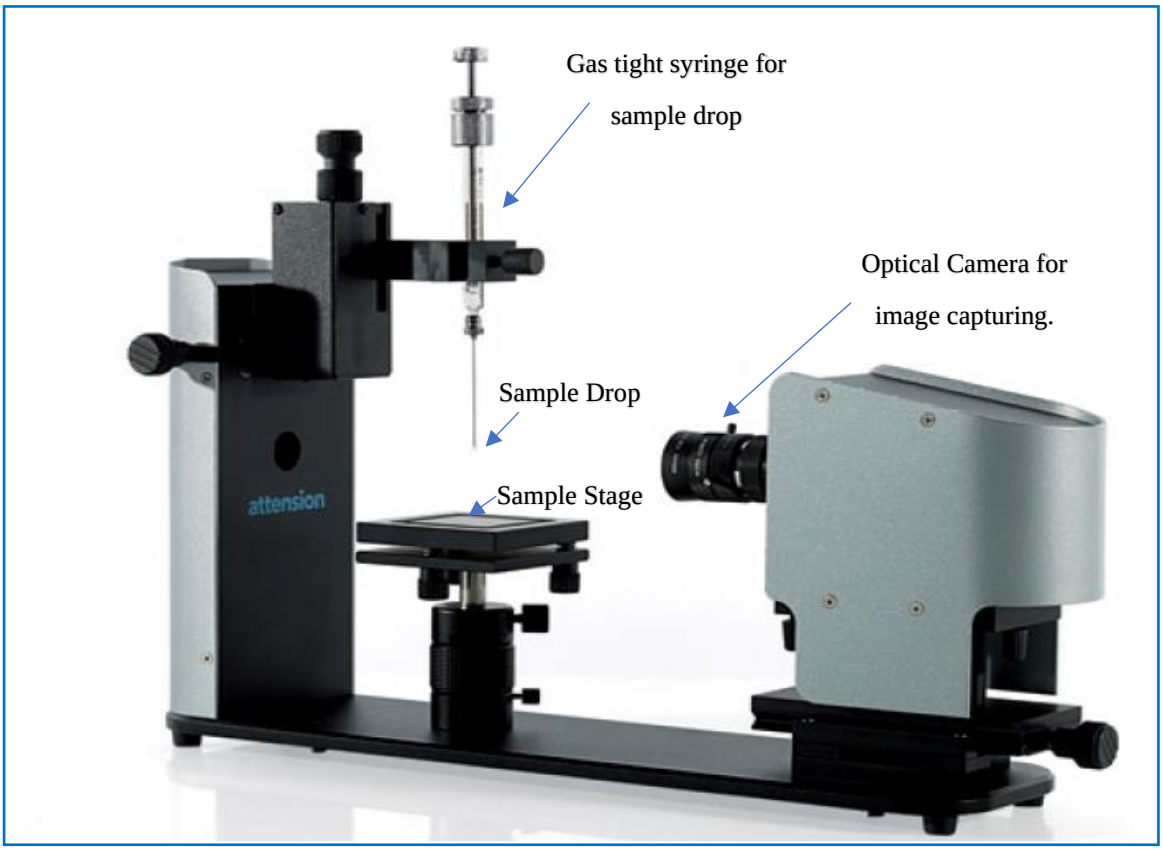

Figure 4.14: Theta Lite optical tensiometer used for measuring surface tension, interfacial tension and contact angles. (source: https://dynetesting.com/contact-angle-measurement-equipment/theta-lite-optical-tensiometer/)

Measurement Principle

Pendant drop method offers a simple and elegant solution to determining surface and interfacial tension of a liquid sample. The measurements can be performed optically using a pendant drop shape analysis. The shape of the drop hanging from a needle is determined from the balance of forces which include the surface tension of the liquid being investigated. The technique involves the acquisition of a silhouette of an axisymmetric fluid droplet, and iterative fitting of the Young–Laplace equation that balances gravitational deformation of the drop with the restorative interfacial tension [115],[116]. Since the advent of high-quality digital cameras and desktop computers, this process has been automated with high speed and precision.The surface or interfacial tension can be related to the drop shape with the following correlation [116].

$$\gamma = \frac{\Delta\rho g R_0}{\beta} \tag{4.5}$$

where γ is the surface tension, Δρ is the density difference between fluids, g is the gravitational constant, R0 is the drop radius of curvature at the apex, and β is the shape factor. β can be defined through the Young-Laplace equation expressed as 3 dimensionless first-order equations in terms of the arc length s measured from the drop apex, derive from variables of the drop shape shown in Fig. 4.15 [115].

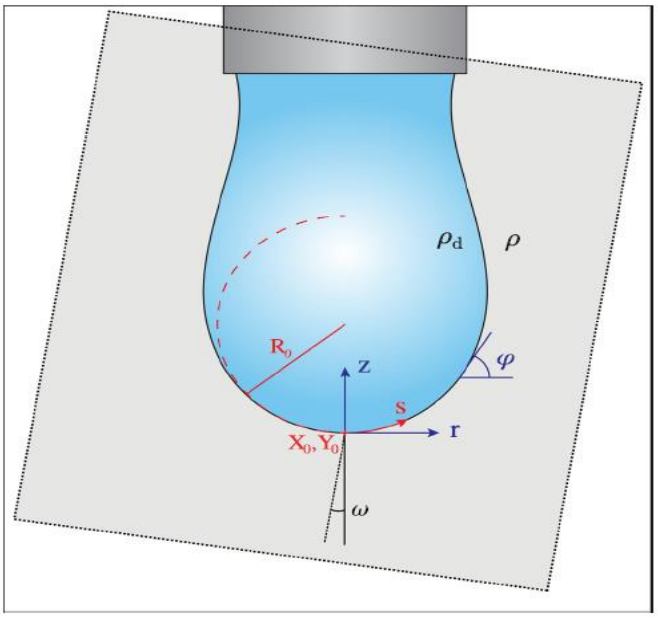

Figure 4.15: A schematic of a pendant drop below a needle. The shaded region represents the image area captured by the camera. The associated variables used in the computational routine to determine the shape factor, and thus the surface and interfacial tension [115].

$$\frac{\mathrm{d}\varphi}{\mathrm{d}s} = 2 - \beta\, \mathrm{z} - \frac{sin\varphi}{r} \tag{4.6}$$

$$\frac{\mathrm{d}r}{ds} = cos\varphi \tag{4.7}$$

$$\frac{\mathrm{d}z}{ds} = sin\,\varphi \tag{4.8}$$

Where, r and z are the cylindrical coordinates, s is the arch length from the drop apex and φ is the tangent angle.

Modern computational methods using iterative approximations allow for solutions of the Young-Laplace equation to be found. Thus, the surface or interfacial tension between any two immiscible fluids with known densities can be determined. For optical tensiometer the size of the droplet is important, and it should have a tear or pendant shape [115]. Care must be taken to ensure that the needle tip is not influencing the drop shape. When measuring surface tension, the density difference between liquid and gas (usually air) is large enough that volumes between 5 µl to 20 µl are generally sufficient to provide pendant or tear shapes. When measuring interfacial tensions, both density difference and interfacial tension influence the required volume to achieve a pendant or tear shape drop. As a guideline, the smaller the density difference, the larger the volume required [116].

Sessile drop measurement is the most used contact angle measurement method adopted by the Theta Lite optical tensiometer. It is a direct measurement of the tangent angle at the three-phase contact point on a sessile drop profile shown in Fig.4.16. In practice, a droplet is placed on the solid surface and an image of the drop is recorded. The static contact angle is then defined by fitting Young-Laplace equation around the droplet, although other fitting methods such as circle and polynomial can also be used [63].

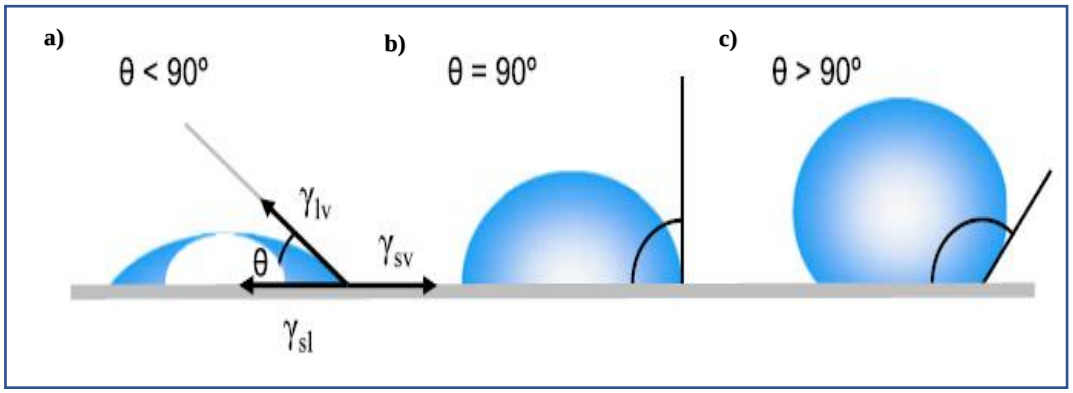

Figure 4.16: Graphical image Illustration of contact angles formed by sessile liquid drops on a smooth homogeneous. Solid surface of three scenarios. a) contact angle Θ less than 90^0 ,b) contact angle equal to 90^0 ,c) contact angle more than 90^0 [63].

The principle measurement of sessile drop method is similar as pendant drop method for optical tensiometer as explained earlier of this section. It is almost trivial in its simplicity, all that is required is a needle, a camera, and a light source. A basic schematic setup and the drop image are shown in Fig.4.17.

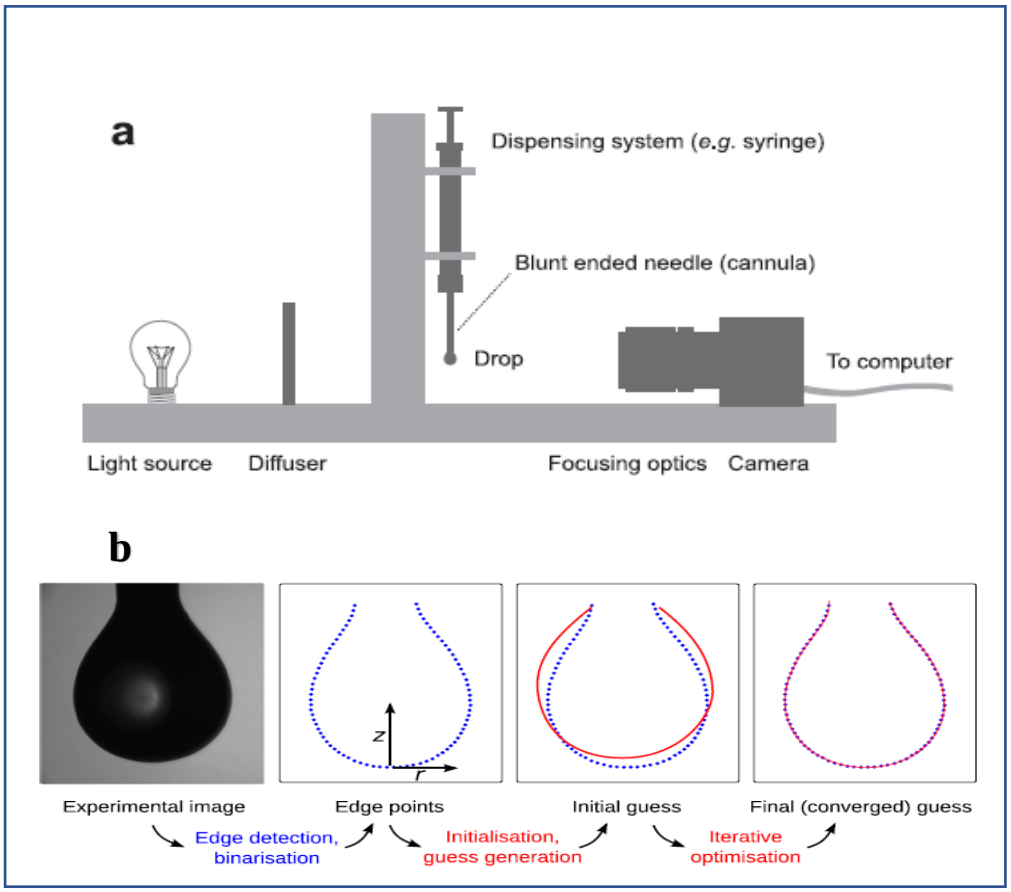

Figure 4.17: a) schematic of principal of optical tensiometer set-up, b) typical drop image captured and process of going from a raw experimental image to a fitted solution from which contact angles, Θ can be obtained [115].

Procedure

A pendant drop or Sessile drop measurement are carried out simply and quickly. The following section describes the procedure with the description of the hardware diagram of Theta Lite optical tensiometer as shown in Fig. 4.18 for ease of reference.

1) Turn Theta Lite machine on and open the **OneAttension** program. Choose measurement method by clicking pendant drop or sessile drop icon. Click adjust camera parameters and choose automated camera adjustment by clicking **Auto** adjust. You can adjust the camera settings also manually if needed.

2) Place a calibration ball and its magnetic holder on the sample stage. Bring the ball into the image on screen and zoom it appropriately by altering the lens zoom adjustment **(#15)** and the lens focus adjustment **(#14)** between the camera and the ball. Press Calibration invalid and accept the calibration ball diameters (standard 4 mm) to complete the calibration.

3) Clean the syringe, place the liquid into it and attach it to the syringe clamp **(#11).** For surface tension of single liquid, sample are drawn into syringe by using the automated fill function and chose the pendant drop method from the main **Theta tab**. For the standard interfacial tension of two liquid measurement, place the less dense liquid in the syringe, the denser liquid in a cuvette and place it on the sample stage **(#13).** Change the syringe needle to a hook needle and attach the filled syringe to the syringe **clamp (#11).** From the main **Theta** tab choose the pendant drop method. The less liquid will be the paraffin oil and the denser liquid will be the nano fluid samples.

4) Fill in the relevant data in the recipe sheet. It might be necessary to add users, liquids or solids to the database manager found in the **Setup** tab. With a surface tension measurement simply lower an appropriate drop and start measurement and image recordings. For the interfacial tension measurement, lift the sample stage **(#13)** until the cuvette is visible, lower the hook needle into it. Lower an appropriate drop and select **Flip Y**. Contact angles are measured by choosing Sessile drop method tab from the **Theta** and a droplet is placed on the solid surface and an image of the drop is

recorded. The static contact angle is then defined by fitting Young-Laplace equation around the droplet.

5) Press **Start** from the controls and wait for the images to be recorded.

6) After recording, choose the analysis tab and double click your experiment. Accept either the default fitting parameters or adjust them from the Drop analysis window. The software will then process all of the chosen images. The red line represents the baseline, and it should connect the widest points of the curve profile and its reflection to each other. Check this visually, and if unsatisfied unselect Use automatic baseline and set it manually. In sessile drop contact angle experiments, the baseline is set at the solid surface, whereas in pendant drop experiments it is adjusted at the end of the needle. By right clicking on the **Results** you can perform further data analysis for drawing graphs or by creating statistics from the chosen data points. There is option to export data by right clicking on the **Results**. By right clicking on the drop image, you can save the separate pictures or the video. Result report in pdf format can be also created by clicking **Generate** report.

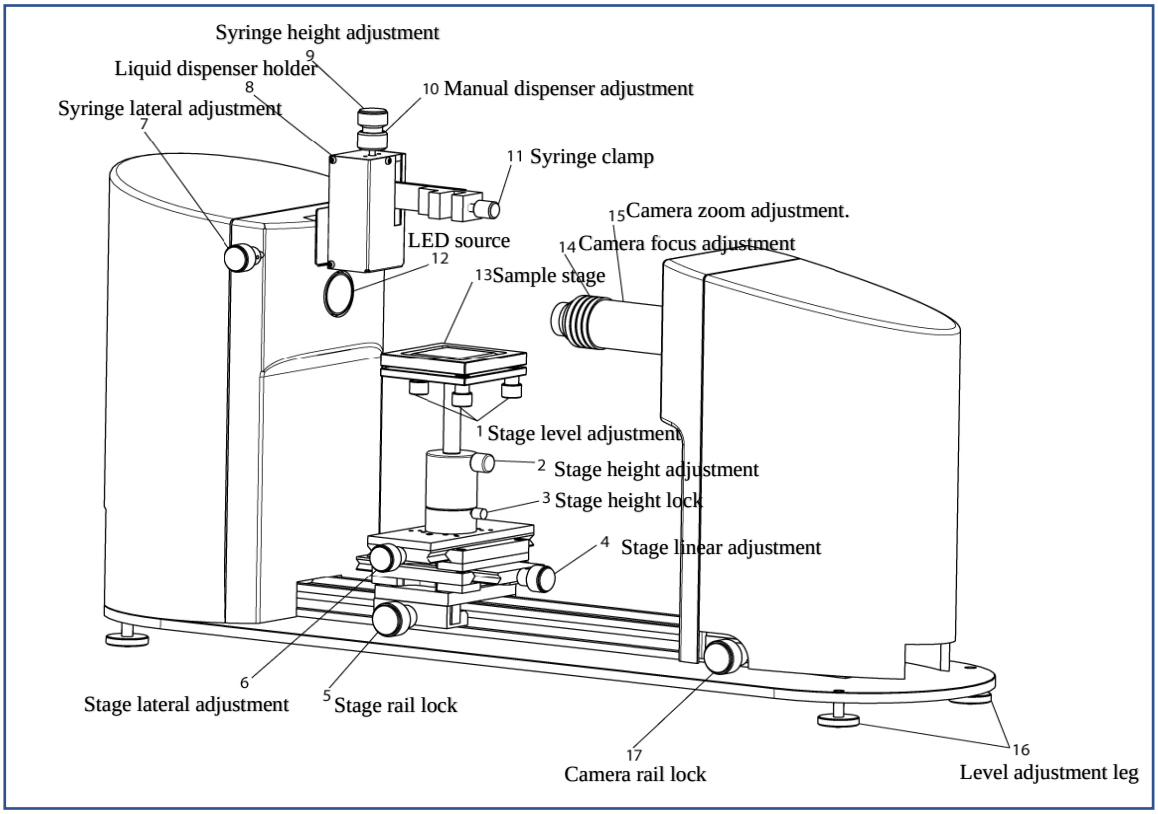

Figure 4.18: Hardware diagram of Theta Lite optical tensiometer. (source: https://www.manualslib.com/manual/1359167/Attension-Theta.pdf)

4.4 Observation and Remarks

The following section will discuss the observations and analysis done on the nanofluids physio-chemical properties characterisation for both the isothermal and non-isothermal conditions.

4.4.1 Density

Isothermal Condition

Table 4.4 records the of density of nanofluids sonicated at five different amplitudes % with a fixed 500-watt power and 20 KHz frequency ultrasonic equipment. For each sample three density readings were measured, and an average value taken as final reading for statistical assurance. All the five samples were maintained at 30 ^{0}C constant room temperature during sonication and measurement of density. The observation indicates that density increased when the amplitude was increased from the base case at 0% amplitude to 20 %. However, interesting observation was noticed between 20% and 40% amplitudes, the density decreased slightly. The density was on incremental trend again once amplitude was increased from 40% to 100%. The increase in density of the nanofluids observed due to the volume contraction of the nanofluids sample causing less spacing between the molecules of the nanofluids leading to a more ordered or compact structure because of increase in the cohesive force between the molecules of the fluids as we maintain the system temperature constant. In one of the previous researchers works, this observation of the micellar structural changes is referred as 'water maker' [117]. The Isothermal condition has reversed the temperature effect on micellar structure during sonication, thus resulting in overall density increase trend with amplitude. The 20% and 40% amplitudes range could be the micellar structural relaxing range referred as 'water breaker' structural before its start agglomerating rapidly. This phenomenon also can be explained with the free volume theory [117]. Free volume is the space present inside the molecular structure of a substance or mixture, and it can be measured by positron annihilation method. Free volume changes as the molecules oscillate or changes in structural. If the intermolecular cohesion increases the free volume decreases [118]. Free volume controls the molecular mobility of large segments of the micellar chains of the nanofluids, which in turn influence the physical and mechanical properties, such as volume, density, molecular packing parameters, elasticity, and viscosity.

Table 4.4: Density at various amplitudes measured an recorded under Isothermal conditions

Amplitude %	Temperature (^{o}C)	Average Density (g/ml)	Standard Deviation +/-
0	30	1.0186	0.00021
20	30	1.0216	0.00057
40	30	1.0206	0.00026
60	30	1.0236	0.00074
80	30	1.0252	0.00040
100	30	1.0274	0.00076

Non-Isothermal Condition

Table 4.5 shows the results of density of nanofluids sonicated at five different amplitudes % with a fixed 500-watt power and 20 KHz frequency ultrasonic equipment. All the samples temperature was let to increase during sonication and measurement of density was taken at the corresponding temperature. The result shows density spiked during the amplitude increased from 0% of base case to 20%. However, from 20% to 60% amplitudes, the density of the nanofluids decreased significantly. The density was constant from 60 to 80 % amplitude before it started to increase again when we applied 100% amplitude. All the measurements were duplicated three times and average readings were taken for confirming the trend and statistical assurance. It is obvious that under the non-isothermal condition the density trend against the amplitude was overall behaved opposite compared to isothermal condition with an exception for the 0% to 20% and 60 to 100% amplitudes range. The temperature increase during sonication of the nanofluids results in the volume expansion causing more spacing between the molecules of the nanofluids leading to a less ordered structure due to the decrease in the cohesive force between the molecules of the fluids and referred as ‘water breaker structure’ [117]. Thus, the density of nanofluids of the studied surfactants system, Triton CG-425 decreases with the rise in temperature during sonication with amplitude range of 20 to 60 %. However, the opposite was observed for 0 to 20% and 60 to 100% amplitude range where density increase was observed. This observation can be explained by the compaction and relaxation of micellar chain due to the external perturbation of ultrasound that relates back to the free volume theory [117], suggesting we could have different physio-chemical properties due micellar structure chain parting and agglomerating [119].

Table 4.5: Density at various amplitudes measured and recorded under non- isothermal conditions

Amplitude %	Temperature (°C)	Average Density (g/ml)	Standard Deviation +/-
0	30	1.0186	0.00021
20	47	1.0191	0.00051
40	48	1.0172	0.00046
60	51	1.0144	0.00031
80	50	1.0144	0.00026
100	52	1.0164	0.00050

Remarks

A comparative density chart against amplitude % was plotted as shown in Fig. 4.19 for both scenarios, isothermal, and non-isothermal. The trend indicates, for the non - isothermal condition, density declines with amplitude increases and for isothermal condition it is in opposite trend. We believe that ultrasonic induction on nanofluids for the non-isothermal condition causes the density decrease overall in agreement with literature reported. The temperature effect on the base sodium chloride solution from the literature is show in table 4.6 as reference for comparison [120]. However, for sonication with amplitude 80% to 100%, the opposite trend is observed despite temperature increase possibly from the agglomeration of micellar due to the Kraft temperature effect that was explained in earlier section of literature review of this thesis.

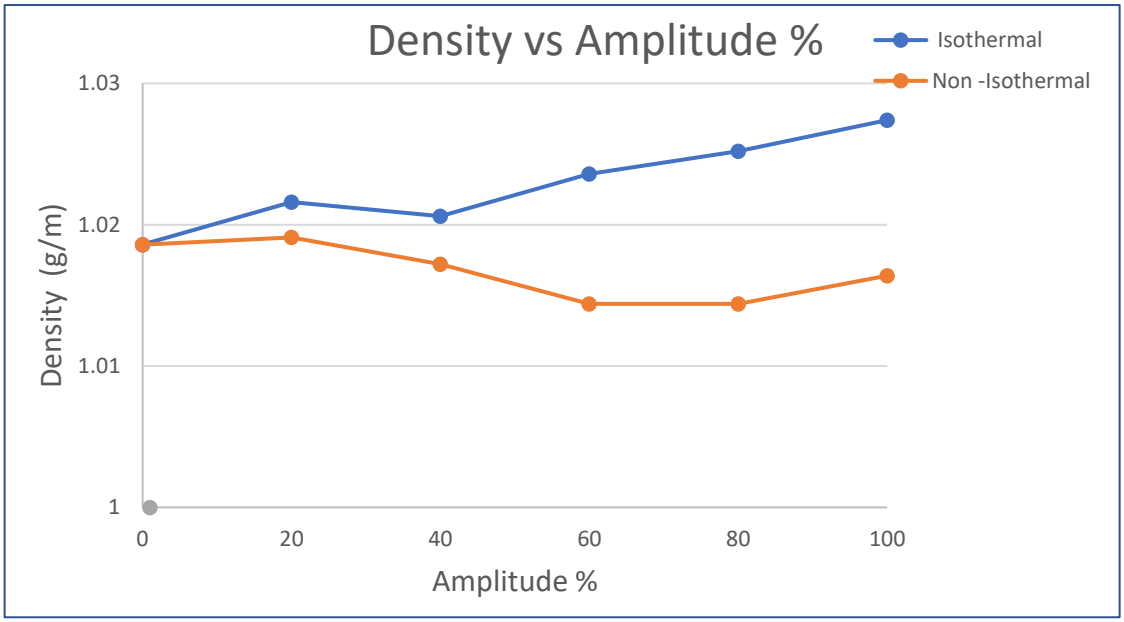

Figure 4.19: Density vs Amplitude % chart for both Isothermal and Non-Isothermal conditions

Table 4.6: Specific gravity or density (kg/l) of aqueous sodium chloride solutions as a function of sodium chloride weight % and temperatures T ^{0}C.

(source: https://www.handymath.com/cgibin/nacltble.cgi?submit=Entry)

Sodium Chloride in Water							
	Temperature in degrees Centigrade (°C)						
	0°C	10°C	25°C	40°C	60°C	80°C	100°C
Concentration (% Weight)	Density (kg/L)						
1	1.00747	1.00707	1.00409	0.99908	0.9900	0.9785	0.9651
2	1.01509	1.01442	1.01112	1.00593	0.9967	0.9852	0.9719
4	1.03038	1.02920	1.02530	1.01977	1.0103	0.9988	0.9855
8	1.06121	1.05907	1.05412	1.04798	1.0381	1.0264	1.0134
12	1.09244	1.08946	1.08365	1.07699	1.0667	1.0549	1.0420
16	1.12419	1.12056	1.11401	1.10688	1.0962	1.0842	1.0713
20	1.15663	1.15254	1.14533	1.13774	1.1268	1.1146	1.1017
24	1.18999	1.18557	1.17776	1.16971	1.1584	1.1463	1.1331
26	1.20709	1.20254	1.19443	1.18614	1.1747	1.1626	1.1492

4.4.2 pH

Isothermal condition

Table 4.7 reflects the results of pH variation when we vary the amplitude % on the nanofluids samples at isothermal condition of 30 ^{0}Celsius. The pH measurements were taken at 30 ^{0}C room temperature as well. The pH increased initially from 2.9 to 3.0 when we raise the amplitude from the base to 20%. This increase in pH could be due to release of free radicals from water molecules, H_20 --- $H^+ + OH^-$ from the sonication effect [121]. The OH^- radicals reacted with other molecules to increase the pH. However, further increased in amplitude did not have impact on pH, as it remained constant at 3, suggesting sonication parameters such as amplitude has no impact on pH of nanofluids system [56].

Table 4.7: pH at various amplitudes measured and recorded under isothermal condition

Amplitude %	Temperature (^oC)	pH	Standard Deviation +/-
0	30	2.9	0.02
20	30	3.0	0.06
40	30	3.0	0.05
60	30	3.0	0.06
80	30	3.0	0.04
100	30	3.0	0.03

Non-Isothermal condition

Table 4.8 reflects the results of pH variation when we vary the amplitude of the nanofluids samples at non-Isothermal condition. The pH measurements were taken at corresponding temperature. The pH increased initially from 2.9 to 3.0 when we raise the amplitude from the base to 20%. This increase in pH could be due to release of free radicals from water molecules, H_20 --- $H^+ + OH^-$ from the sonication effect as explained earlier in isothermal condition. The OH^- radicals reacted with other molecules to increase the pH. However, further increased in amplitude did not have impact on pH despite we allow temperature build-up of the nanofluids. It remained constant at 3, suggesting sonication parameters such as amplitude has no impact on pH of nanofluids system for both conditions. The temperature rises significantly when the nanofluids were induced sonication of 20% amplitude and it started to flatten from 40 % to 100 % amplitude. Temperature and pH changes for the non-isothermal condition for various amplitude plotted in Fig.4.20. The temperature rise has no effect on the pH of the nanofluids Thus, we can conclude temperature and amplitude of ultrasonic has no effect on pH of nanofluids [56].

Table 4.8: pH at various amplitude under non- isothermal condition

Amplitude %	Temperature (^oC)	pH	Standard Deviation +/-
0	30	2.9	0.03
20	47	3.0	0.1
40	48	3.0	0.06
60	51	3.0	0.08
80	50	3.0	0.06
100	52	3.0	0.06

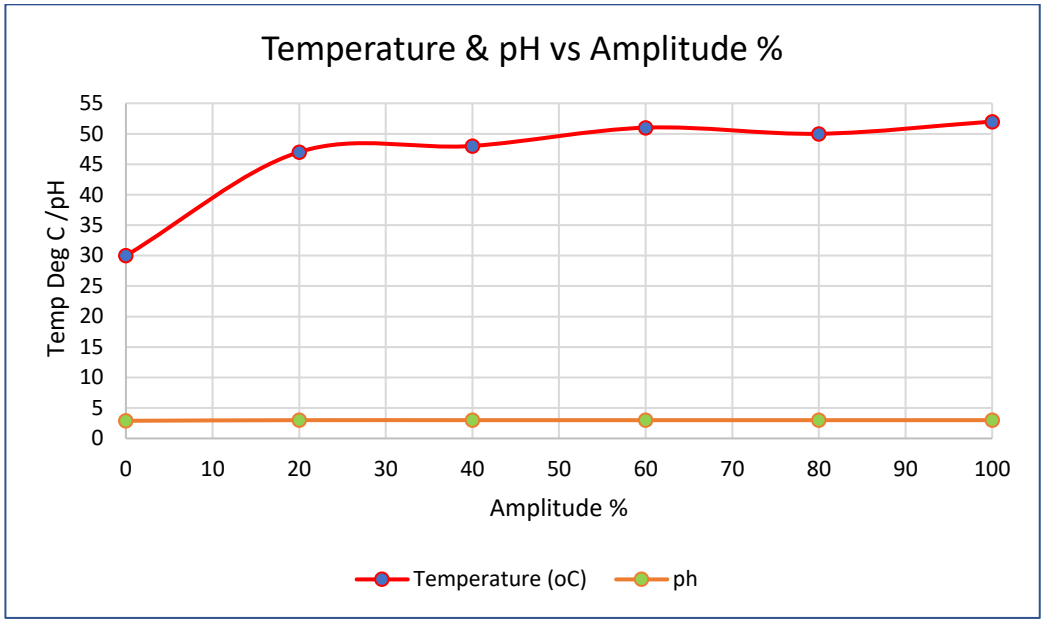

Figure 4.20: Temperature and Ph Chart vs Amplitude% for non-isothermal condition.

4.4.3 Viscosity

Isothermal Condition

Table 4.9 shows the results of dynamic viscosity of nanofluids sonicated at five different amplitudes % with a fixed 500-watt power and 20 KHz frequency. All the five samples were maintained at 30 ^{0}C constant room temperature during sonication and measurement of dynamic viscosity. The result shows viscosity decreased gradually when the amplitude was increased from the base case at 0% amplitude to 20 %. However, interesting observation was noticed between 20% and 40% amplitudes, the viscosity almost flat before the drastic incremental trend observed when amplitude was increased from 40% to 100%. The measurements were repeated three times and average readings was taken for confirming the trend and statistical assurance. The decrease in viscosity of the nanofluids results from the transformation of molecules structure of the nanofluids leading to a less ordered or loose structure due to the strong shear force generated during sonication between the molecules of the fluids. This also would result in system in-situ temperature rise. However, as we maintain the system temperature constant with external cooling, has reversed the temperature increase effect on micellar structure during sonication causing more agglomerated micellar structure, thus resulting in overall viscosity increase trend with amplitude. The 20% and 40% amplitude range could be the

micellar structural relaxing range before its start agglomerating rapidly [119],[122]. These observations can be explained from the free volume theory.

Table 4.9 : Viscosity at various amplitude under isothermal condition

Temperature (^{0}C)	Amplitude %	Dynamic viscosity [mPa.s]	Standard Deviation +/-
30	0	2.5085	0.017
30	20	2.4191	0.040
30	40	2.4273	0.010
30	60	3.3581	0.153
30	80	3.4895	0.076
30	100	3.7765	0.093

Non-Isothermal Condition

Table 4.10 shows the results of dynamic viscosity of nanofluids sonicated at five different amplitudes % with a fixed 500-watt power and 20 KHz frequency. All the samples temperature was let to be increased during sonication and measurement of viscosity was taken at the corresponding temperature. The result shows viscosity decreased significantly during the amplitude increased from 0% of base case to 20%. However, from 20% to 60% amplitude, the viscosity of the nanofluids almost flat. The viscosity increased linearly supersede the original viscosity of the nanofluids at the amplitude of 60 to 100 % range. All the measurements were repeated three times and average readings were taken for confirming the trend and statistical assurance. It is obvious that under the non-isothermal condition the viscosity trend against the amplitude was overall lower compared to the original viscosity of the nanofluids with exception for the 80% to 100% range. The temperature increases during sonication of the nanofluids results in the volume expansion causing more spacing between the molecules of the nanofluids leading to a less ordered structure due to the increase in the shear force that results in breakup of micellar structure chain. However, the opposite happens beyond a specific temperature limit called Kraft temperature, where the micellar structure starts the agglomeration and resulting in viscosity build-up of the nanofluids [119],[122].

Table 4.10: Viscosity at various amplitude under non-isothermal condition

Temperature ^{0}C	Amplitude %	Dynamic viscosity [mPa.s]	Standard Deviation +/-
30	0	2.5085	0.017
47	20	2.0796	0.020
48	40	2.0359	0.041
51	60	2.0269	0.009
50	80	2.3847	0.075
52	100	2.6789	0.057

Remarks

A comparative viscosity against amplitude % chart was plotted as shown in Fig. 4.21 for both scenarios, isothermal, and non-isothermal. The trend indicates, for the non - isothermal condition, viscosity declines with amplitude increases to certain extend where it starts to increase again after 60 % amplitude and for isothermal condition it is in opposite trend where it almost maintain the viscosity in flat line till 40% amplitude and there after showing incremental trend beyond initial base viscosity. The viscosity trend against temperature and sonication time for conventional nanofluids prepared with two stage nano particle dispersion method using aluminium oxide from literature shown in Fig 4.22 [123]. The important observation from comparing trend between nanofluids in Fig.4.21 and Fig.4.22 is that nanofluids prepared in conventional two stage method has lower viscosity at end of sonication mainly caused by dispersion and settling. The micellar nanofluids has different behaviour during sonication as the viscosity decrease and increase are mainly from the self-assembly [45], [48] and structural changes of the micellar itself without causing settling of particles.

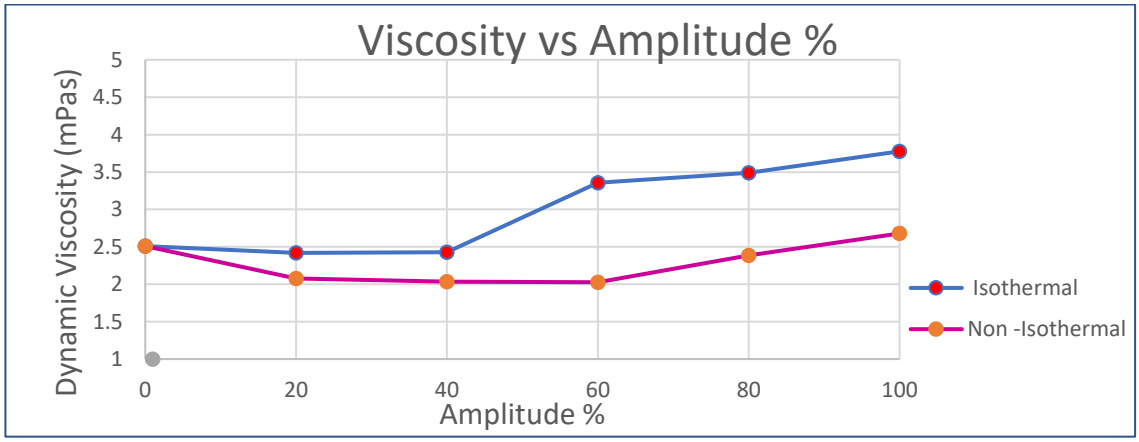

Figure 4.21: Viscosity vs Amplitude % chart for both Isothermal and Non-Isothermal conditions

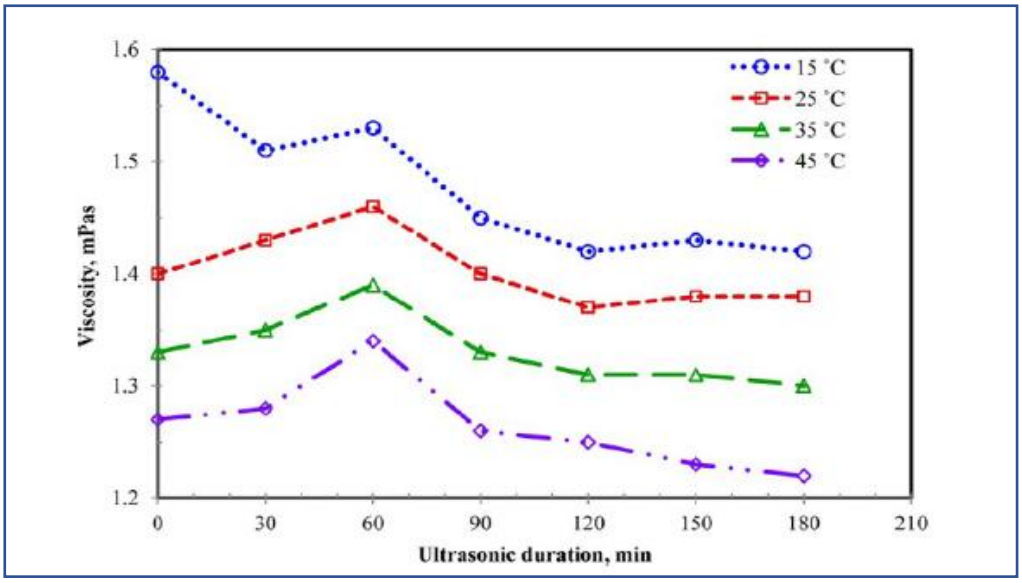

Figure 4.22: The viscosity variations concerning ultrasonication time at different temperatures of conventional Al_2O_3 nanofluids [123].

4.4.4 Electrical Conductivity

Isothermal Condition

The results of electrical conductivity of nanofluids sonicated at five different amplitudes % with a fixed 500-watt power and 20 KHz frequency ultrasonic equipment are presented in table 4.11. All the five samples were maintained at 30 ^{0}C constant room temperature during sonication and measurement of electrical conductivity. It was observed that electrical conductivity increased gradually when the amplitude was increased from the base case at 0% amplitude to 20 %. However, interesting observation was noticed between 20% and 40% amplitude, the electrical conductivity dropped before the drastic incremental trend observed when amplitude was increased from 40% to 100%. The measurements were repeated three times and average readings was taken for statistical consistency. The electrical conductivity trend observed of the nanofluids results in agreement with the theory i.e., direct proportional correlation between electrical conductivity and temperature [124]. However, as we maintain the system temperature constant with external cooling, has reduce the temperature increase effect on conductivity to a certain degree during sonication. The only unusual conductivity decrease trend observed was for the amplitude range between 20 to 40 % range. This observation suggest that electrical ionic free movement was reduced for this amplitude range when external

energy input from sonication been countered with external colling generating a particular micellar structural.

Table 4.11 : Electrical conductivity at various amplitude under isothermal condition

Temperature ^{0}C	Amplitude %	Electrical Conductivity(mS/CM)
30	0	114.1
30	20	131.7
30	40	121.0
30	60	127.0
30	80	141.0
30	100	149.1

Non-Isothermal Condition

Table 4.12 presents the results of electrical conductivity of nanofluids sonicated at five different amplitudes % with a fixed 500-watt power and 20KH frequency ultrasonic equipment. All the samples temperature was let to be increased during sonication and measurement of electrical conductivity was taken at the corresponding temperature. The result shows electrical conductivity in an upward trend during the amplitude increased from 0% of base case to 100%. All the measurements were repeated three times and average readings were taken for confirming the trend and statistical assurance. It is obvious that under the non-isothermal condition the electrical conductivity is directly proportional to temperature supporting the general correlation between electrical conductivity and temperature [124].

Table 4.12 : Electrical conductivity at various amplitude under mon-isothermal condition

Temperature ^{0}C	Amplitude %	Electrical Conductivity(mS/CM)
30	0	114.1
47	20	134.3
48	40	139.7
51	60	142.5
50	80	151.3
52	100	172.0

Remarks

The graph plot of electrical conductivity against amplitude for both the conditions are shown in Fig.4.23. The chart indicates the non-isothermal condition has higher electrical conductivity compared to isothermal conditions. Thus, we can conclude sonication does improve electrical conductivity for both the conditions with exception for amplitude range 20 to 40 % under isothermal condition.

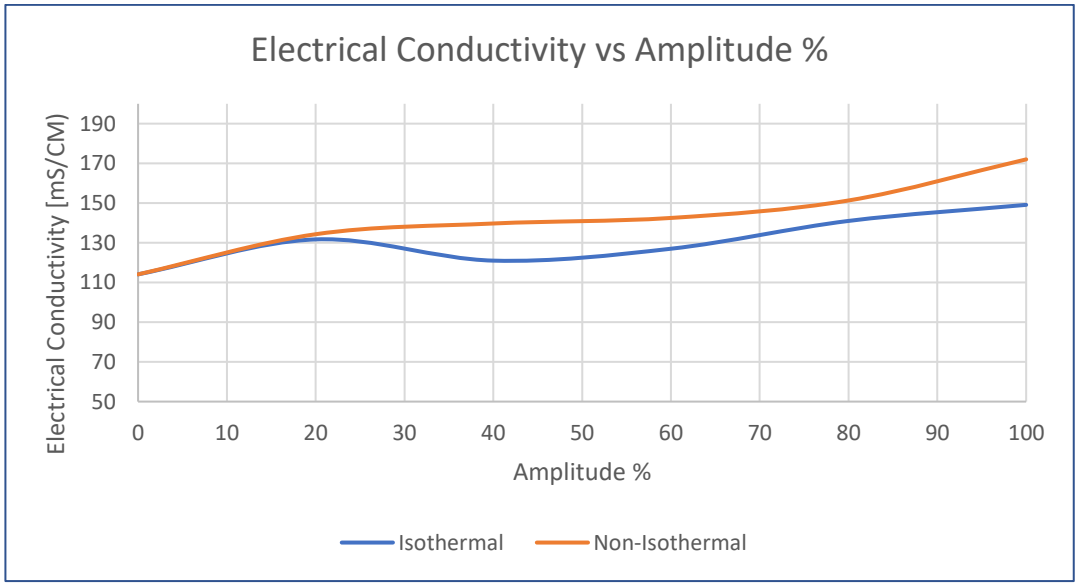

Figure 4.23: Electrical conductivity vs Amplitude % chart for both Isothermal and Non-Isothermal conditions.

4.4.5 Particle Size

Isothermal Condition

Table 4.13 summarise the measurement and analysis of particle size of nanofluids treated at five different amplitudes with a fixed 500-watt power and 20 KHz frequency ultrasonic equipment. All the five samples were maintained at 30 ^{0}C constant room temperature during sonication and measurement of particle size. The analysis indicates that the mean average particle size increase when the amplitude was increased from the base case at 0% amplitude to 20 %. However, the opposite observation was noticed between 20 and 40 % amplitudes. The average mean particle size decreased slightly. The mean average particle size was on incremental trend again with multiple peaks when amplitudes were increased from 40% to 100%. The measurements were repeated three times and average readings was taken for confirming the trend and for statistical assurance. The example results plot for base nanofluids at 0% amplitude from Zetasizer analysis software are shown in figure 4.24 and 4.25. The increase in particle size of the nanofluids results in the volume contraction causing less spacing between the molecules of the nanofluids leading to a more extended micellar structure due to the increase in the cohesive force between the molecules of the fluids when the amplitude increased to 20%. As we maintain the system temperature constant, the isothermal condition has reversed the temperature increase effect on micellar structure changes during sonication, thus resulting in overall particle size increasing trend with amplitude. The 20% and 40% amplitude range could be the micellar structural relaxing range before its start agglomerating rapidly. This phenomenon also can be explained with the free volume theory. Free volume controls the molecular mobility of large segments of the micellar chains, which in turn influence the physical and mechanical properties, such as particle size.

Table 4.13: Mean average particle size at various amplitude under isothermal conditions.

Amplitude %	Mean average Particle Size(nm)	Temperature (^{o}C)
0	49.22	30
20	81.45	30
40	56.10	30
60	92.62	30
80	105.00	30
100	134.10	30

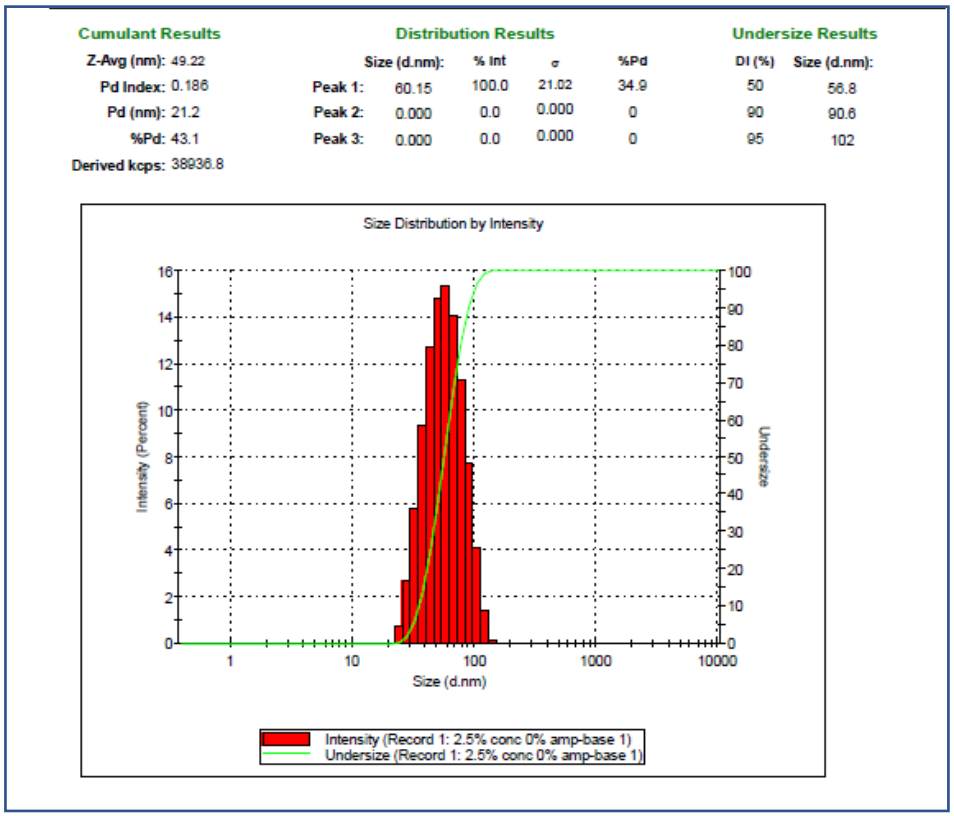

Figure 4.24: Size distribution vs Intensity for base sample at 0 % amplitude for isothermal condition

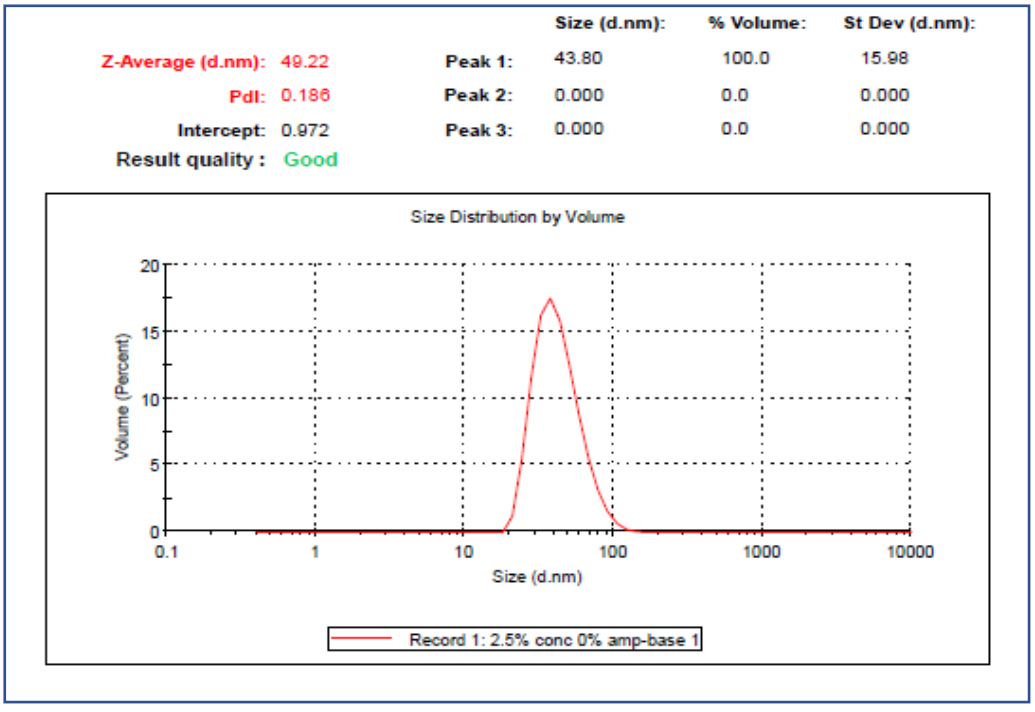

Figure 4.25: Size distribution vs Volume for base sample at 0 % amplitude for isothermal condition

Non-Isothermal Condition

Table 4.14 shows the results of mean average particle size of nanofluids treated at five different amplitudes % with a fixed 500-watt power and 20 KHz frequency ultrasonic equipment. All the samples temperature were let to increase during sonication and measurement of particle size was taken at the corresponding temperature. The result shows mean average particle size decreased during the amplitude increased from 0% of base case to 20%. However, from 20% to 40% amplitudes, the mean average particle size of the nanofluids increased significantly. The particle size decreased significantly for treatment with 60 % amplitude before it started to increase drastically again when we applied 80 to 100% amplitude. All the measurements were repeated three times and average readings were taken for statistical assurance and confirming the trend. The example results plot for base nanofluids at 0% amplitude from Zetasizer analysis software are shown in figure 4.26 and 4.27. It is obvious that under the non-isothermal condition the mean average particle size trend against the amplitude was volatile compared to the isothermal condition that has upward trend with exception for the 40% amplitude. The temperature increases during sonication of the nanofluids results in the compaction and relaxation of micellar chain due to the external perturbation of ultrasound that relates back to the free volume theory, suggesting we could have different physio-chemical properties due to micellar structure chain parting and agglomeration.

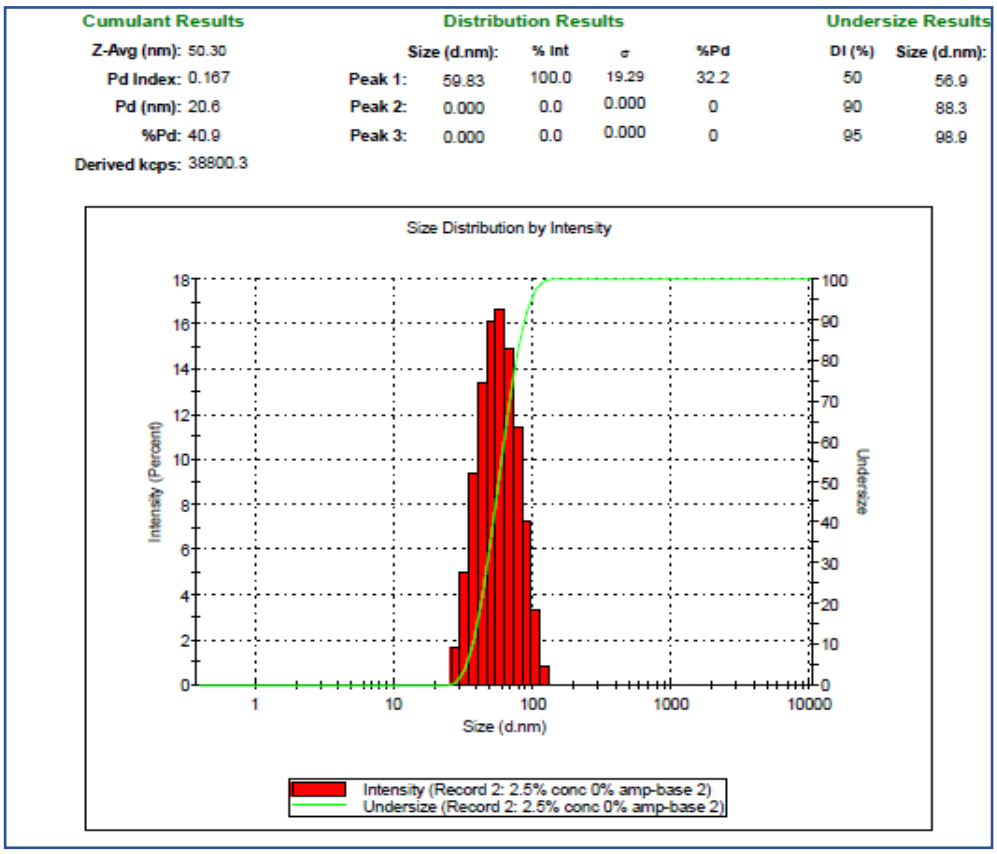

Figure 4.26: Size distribution vs Intensity for base sample at 0 % amplitude for non-isothermal condition

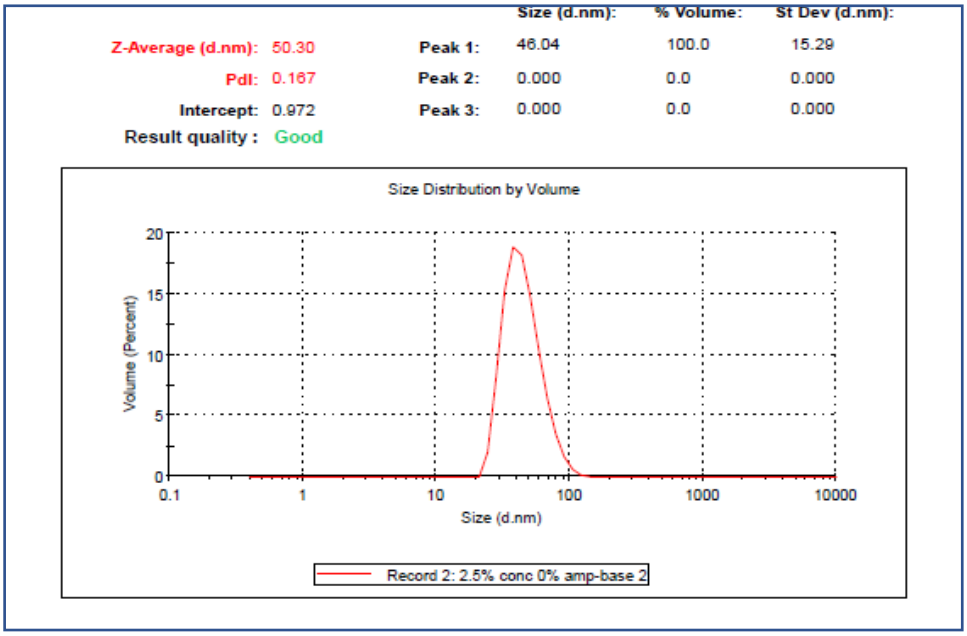

Figure 4.27: Size distribution vs Volume for base sample at 0 % amplitude for non- isothermal condition.

Table 4.14: Mean average particle size at various amplitude under non- Isothermal conditions

Amplitude %	Mean average particle size (nm)	Temperature (^{o}C)
0	50.30	30
20	31.23	47
40	56.10	48
60	9.38	51
80	216.4	50
100	953.6	52

Remarks

A comparative chart of mean average particle size against amplitude % was plotted as shown in Fig. 4.28 for both scenarios, isothermal, and non-isothermal. The trend indicates, for the non -isothermal condition, particle size is minimal for amplitude 20% and 60%. The isothermal condition shown a steady gradual mean particle size incremental when amplitude is increased.

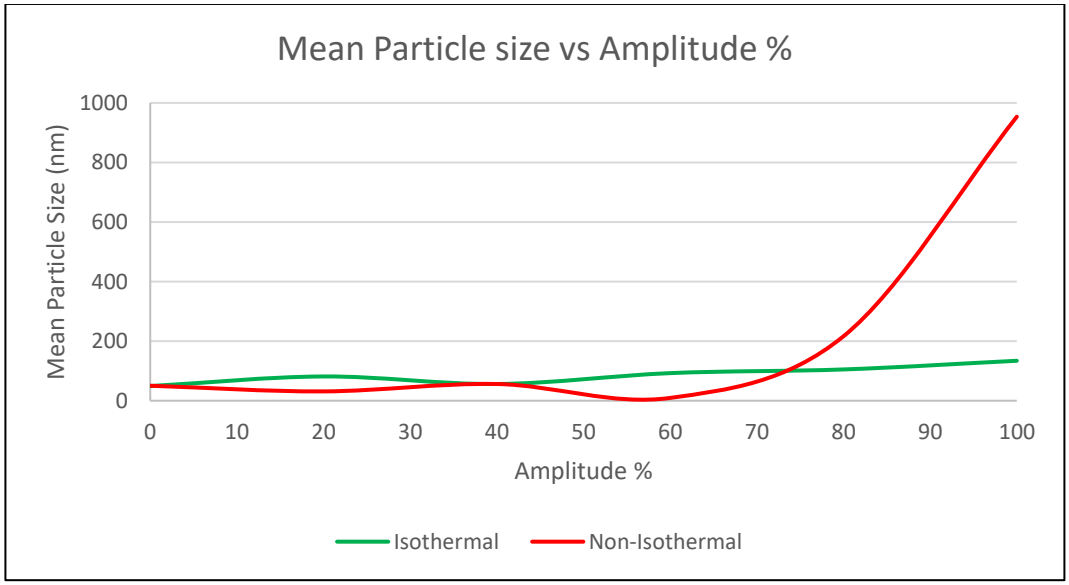

Figure 4.28: Mean average particle size vs amplitude % graph for both Isothermal and Non-Isothermal conditions.

4.4.6 Zeta Potential

Zeta potential results for the nanofluids treated at five different amplitudes with a fixed 500-watt power and 20 KHz frequency ultrasonic equipment for both the isothermal and non-isothermal conditions been tabulated in table 4.15. The zeta potential measurement for the isothermal condition was set at 30 degrees Celsius [125]. However, Zeta potential for the non-isothermal were varied according to the corresponding temperature recorded for each amplitude. The results indicate that, zeta potential is negative charge for the nanofluids design with alky polyglycolide surfactant (APG). Under the isothermal condition the value show more of a flat line trend compared to a decreasing trend for the non-isothermal condition. The results are plotted in Fig. 4.29. Typical zeta potential value for various non-ionic APG surfactant and few other types of surfactants-based fluids from the literature [126] are as per Fig 4.30. The reference value will provide us some assurance that the measurements obtained for this experiment are reliable. Zeta potential is very much depended on the type of surfactant and pH. It is obvious ultrasound induction did not have effect on pH from our earlier results, thus has minimal effect on zeta potential. However, at higher amplitude under non isothermal condition, observed zeta potential decline due to temperature effect.

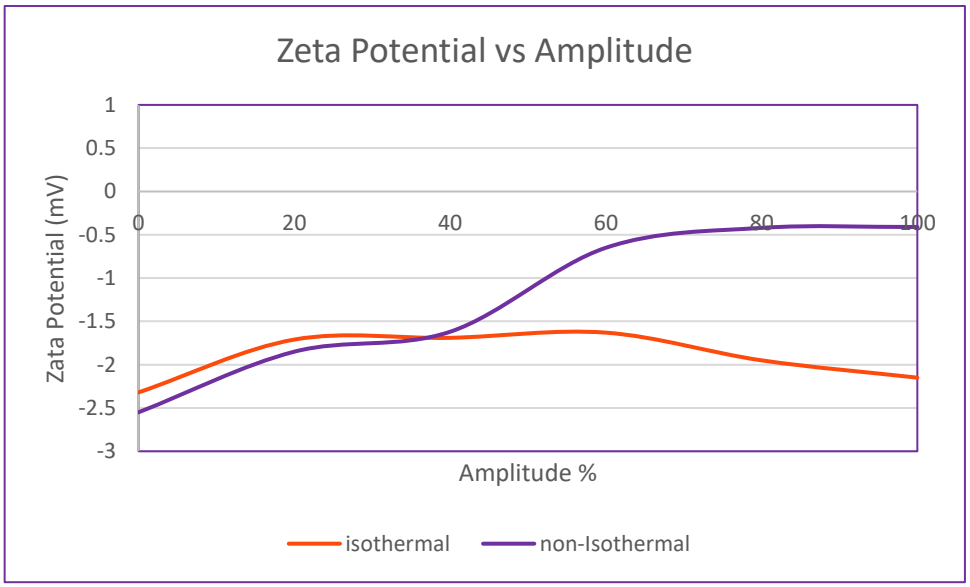

Figure 4.29: Graph comparison of zeta potential vs amplitude for isothermal and non -isothermal condition

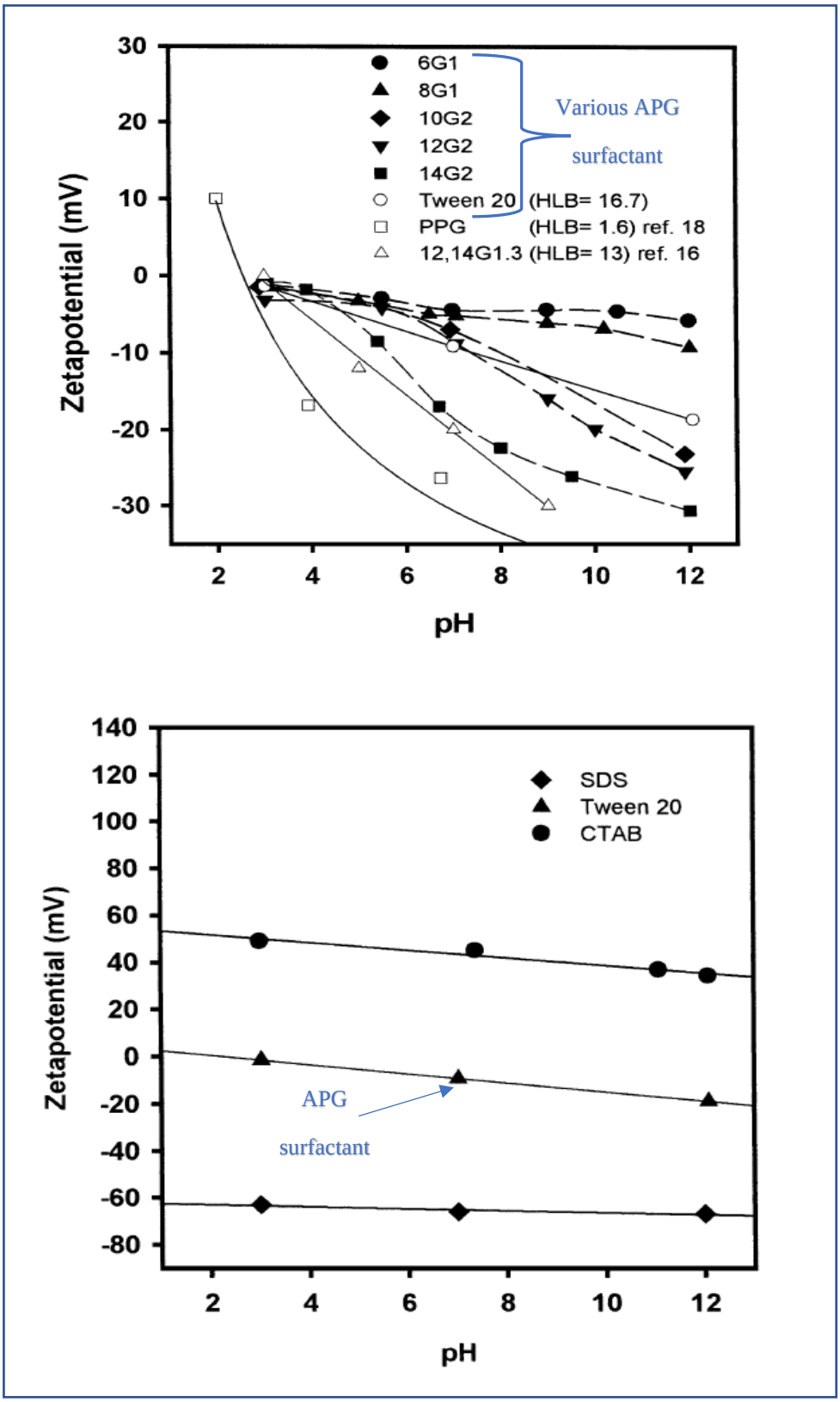

Figure 4.30: Typical zeta potential value vs pH of various surfactant fluids [126].

Table 4.15: Zeta potential at various amplitude % for both isothermal and non-isothermal conditions

Isothermal			Non-Isothermal	
Amplitude %	Zeta Potential (mV)	Temperature ^{0}Celcius	Zeta Potential (mV)	Temperature ^{0}Celcius
0	-2.32	30	-2.55	30
20	-1.71	30	-1.85	47
40	-1.69	30	-1.62	48
60	-1.63	30	-0.65	51
80	-1.95	30	-0.42	50
100	-2.15	30	-0.41	52

4.4.7 Surface tension, Interfacial tension, and contact angles.

Surface tension, interfacial tension and contact angles results for the nanofluids sonicated at five different amplitudes % with a fixed 500-watt power and 20 KHz frequency ultrasonic equipment under both the isothermal and non-isothermal conditions been tabulated in table 4.16. All the measurement for the isothermal condition was set at 30 degrees Celsius. However, for the non-isothermal were varied according to the corresponding temperature recorded for each amplitude. Each measurement was repeated three times for statistical consistency. Example of images recorded for the surface tension and contact angles measurement are shown in Fig. 4.31. Surface tension, interfacial tension, and contact angles against amplitudes % graphs were plotted and shown in Fig.4.32, Fig.4.33 and Fig.4.34 respectively. The surface tension for both isothermal and non-isothermal sonication shows reduction trend when we increase amplitude %. However, surface tension value has the lowest value under the non-isothermal condition at amplitude 60%. This observation trend was seen for all three parameters, surface tension, interfacial tension, and contact angles.

Remarks

The three parameters, surface tension, interfacial tension and contact angles are vital for a fluid's wettability studies [23]. The trends indicate that nanofluids sonicated at non-isothermal conditions have higher wetting characteristic compared to nanofluids sonicated under isothermal condition.

Table 4.16: Surface tension, interfacial tesnion and contact angles at various amplitude % for both isothermal and non-isothermal conditions

Isothermal				Non-Isothermal			
Amplitude %	Surface tension (mN/m)	Interfacial Tension (mN/m)	Contact angles (degree)	Surface tension (mN/m)	Interfacial tension (mN/m)	Contact angles (degree)	Temperature ^{0}C
0	31.8	1.25	16.69	31.8	1.25	16.81	30
20	28.5	0.85	13.93	26	0.60	11.28	47
40	27.5	0.83	12.85	23.8	0.45	8.65	48
60	26	0.81	12.15	18.5	0.23	6.89	51
80	26.5	0.75	16.17	20.8	0.28	7.53	50
100	26.3	0.62	16.34	21	0.31	8.14	52

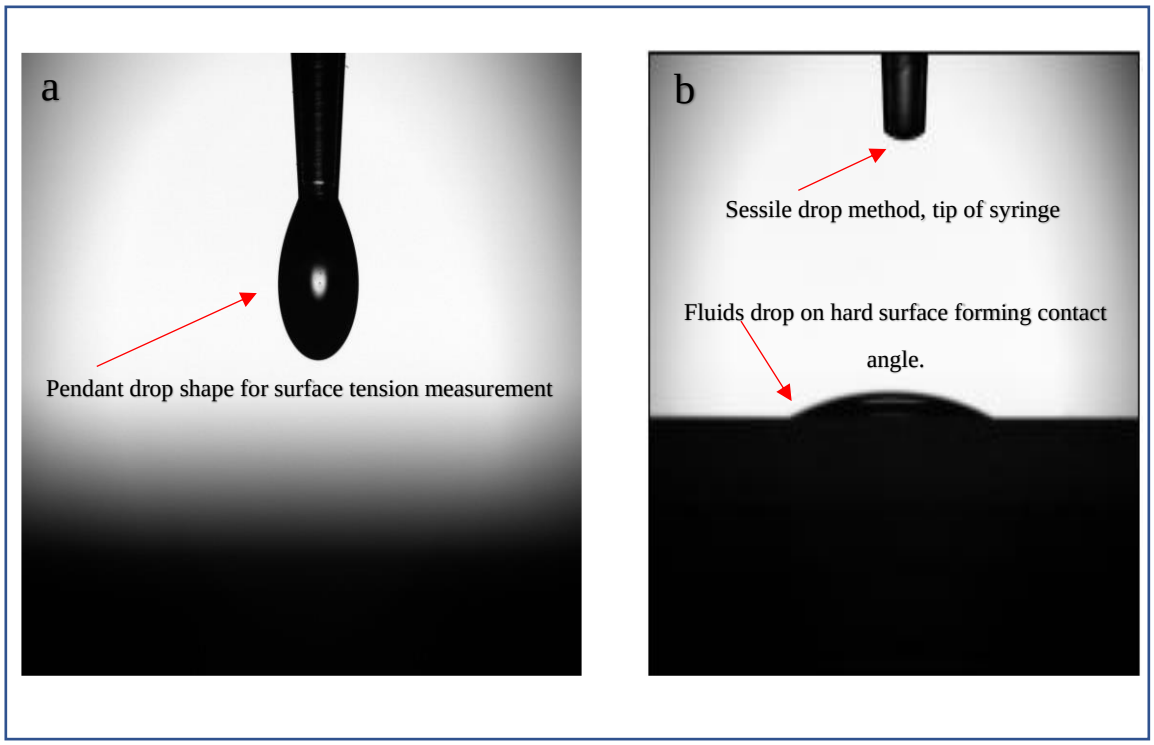

Figure 4.31: a) image of surface tension measurement, b) image of contact angles measurement

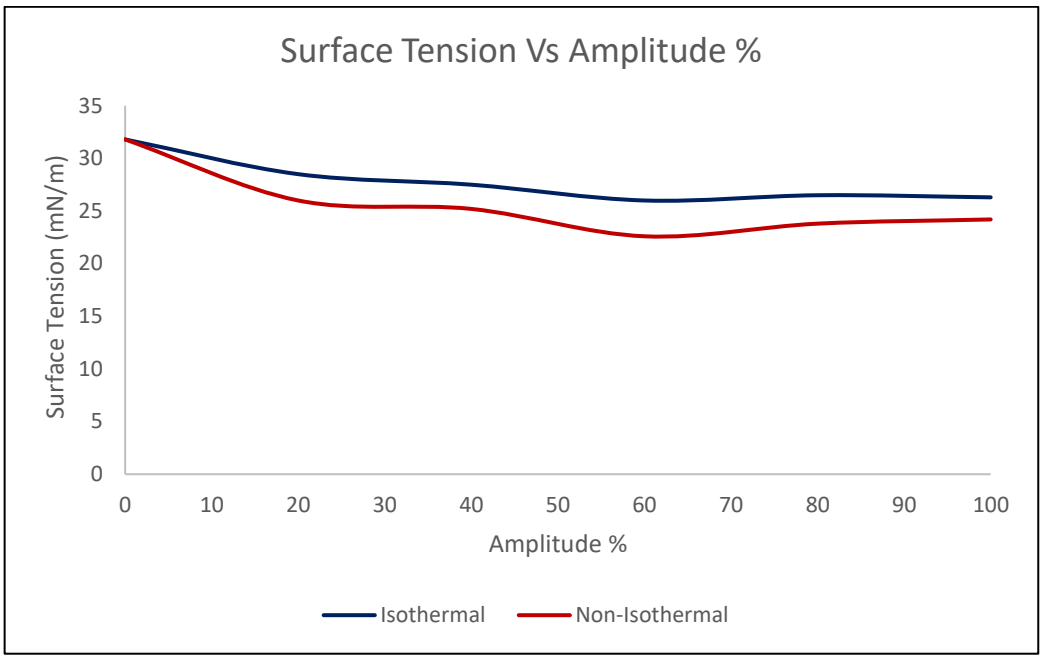

Figure 4.32: Graph comparison of surface tension vs amplitude % for isothermal and non -isothermal condition

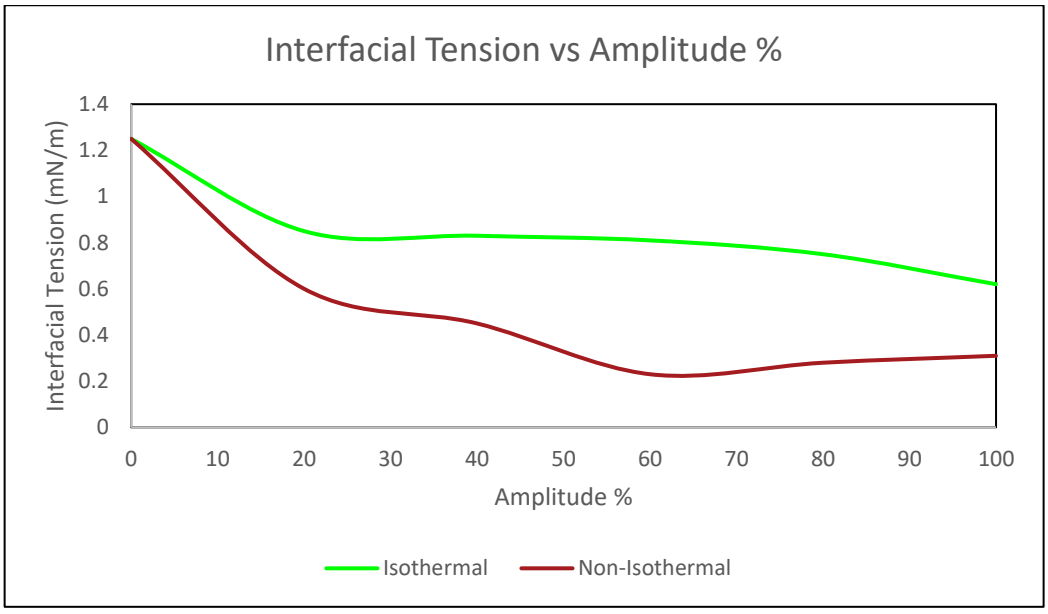

Figure 4.33: Graph comparison of interfacial tension vs amplitude % for isothermal and non -isothermal condition

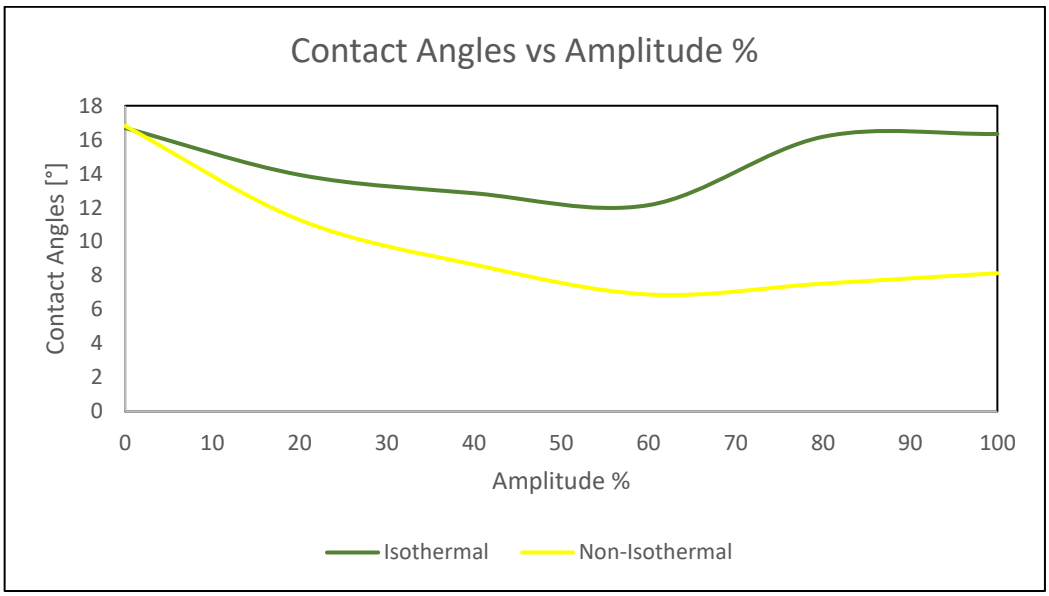

Figure 4.34: Graph comparison of contact angles vs amplitude % for isothermal and non -isothermal condition

4.5 Closure

This chapter presents the observation and analysis done on nanofluids physio-chemical properties characterisation that undergone sonication with 20 KHz frequency and 500-watt power output at five different amplitudes % under isothermal and non-isothermal conditions. The physio-chemical properties that were investigated have key influence on nanofluids design for its potential application for near well remediation for mass transfer kinetics enhancement. The observation from the experiments conducted indicate that external perturbation such as ultrasonic does alter the physio-chemical properties and by varying the operating parameters, such as the sonication amplitude and process conditions [127],[128],[129], we able to manipulate and achieve the desired physio-chemical properties that suitable for our application. It's obvious from the observation that non-isothermal process condition and an optimum 60 % amplitude provide the most favourable physio-chemical properties of the nanofluids for near wellbore remediation enhancement [14],[40],[92].

The results of physio-chemical characterisation under various amplitudes % and process conditions from this chapter will be used to conduct further studies to simulate the near wellbore remediation and mass transfer kinetics evaluation experiments in the next chapter. Those experiments will provide the optimum selection of amplitude %, process condition and physio-chemical properties correlation to identify main factors influencing the mass transfer kinetics performance of the nanofluids.

CHAPTER 5 Nanofluids Mass Transfer Kinetics Evaluation

5.1 Introduction

In the previous chapter, we have experimentally studied the effect of various amplitude % of the ultrasonic induction on physio-chemical properties of nanofluids. The manipulation of physio-chemical properties of nanofluids by changing the ultrasonic operating parameters have many application benefits in oil and gas industry, particularly the near wellbore remediation. Chemical treatment for near wellbore remediation is purely dependent on mass transfer mechanism and its kinetics. The mechanisms involved in near wellbore remediation are solubilisation and dissolution processes that occur between the nanofluids and the contacting damage media. Solubility and dissolution are two different concepts, but they are interrelated. Solubility is the measure of the maximum amount of solute that may be dissolved in solution at equilibrium, which produces a saturated solution and dissolution generally refers to the process of dissolving or breaking apart of a substance [70],[71]. Thus, the near wellbore remediation mechanism can be described in the following four stages.

1) Diffusion of interacting substances to the damage media surface.
2) Adsorption on the damage media surface.
3) Reaction on the damage media surface.
4) Mass transfer of products i.e., the disintegrate damage media particles away from surface.

Chemical treatment alone has its limitation on the mass transfer kinetics happening during near wellbore remediation. The combination of chemical and external perturbation such as ultrasound treatment for near wellbore remediation will be studied in this chapter to understand the optimum amplitudes of the ultrasonic induction under both isothermal and non-isothermal condition that influence the physio-chemical properties of nanofluids for an effective near wellbore remediation. To achieve the objective, mass transfer kinetics evaluation experiments will be conducted to simulate the near wellbore remediation processes. The following are the experiments outlined for this chapter.

a) Filter cake dissolution test
b) Sand packed column flow test

5.2 Filter Cake Dissolution Test

During overbalanced drilling, an impermeable layer "filter cake" usually forms that often contains an inorganic portion and an organic portion of the drilling fluids. The filter cake must be removed from the near wellbore to prevent hydrocarbon production flow impairment. Conventional methods of filter cake removal consist of contacting and soaking the filter cake with suitable fluids such as solvent, mutual solvent and acids mixed in clear brine [130]. In this research work, we will use nanofluids synthesised using the new method [46] described in chapter 3 to remove the filter cake by the dissolution mechanism. The driving mechanism of this technology is to obtain a near zero free energy state between the novel nanofluids and non-aqueous filter cake which promotes the diffusion of oil phase into nanofluids to form nano emulsion. The spontaneous action of reversing wettability of filter cake from oil wet to water wet disintegrate the solid particles of the filter cake. The effectiveness and reaction time of a breaker fluid in breaking a filter cake on the wall of a wellbore penetrating a subterranean formation is determined by forming a filter cake on a filter medium such as the aloxite disk using drilling mud inside the high temperature high pressure (HTHP) filter press equipment. The filter cake will be soaked with nanofluids generated with various amplitude under isothermal and non-isothermal conditions. The volume fluid passing across the filter medium under static conditions is monitored and recorded over time. An increase in the rate of fluid passing across or through the medium indicates efficiency of the filter cake break -up [131]. The section below details the materials, equipment's and procedure used for filter cake dissolution test.

5.2.1 Materials and Equipment

The following materials and equipment are used for the filter cake dissolution test.

a) 2.5"x0.25" 20-micron Ceramic Filter Disc (aloxite disk)
b) 150ml of each sample of nanofluids labelled as per table 4.1 in chapter 4
c) Saraline 185 V base oil from Shell
d) Double end HTHP filter press cell
e) Measuring cylinder 100ml and 20 ml

f) 10 ppg Oil based Mud from NexusChem
g) Electronic weighing balance

5.2.2 Procedures.

The following procedures are used for the filter cake dissolution test [132],[133].

1) Use 2.5”x0.25” 20-micron Ceramic Filter Disc, 5 Darcies (part No.170-51) as shown in Fig. 5.1 and saturate ceramic filter disc by soaking it in saraline 185 V base oil for 30 minutes to mimic the initial oil saturation reservoir condition.
2) At room temperature pour 300 ml of fresh mud sample into HTHP Cell and start heating the cell to 250°F, and 500 psi differential pressure i.e., 600 psi on top and 100 psi bottom. Once a steady state temperature and pressure of 250°F and 500 psi maintained inside the HTHP cell, allow for filter cake build up for 30 minutes as shown in Fig. 5.2. The details schematic of each part of the HTHP cell are shown in Fig.5.3.
3) After 30 minutes of incubation, cool down the cell to room temperature, and carefully pour the mud out without affecting and disturbing the mud filter cake.
4) Take out the filter cake & the ceramic disc carefully and weigh ceramic disc with filter cake on top and record it as initial weight ***M***i. Carefully place back the filter cake with ceramic disc into the double end cap HTHP cell.
5) Pour 100ml of sonicated nanofluids treated with 0 % amplitude solution into the double end cap HTHP Cell. Taking care not to pour directly onto the filter cake.
6) Apply 100 psi pressure at 250°F temperature into HTHP cell until it reaches steady state and allow the nanofluids soak the filter cake instantly.
7) Open the bottom valve and record the time to collect filtrate and volume while filtrate solution passes through the filter cake disc.
8) Record for every 5-minute intervals until 100 ml filtrate is collected or till there is no more filtrate flow. Retort filtrate for oil-water-solid analysis.
9) Take out ceramic disc with filter cake and weigh ceramic disc with filter cake and record as final weight, ***M*f**. Take photo at the end of the test the condition of the filter cake.
10) Repeat step 1 to 9 for the remaining samples labelled as per table 4.1 in chapter 4.

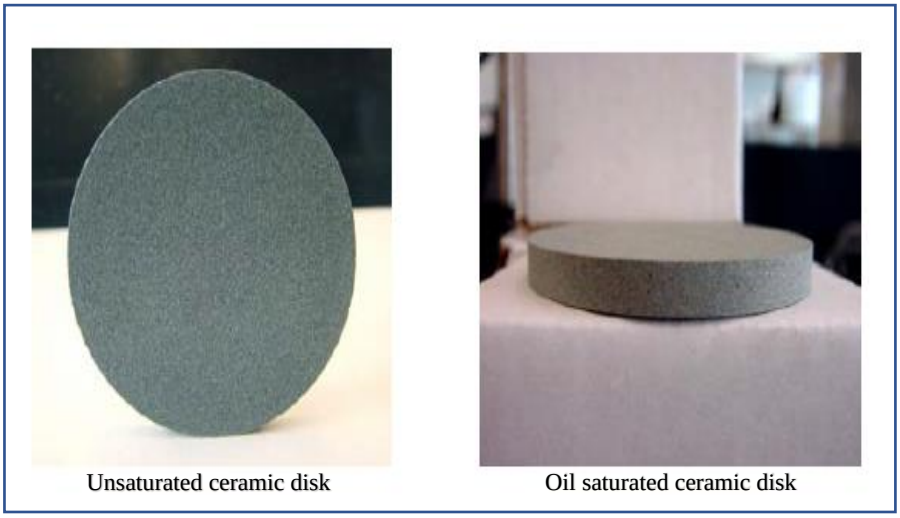

Figure 5.1 : 2.5"x 0.25" 20-micron Ceramic Filter Disc used to mimic standard reservoir pores. A) picture of unsaturated ceramic disc condition, B) Oil saturated ceramic disc condition mimic reservoir with oil wet

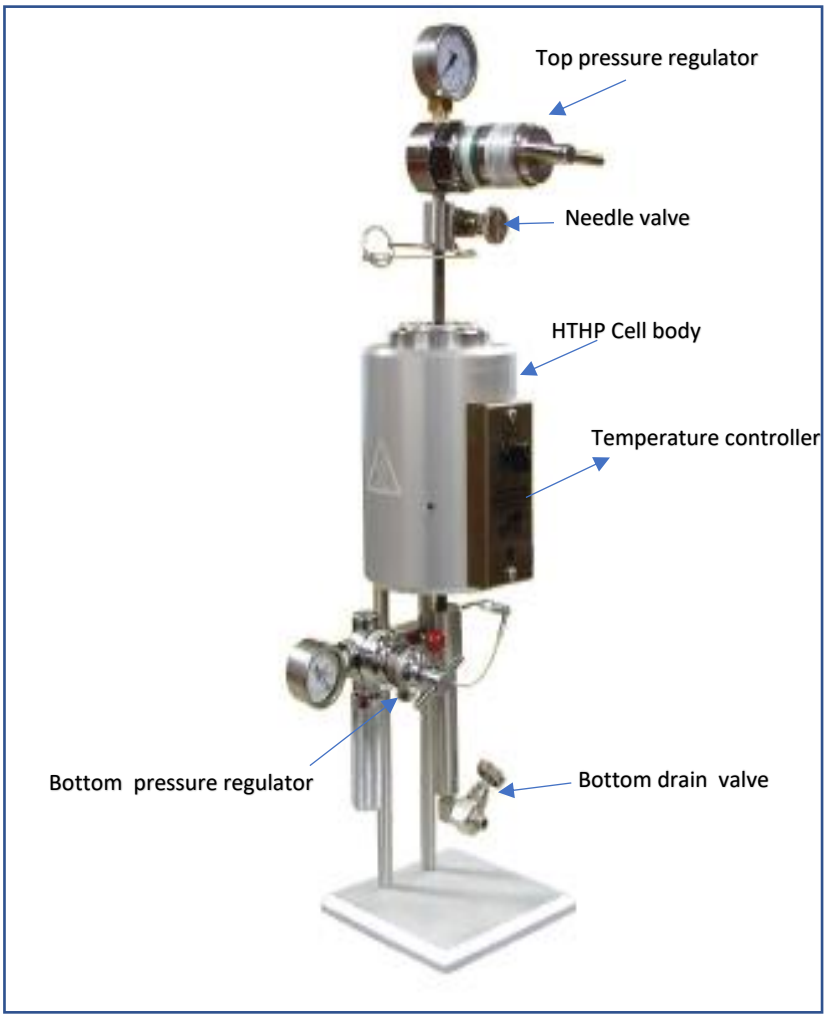

Figure 5.2: Double end cap HTHP filter Press cell experiment kit used in filter cake dissolution test.

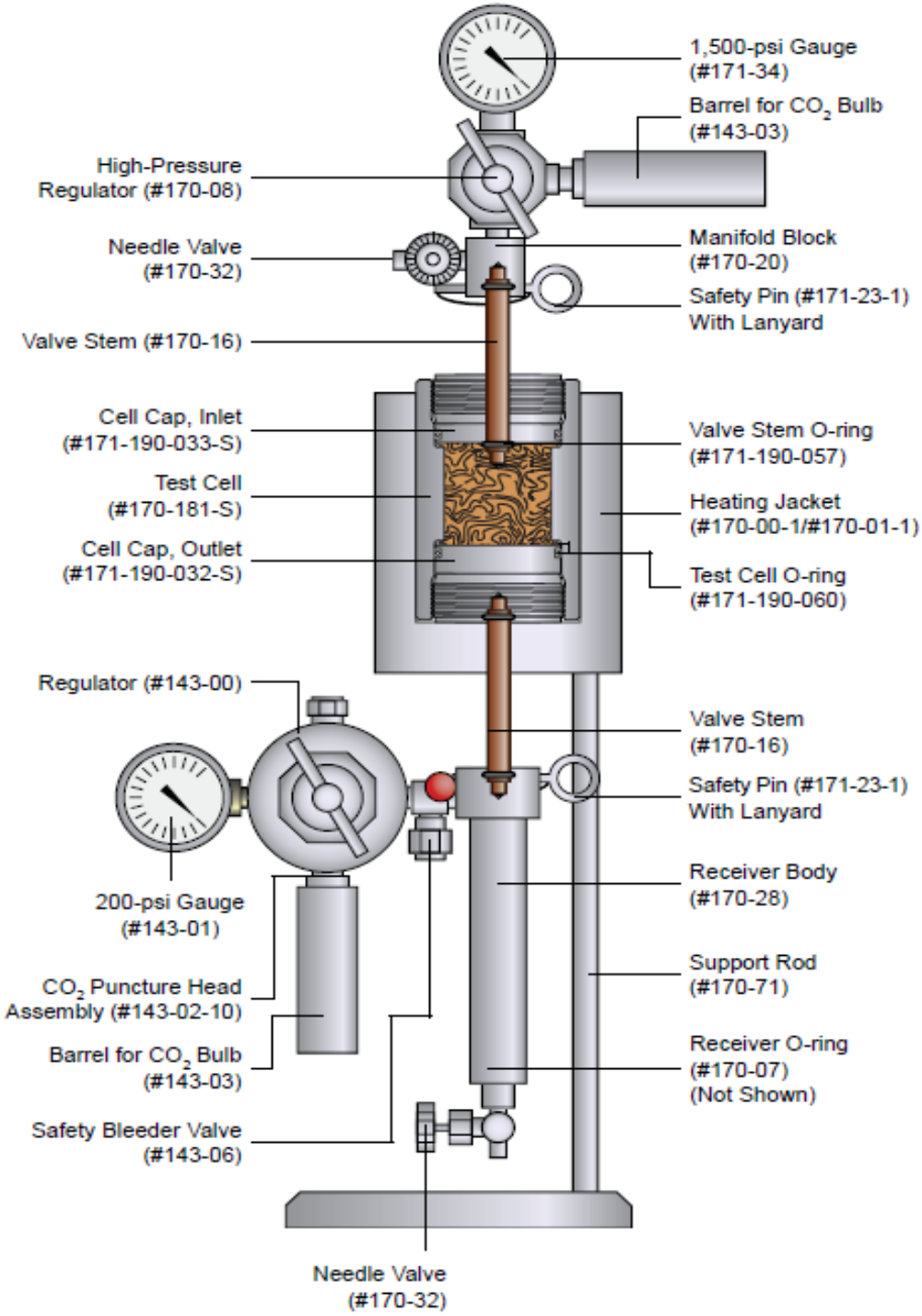

Figure 5.3: Details schematic of HTHP filter Press parts (source: https://www.ofite.com/doc/170-00-7_instructions.pdf).

5.3 Sand Packed Column Flow Test

The sand packed column flow test will be used to evaluate the effectiveness of nanofluids in removing emulsion damage in a reservoir. Emulsion damage is a type of formation damage in which there is a combination of two or more immiscible fluids, including gas condensate, that will not separate into individual components. Emulsions can form when fluid filtrates from drilling or completion brine mixed with reservoir crude oil. This emulsion can create a blockage or reduced permeability of reservoir for the hydrocarbon to flow. A laboratory set up sand packed glass column will be used to conduct this experiment. The dimension of this apparatus will be 370mm x 230mm x 1500mm with working pressure of 0.69Mpa. The cell will have effective filter area of 18 cm^2 with sand volume of 350 cm^3 and remediation fluids volume of 500 ml. The sieved beach sands with size of 20 mesh and 40 mesh with mixed ratio of 2 to 1 will be used to simulate the sandstone reservoir. Crude oil obtained from Petronas Malaysia from Dulang Field will be used as reservoir hydrocarbon fluids. 5% by weight concentration of Sodium chlorine brine will be used as completion fluids to be mixed with the crude oil and simulate the emulsion damage condition in near wellbore matrix. Nanofluids sonicated at various amplitude at both isothermal and non-isothermal condition will used as remediation fluids to remediate the emulsion damage and reverse the reservoir wettability from oil wet to water wet. The efficiency of the nano fluids sonicated at various amplitude in removing emulsion damage will be evaluated and compared by measuring the flowrate of brine into the sand reservoir pre and post treatment. The flowrate of brine into the sand reservoir pre and post treatment with nanofluids will be measured and plotted for comparison. The section below details the materials, equipment's and procedure used for sand packed column flow test.

5.3.1 Materials and Equipment

The following materials and equipment are used for the sand packed column flow test.

a) Sand Packed column Apparatus
b) 20 and 40 mesh refined beach sand
c) Crude oil from Petronas Dulang field
d) 5 % Sodium Chloride brine
e) 500 ml of each Nanofluids samples labelled as per Table 4.1 in chapter 4
f) Measuring cylinder 10 ml , 50 ml and 100 ml
g) 500 ml Beaker

h) Stopwatch
i) Vacuum Pump

5.3.2 Procedures

The following procedures are used for the sand packed column flow test [134],[135].

1) Set up the sand packed column apparatus as shown in Fig. 5.4.
2) Placed 350 ml of sand with particle sized between 20 mesh and 40 mesh with ratio of 2 to 1 into the transparent glass column fitted with 10 mesh filter screens at the bottom cap.
3) Pour 350 ml of sodium chloride brine and close both upper and bottom seal cap and apply 100 psi pressure from the top for 10 minutes. Bleed the pressure off and open the valve at bottom to drain the sodium chloride brine. This will make the sand particles compacted.
4) Use vacuum pump to suck dry the sodium chloride brine from the bottom outlet.
5) Mix 35ml of crude oil and 35 ml of 5 % by weight sodium chloride brine in Hamilton mixer to make emulsion.
6) Open the top seal cap of the sand packed column and pour the mixture emulsion into the sand packed column and let it soak and settled within the sand porous matrix for 30 minutes.
7) Pour 350 ml of 5% by weight of sodium chloride brine and closed the top cap. Close both the top and bottom valve and apply 100 psi pressure and regulate till the pressure is constant for an hour.
8) Record the volume of brine filtrate volume for every 15 minutes interval for 120 minutes. Establish this flowrate as pre-treatment data.
9) Once the brine fully drained out, follow procedure 7 by replacing brine with 350 ml of nanofluid that was sonicated. After an hour fully drain the nanofluids.
10) Repeat procedure 7 and 8 and established this flowrate as post treatment data.
11) Repeat procedures 1- 10 for all the samples of nanofluids labelled as per table 4.1 in chapter 4. Make sure the glass cylinder is cleaned each time prior to repeat the test with nanofluids. Use clean sand for each test. Record the results and take photo for each test.

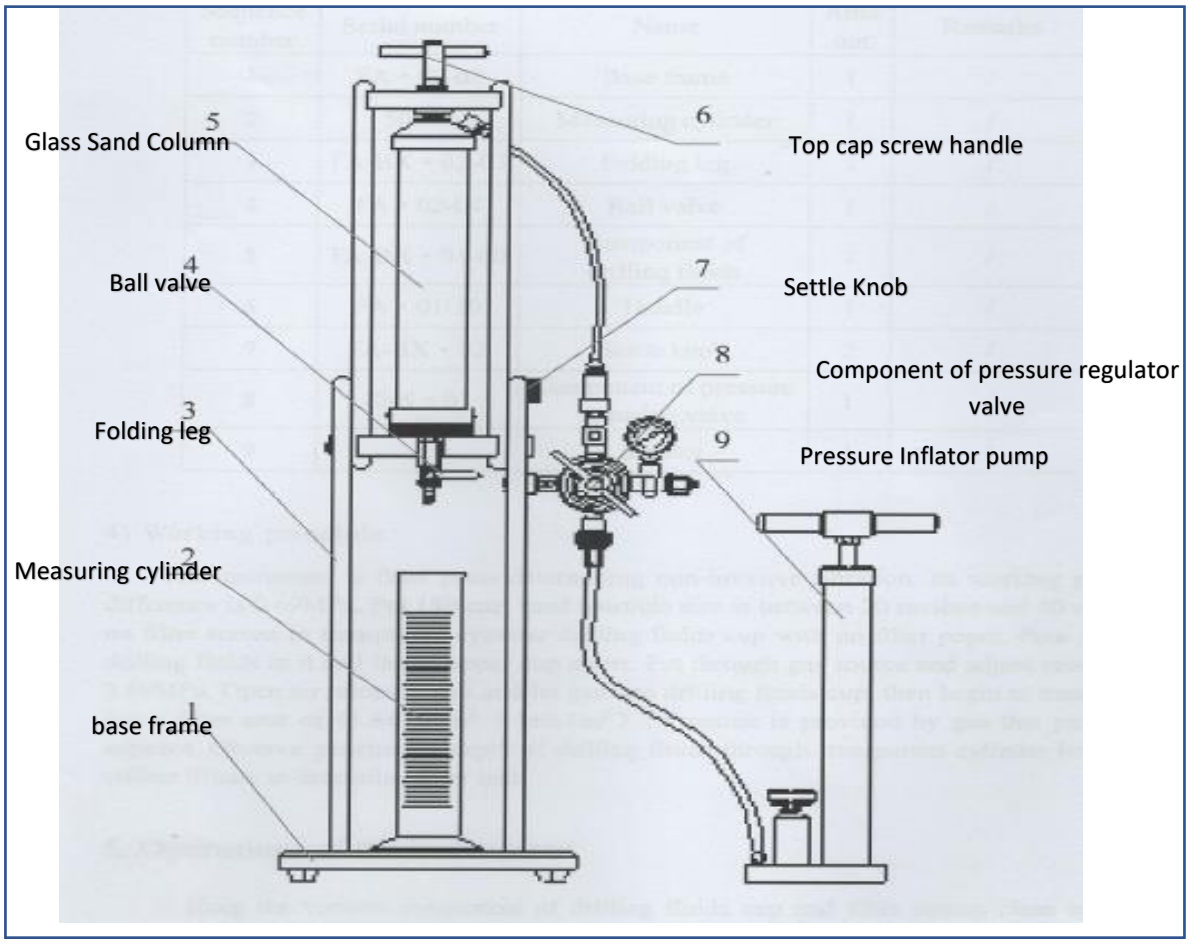

Figure 5.4: Schematic of sand packed column apparatus

5.4 Observation and Remarks

The following section will discuss on observations and analysis done on the mass transfer kinetics evaluation based on the theoretical fundamentals of mass transfer mechanism during near wellbore remediation [85], [136] and its correlation to enhance oil recovery.

5.4.1 Filter Cake Dissolution Test

The filter cake dissolution test can be evaluated based on three key parameters, **average filter cake dissolution rate, cake removal % efficiency and oil/water content % analysis.**

1) Filter cake dissolution rate results for the nanofluids treated at five different amplitudes with 500-watt power and 20KH frequency for both the isothermal and

non-isothermal conditions been tabulated in table 5.1. The operating parameters for the experiment inside the HTHP cell were fixed to match a typical reservoir condition of 250 ^{o}F and 500 psi differential pressure as shown in Fig. 5.5. The results are plotted as Fig. 5.6 for isothermal and Fig. 5.7 for non -isothermal condition. The base case, at 0% amplitude plotted in Fig. 5.8. The average filter cake dissolution rate is directly proportional to the rate of filtrate volume flow pass through the filter cake and ceramic disk referred as total filtrate volume [137],[138]; thus, it is calculated based on the following formula.

(source: https://mathinsight.org/approximating_nonlinear_function_by_linear).

Average filter cake dissolution rate = (Total filtrate volume)/(Total Time) (5.1)

Table 5.1: Average filter cake dissolution rate at various amplitudes for both isothermal and non-isothermal conditions

Isothermal				Non-Isothermal		
Amplitude %	Total Filtrate volume (ml)	Total Time (min)	Avg Filter cake dissolution rate (ml/min)	Total Filtrate volume (ml)	Total Time (min)	Avg filter cake dissolution rate (ml/min)
0	100	70	1.43	100	70	1.43
20	100	105	0.95	99	55	1.80
40	100	80	1.25	98	63	1.56
60	99	70	1.41	98	45	2.18
80	100	60	1.67	98	165	0.59
100	100	50	2.00	100	145	0.69

Remarks

The observation from the above table indicates that the average filter cake dissolution was highest for the nanofluids sonicated at 60% amplitude under non isothermal condition. We can say that the rate dissolution rate almost double for when the fluids sonicated at 60% amplitude under non-isothermal compared to isothermal condition for the same amplitude. However, the average dissolution rate dropped almost one third for the amplitude higher than 60% under non isothermal condition in comparison to isothermal condition.

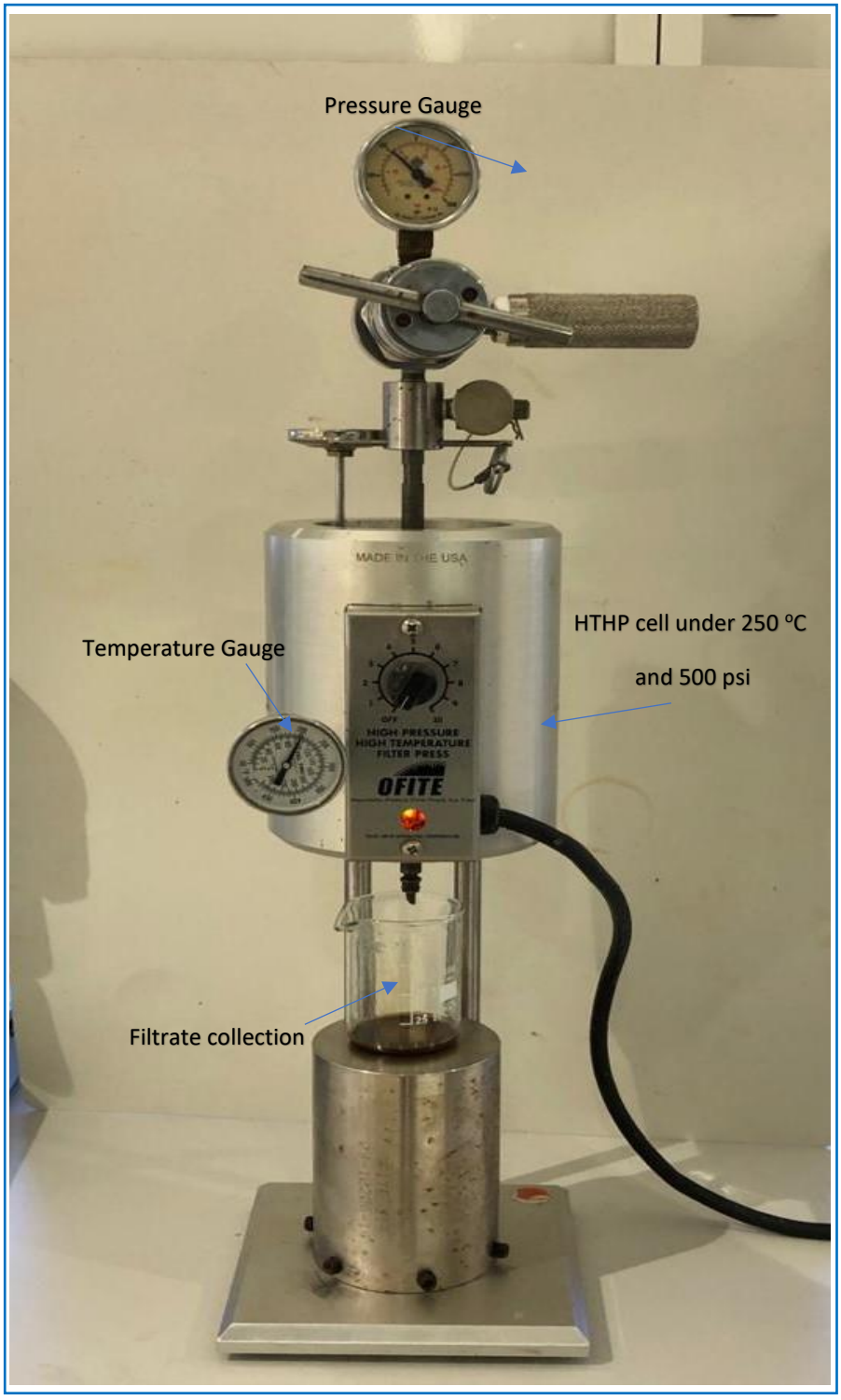

Figure 5.5: Filter cake dissolution test with HTHP filter press cell

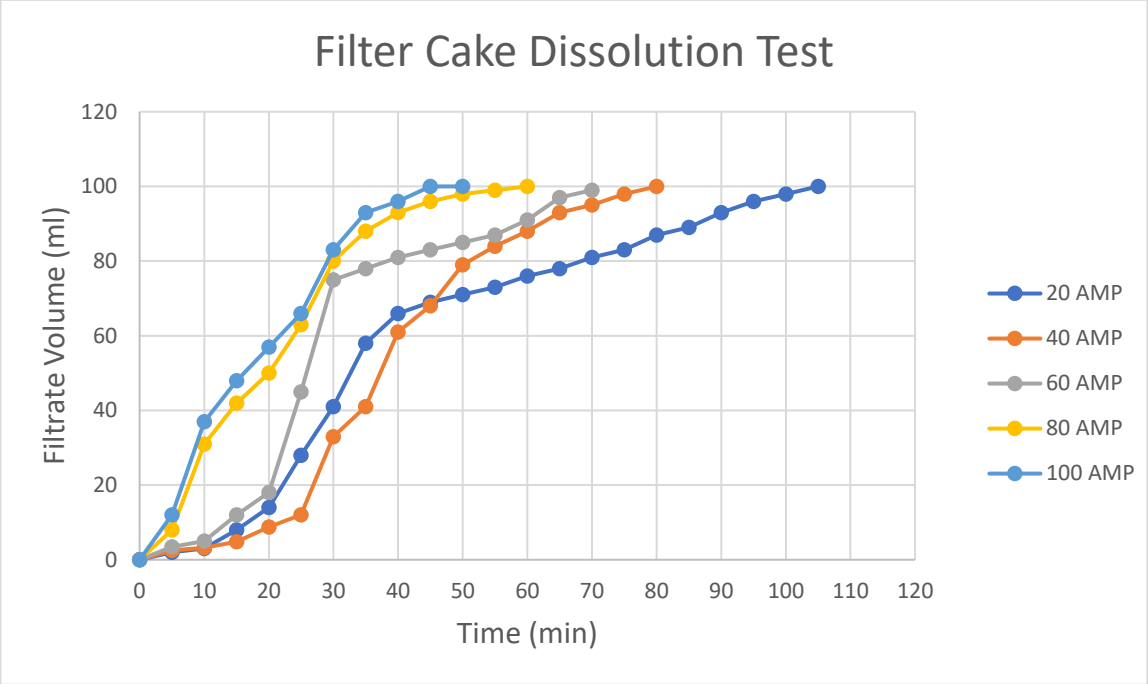

Figure 5.6: Filter cake dissolution rate under isothermal condition

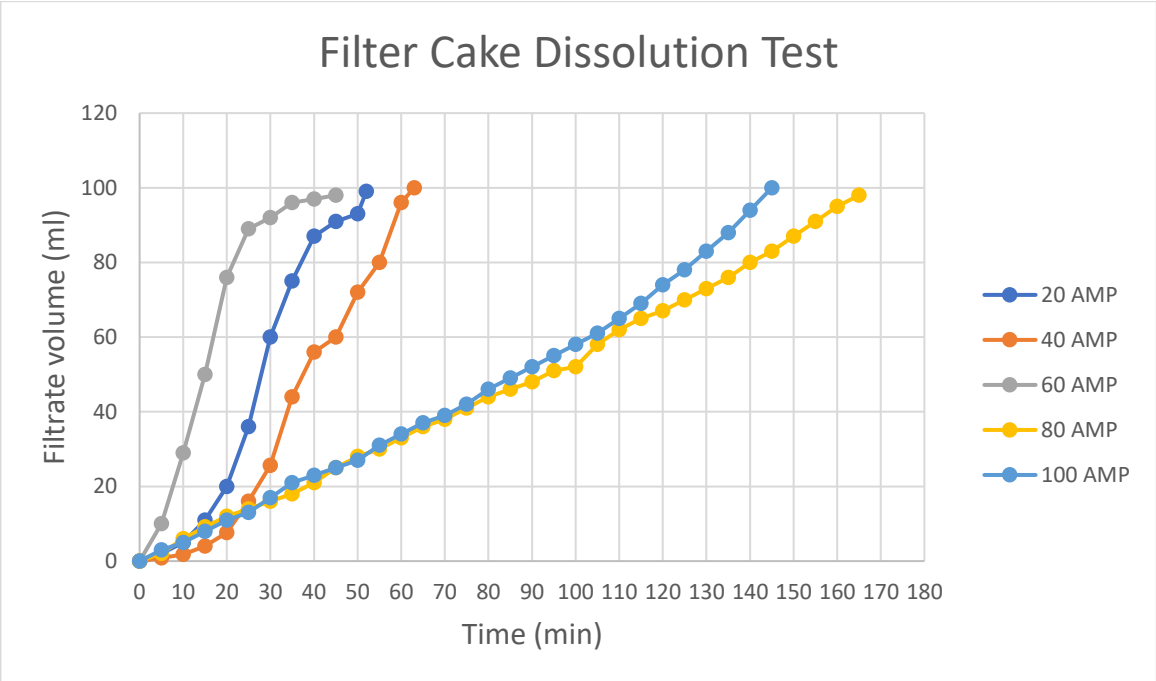

Figure 5.7: Filter cake dissolution rate under non-isothermal condition

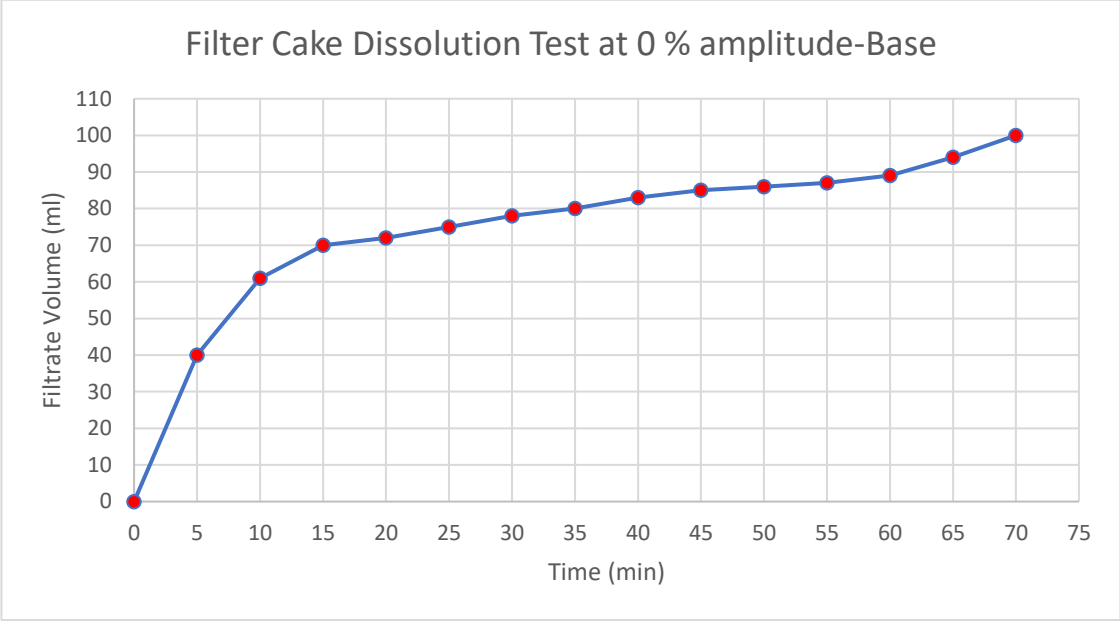

Figure 5.8: Filter cake dissolution rate for the base case, 0% amplitude

2) The filter cake removal % efficiency is calculated based on the following formula [138],[139].

$$\textbf{Filter Cake removal \% efficiency} = [(M_i - M_f)/(M_i - M_{fp})] \times 100\ \% \quad (5.2)$$

Where,

***M*i** is the weight of initial filter cake with filter paper.

***M*f** is the weight of final filter cake with filter paper.

***M*fp** is the weight of blank filter paper = 0.3 gram.

The filter cake condition before and after dissolution is shown in Fig. 5.9 as an example. The summary of filter cake removal efficiency % are tabulated in table 5.2 for samples of nanofluids treated at various amplitude % for both the isothermal and non-isothermal conditions.

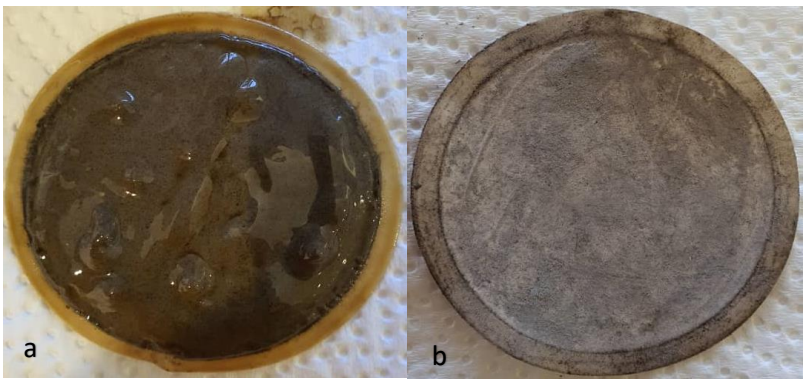

Figure 5.9 : a) initial filter cake condition , b) After treatment filter cake condition

Table 5.2: Summary of Filter Cake removal % Efficiency

				Non-Isothermal		
Amplitude %	Initial Filtercake weight ,g (***M***i)	Final Filtercake Weight ,g(***M***f)	Filter Cake removal % efficiency	Initial Filtercake weight,g (***M***i)	Final Filtercake Weight,g(Mf)	Filter Cake removal % efficiency
0	5.14	3.35	37.0	5.20	3.45	35.7
20	5.18	3.86	27.0	5.16	1.78	69.5
40	5.12	3.61	31.3	5.18	2.12	62.7
60	5.08	3.10	41.4	5.16	1.43	76.75
80	5.12	2.25	59.5	5.10	3.98	23.3
100	5.14	2.05	63.8	5.13	3.75	28.6

Remarks

The observations indicate the maximum filter cake efficiency is achieved when the nanofluids was sonicated at 60% amplitude under non-isothermal conditions. It was observed also that the filter cake removal efficiency dropped significantly for higher amplitude under non-isothermal condition. Totally opposite trend observed for isothermal condition where higher amplitude improve filter cake removal efficiency. We can corelate such behavior to free volume theory and structural changes of the micellar. Under isothermal condition the "relaxed" micellar structural changes were favouring the enhancement of mass transfer as we increased the amplitude with exception for the 20% amplitude. However, for the non-isothermal condition, a fluctuating trend was observed

where the micellar structural changes back and forth between “relaxed and agglomerated structured” when we varied the amplitude. The optimum loose structure of the micellar was achieved at 60% amplitude promoting the maximum mass transfer enhancement during the well remediation process. This observation further validates the viscoelastic behavior of nanofluids due to changes in amplitude.

3) The Nanofluids initial condition and after remediation treatment condition is compared as shown in Fig. 5.10. The oil phase from the filter cake was fully diffused into the nanofluids which is an aqueous phase forming a stable single-phase fluid collected as filtrate [140].

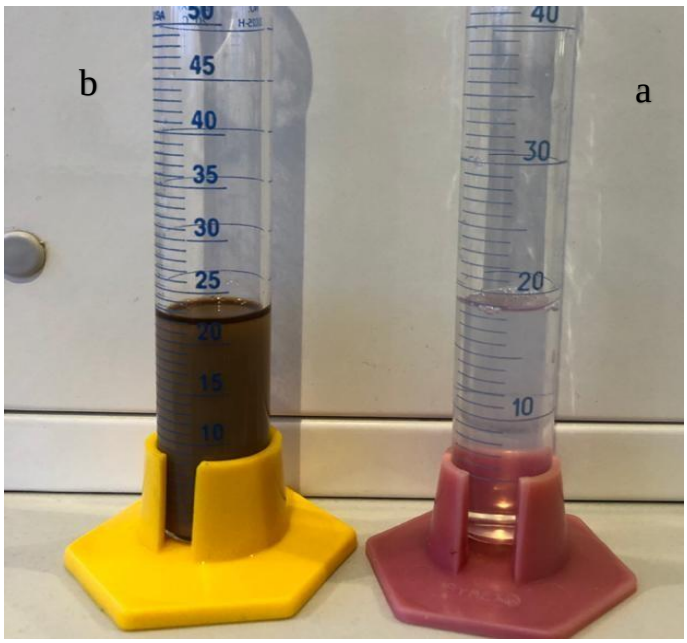

Figure 5.10: a) initial nanofluids condition, b) After treatment nanofluids (filtrate) condition

The stable filtrate phase, oil and water content analysis was done using the Retort apparatus. The retort works on distilling concept to separate the oil and water phase. Retort oil and water analysis was done on the filtrate collected over five minutes time interval to study the diffusion of oil into nano fluids for all the nanofluids sample sonicated at various amplitudes under both the isothermal and non-isothermal conditions. The example of filtrate retort test is shown in Fig. 5.11. Table 5.3 and 5.4 summarise the oil and water phase (nanofluid) analysis of the filtrate collected for both conditions at various amplitudes. The example of distilling fluid for oil and water separation using retort is shown in Fig. 5.12.

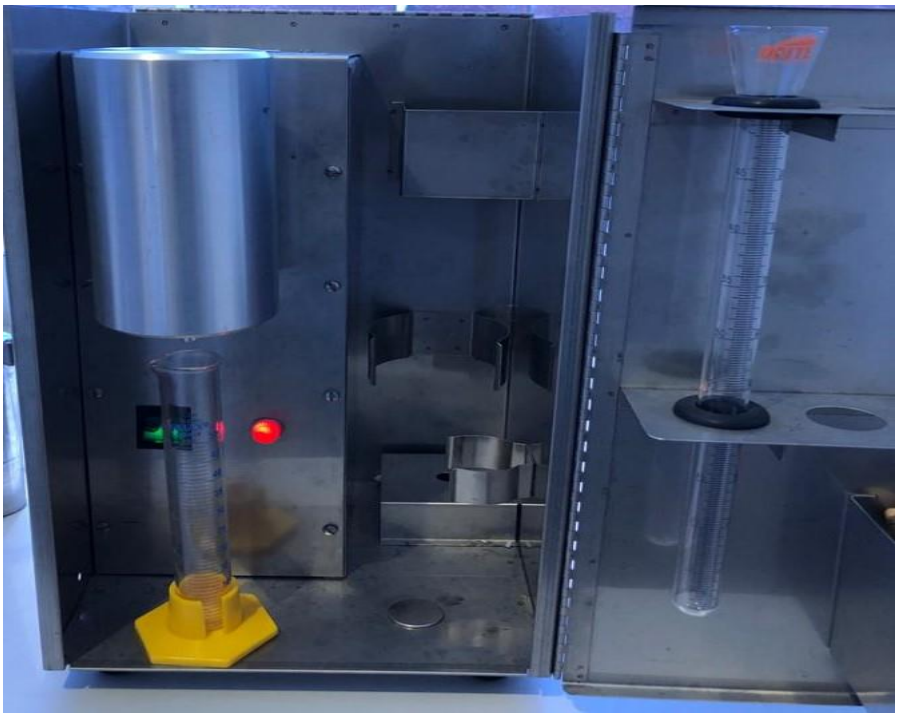

Figure 5.11: Retort test for analysing oil and water contents of filtrate

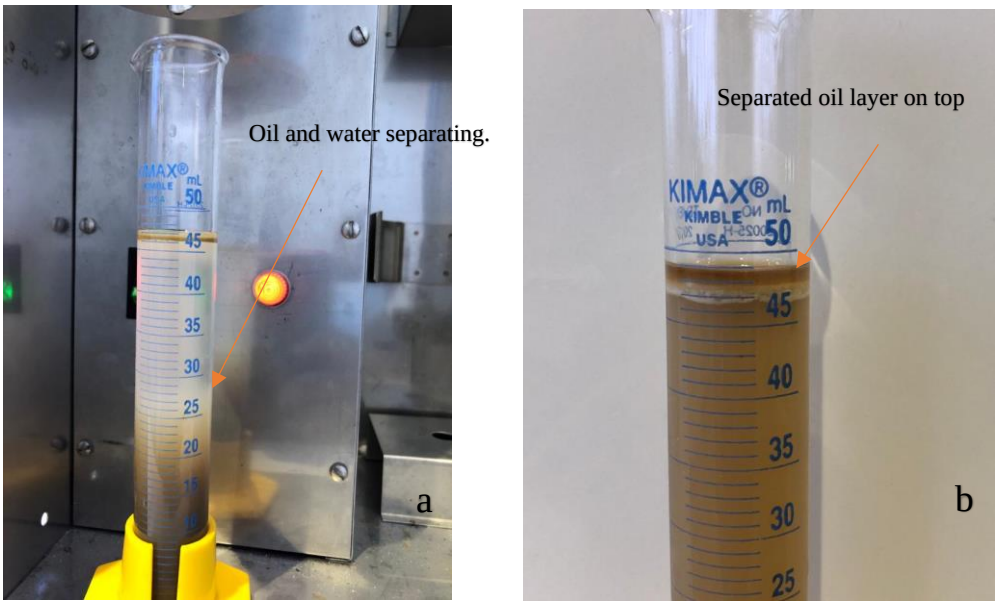

Figure 5.12: a) Filtrate phase separating between oil and water phase, b) After phase separation settled.

Table 5.3: Summary of filtrate retort oil-water % analysis for isothermal and non-isothermal conditions.

Isothermal				Non-Isothermal		
Amplitude %	Final Filtrate Volume (ml)	Oil contents (ml)/%	Water contents (ml)/%	Final Filtrate Volume (ml)	Oil contents (ml)/%	Water contents (ml)/%
0	100	3.2/3.2	96.8/96.8	100	3.2/3.2	96.8/96.8
20	100	3.4/3.4	96.6/96.6	100	4.4/4.4	94.6/94.6
40	100	3.9/3.9	96.1/96.1	100	4.1/4.1	93.9/93.9
60	99	4.1/4.14	95.9/96.9	100	4.9/4.9	93.1/93.1
80	100	4.3/4.3	95.7/95.7	98	2.7/2.8	95.3/97.2
100	100	4.5/4.5	95.5/95.5	100	3.1/3.1	96.9/96.9

Table 5.4: Summary of filtrate oil volume % at various amplitude over period of time for non-isothermal from retort analysis.

Non-Isothermal					
Time (min)	20% Amp Filtrate oil Volume %	40% Amp Filtrate oil Volume %	60% Amp Filtrate oil Volume %	80% Amp Filtrate oil Volume %	100% amp Filtrate oil Volume %
0	0.0	0.0	0.0	0.0	0.0
5	0.0	0.0	0.5	0.0	0.0
10	2.0	0.0	2.2	0.0	0.6
30	2.8	1.5	3.2	1.6	1.8
45	4.1	2.8	4.4	2.1	2.4
60	4.4	3.8	4.7	2.4	2.7
100	4.4	4.1	4.9	2.8	3.1

Remarks

The analysis from the data gathered in table 5.3, we can conclude that the diffusion of oil from the filter cake increase gradually over time when we increased the amplitudes. However, for non-isothermal sonication, the diffusion of oil fluctuates when we increased amplitudes. It was showing opposite behavior as diffusion of oil decreases at higher amplitudes, with exception for the optimum 60% amplitude. These observations support the theory that varying amplitudes under temperature influence provide different micellar structural, leading to changes in physiochemical properties, thus influences the mass transfer kinetics during near well remediation process [140],[141].

The data from table 5.4 was used to plot a comparative graph of the oil volume % in the nanofluids filtrate sonicated at five different amplitudes under non isothermal. The graph is as shown in Fig.5.13. The observation indicates that the maximum oil diffusion into nanofluids achieved at amplitude 60%. This plot shown in Fig.5.13 that derived from experimental will be compared with the plot derived from Ansys Fluent CFD simulation of the filter cake dissolution in chapter 6.

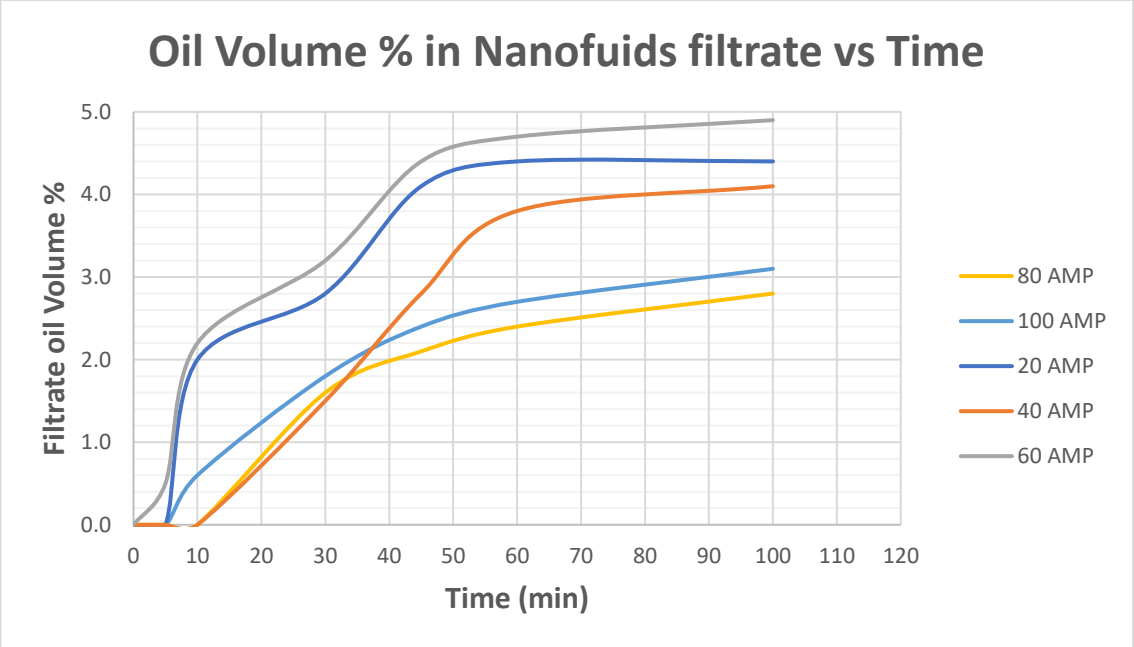

Figure 5.13: Experimental plot of oil volume % of the nanofluids filtrate at various amplitude % over dissolution time using retort experiment for non-isothermal condition.

5.4.2 Sand Packed Column Flow Test

The observation and analysis of sand packed column flow test evaluation[142], [143] on all the nanofluids samples sonicated at five different amplitudes under both isothermal and non-isothermal conditions have been captured in Table 5.5. The pre-treatment brine flow rate experiment as shown in Fig.5.14 was established as a benchmark to compare the flow improvement observed after treatment [144],[145] with all the nanofluids samples labelled in table 4.1 in chapter 4. The comparative plot of brine flowrate recorded after treatment with the nanofluids sample that sonicated at various amplitude under isothermal and non-isothermal are shown in Fig. 5.15 and Fig.5.16.

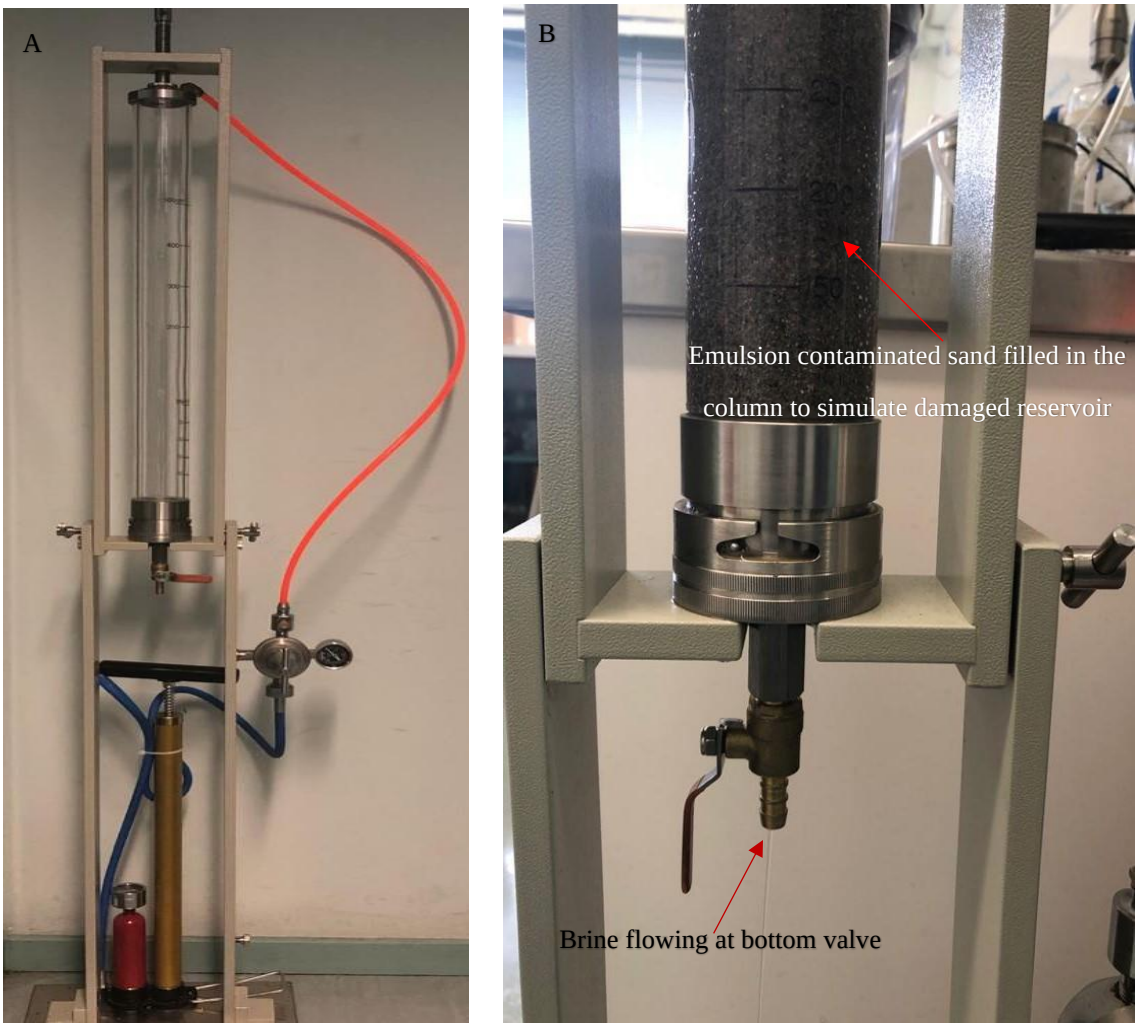

Figure 5.14: A) picture of empty sand packed column, B) picture of sand packed column filled with emulsion contaminated sand. Brine was filled and flowrate was determined for pre-treatment flowrate as a benchmark.

Table 5.5: Summary of brine flowrate of the sand packed column flow test for isothermal and non-isothermal conditions for duration of 120 minutes

Pre-Treatment Brine flow					
Time (min)	Flow volume (ml)				
15	12				
30	18				
45	33				
60	54				
75	68				
90	78				
105	92				
120	103				
Isothermal					
Time (min)	20% Amp Flow Volume (ml)	40% Amp Flow Volume (ml)	60% Amp Flow Volume (ml)	80% Amp Flow Volume (ml)	100% amp Flow volume (ml)
15	31	38	48	45	52
30	63	72	88	96	102
45	89	93	97	105	117
60	108	112	110	118	139
75	123	132	129	136	147
90	133	143	145	152	161
105	156	162	171	185	192
120	182	202	198	208	221
Non-Isothermal					
Time (min)	20% Amp Flow Volume (ml)	40% Amp Flow Volume (ml)	60% Amp Flow Volume (ml)	80% Amp Flow Volume (ml)	100% amp Flow Volume (ml)
15	65	51	95	26	35
30	78	85	125	52	59
45	81	102	147	68	74
60	132	119	172	83	88
75	152	130	195	106	116
90	170	149	229	122	126
105	198	168	265	138	136
120	238	194	302	156	165

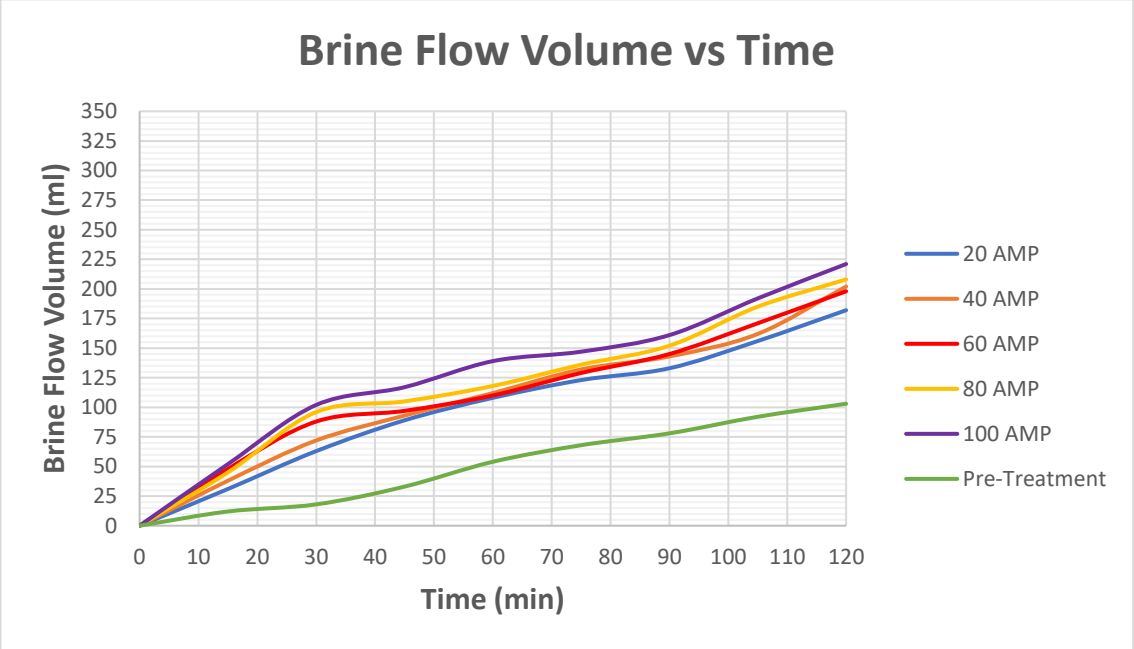

Figure 5.15: Graph plot of sand pack column flow brine flowrate for various amplitude under isothermal condition comparison with pre-treatment flowrate.

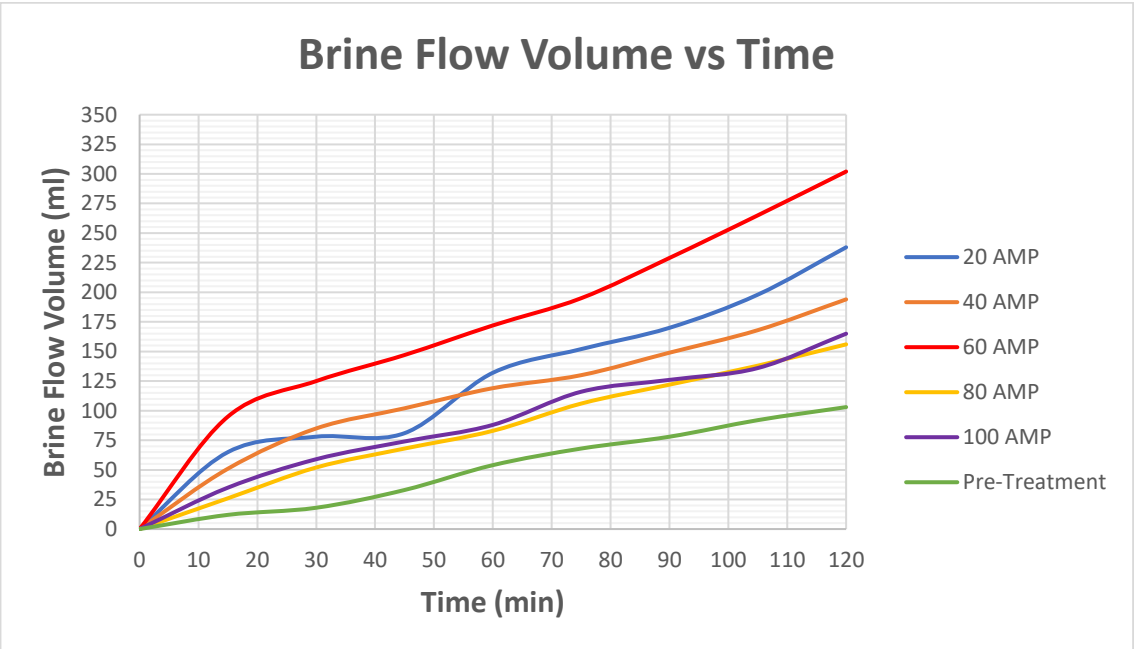

Figure 5.16: Graph plot of sand pack column flow brine flowrate for various amplitude under non-isothermal condition comparison with pre-treatment flowrate

Remark

The sand in the packed column initially been saturated with emulsion to represents the pore matrix damaged by emulsion blocking or reducing the flow channel of brine. Simulating the condition of brine flooding of enhance oil recovery process, the pre-treatment flowrate of brine was established as the benchmark for the damaged reservoir blocking the brine flow. The observations indicate all nanofluids samples improve the brine flowrate after it has been exposed to the damaged sand reservoir as a remediation fluid [146]. The nanofluids removes the emulsion blockages by diffusing the oil from the emulsion trapped in the sand pores, thus improving the brine flow rate. It changes the sand wettability from oil wet to water wet [10]. Nanofluids sonicated at various amplitude under isothermal condition showed a gradual brine flow improvement when we increase the amplitudes. However, for non-isothermal conditions, the maximum improvement achieved at optimum amplitude of 60%. The flow improvement was significant compared to pre-treatment base case, supporting the concept of importance of near wellbore remediation for the success of enhance oil recovery process.

5.5 Closure

This chapter presents the observations and analysis done on nanofluids that undergone sonication at five different amplitudes % under isothermal and non-isothermal conditions for their performance evaluation of enhancing mass transfer kinetics during a near wellbore remediation process. Filter cake dissolution and sand packed column flow experiments were used for this evaluation. Among the key performance indicators were filter cake dissolution rate, filter cake removal efficiency, oil content % retort analysis and brine flow rate or flow volume over a fixed time interval [135],[147],[148]. The observation from the experiments conducted indicate that external perturbation such as ultrasonic does alter the mass transfer kinetics, such as the oil diffusion rate into nanofluids aqueous phase. Changing the operating parameters, such as the sonication amplitude and process conditions that influence the system temperature, we were able to manipulate and achieve the desired physio-chemical properties that suitable for near wellbore remediation application. It is obvious from the observation that non-isothermal process condition and an optimum 60 % amplitude provide the most favourable physio-chemical properties of the nanofluids that promote maximum mass transfer kinetics for near wellbore remediation. We also learned that by varying amplitudes and process

conditions we able to increase or decrease the mass transfer kinetics without changing the nanofluids formulation.

The results of mass transfer kinetics particularly, the oil contents % analysis of the nanofluids from the filter cake dissolution test at 60% amplitude under non-isothermal condition from this chapter will be used for comparison with results obtained from Ansys Fluent simulation of the filter cake dissolution in the next chapter. The nanofluid properties for the Ansys Fluent simulation and operating condition will be based on experiment set up and experiment results obtained in **chapter 4**.

CHAPTER 6 Interphase Mass Transfer Simulation

6.1 Introduction

In the previous chapter, we have conducted an experimental investigation on the effect of various amplitude % of an ultrasonic induction on mass transfer kinetics of a filter cake dissolution process that occur during near wellbore remediation. The experimental results of oil volume % in nanofluids were plotted over time as one of the parameters for mass transfer kinetics evaluation. We have concluded that the non-isothermal sonication provides an efficient nanofluids for near wellbore remediation. In this chapter, we will focus on modelling and simulation of the effect of various amplitude % of non- isothermal sonication on mass transfer kinetics of filter cake dissolution during near wellbore remediation. The main purpose of this simulation is to generalise the outcome of the experimental works carried out in the **chapter 5** and to conceptualize affirmative recommendations for the nanofluids design and synthesis protocol for near wellbore remediation application.

6.2 Modeling Approach

We will use a commercial computation fluid dynamic (CFD), Ansys Fluent for the simulation. The underlying physical process comprises a transport of oil particles from solid phase to the liquid phase of nanofluids. This process takes place across solid–fluid interfaces as shown in Fig. 6.1 and constitute mainly dissolution and disintegration of oil solid phase into liquid nanofluids phase. These mass transfer processes are crucial in near wellbore remediation involving flow and transport in porous media of filter cake. The oil fraction in nanofluids over time interval plot from the CFD simulation will be compared with experimental plot to validate the model chosen.

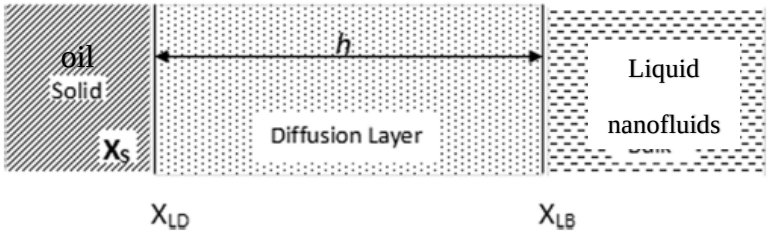

Figure 6.1: Schematics of various dissolution regions and symbols representing the state and location of a solute at solid−liquid interface, diffusion layer, and bulk medium [149].

6.3 Model Description

The CFD particle dissolution model is developed using the multiphase flow solver available in ANSYS-FLUENT (v15.0). The model is assumed isothermal with a constant temperature of 250 ^{0}C. The multiphase model consists of two components: oil solid particles (solute) and liquid nanofluids (solvent). The interphase mass transfer during filter cake dissolution is inherently a micro pore-scale process across fluid–solid interfaces, a situation where two phases, a wetting phase referred as α-phase and a non-wetting phase, referred as β-phase are brought in contact as shown in Fig. 6.2. Ideally, when the two phases are brought in contact (time $t = t_0$), equilibrium is rapidly established directly at the interface. In another word, relating to mass transfer, this means that the concentration of non-wetting phase particles in the wetting phase at the interface as well as the concentration of wetting-phase particles in the non-wetting phase at the interface are both at their equilibrium values, $C^2_{1,eq}$ and $C^1_{2,eq}$. At $t = t_0$, away from the interface, there is still no presence of α-phase particles in the β-phase [150]. After some time, at $t = t_1$, concentration profiles develop within the phases. However, within the bulk phases, the concentrations are still different from the respective equilibrium concentration at the interface. Considering later point of time, $t = t_2$, the equilibrium concentration is finally reached everywhere in the bulk phases as described in Fig. 6.3.

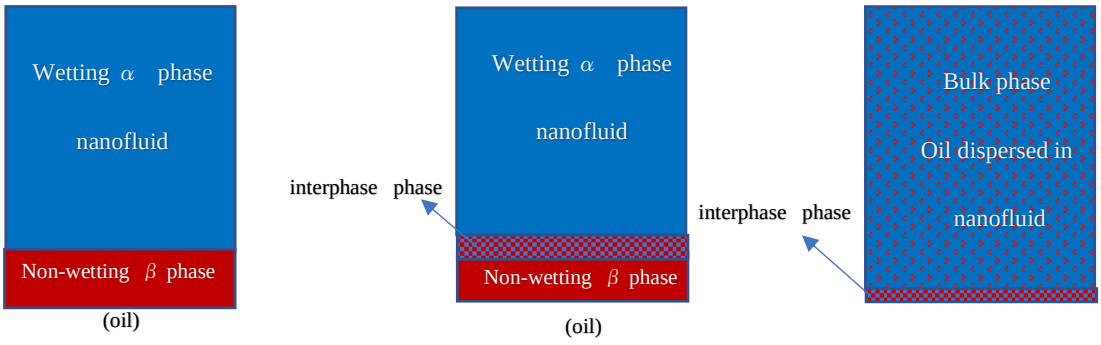

Figure 6.2: Micro pore-scale picture of interphase mass transfer

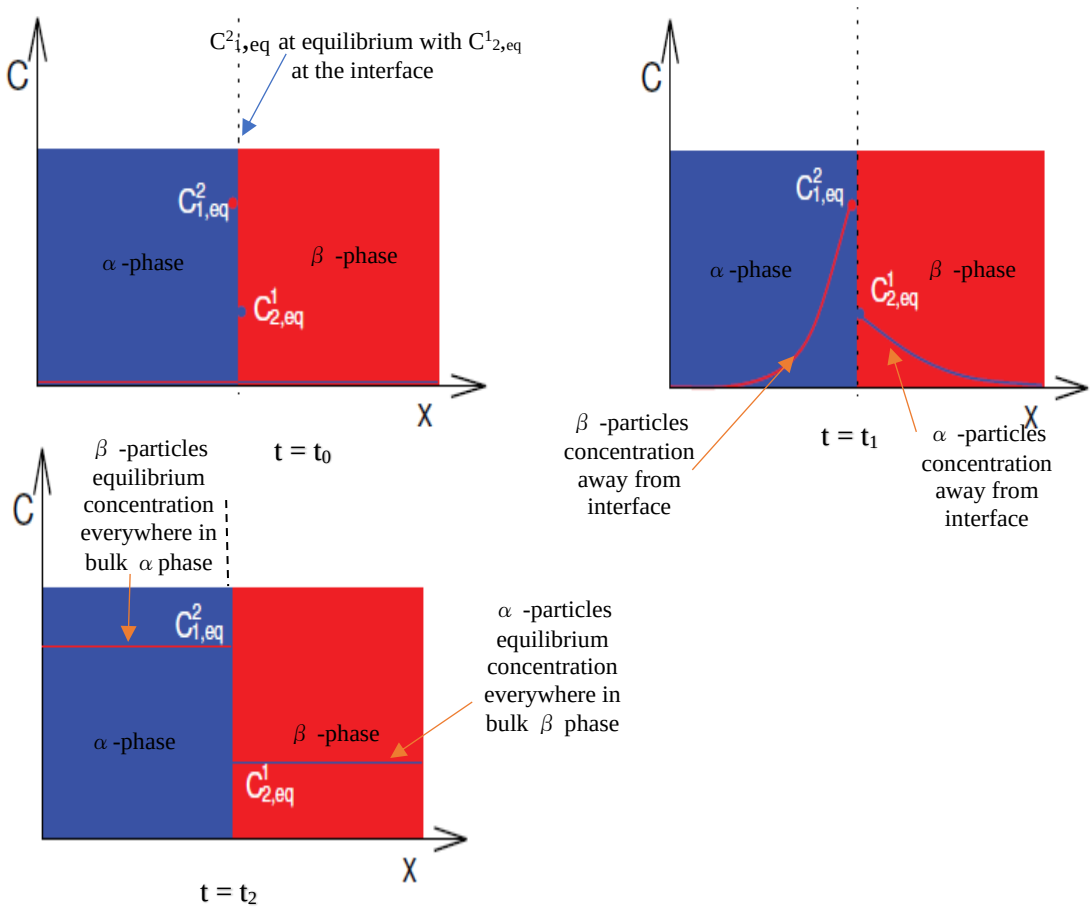

Figure 6.3: α and β phase concentration at various time.

6.3.1 Governing Mass Equation

The dissolution of a solid oil phase into liquid phase seems to be a simple problem. It is a transient flow phenomenon that occurs until the concentration of oil in nanofluids reaches the solubility limit. Dissolution of the solid substance is controlled by the slowest reaction stage, which is the diffusion of dissolved oil compound from the solid surface into nanofluids phase. Thus, our theoretical model will be based on diffusion limited dissolution model [149]. The early mathematical foundations of dissolution as diffusive process are based on the work of Noyes and Whitney. The Noyes−Whitney equation states that the dissolution rate of a solid is proportional to the difference between its solubility and its bulk concentration when constant surface area is maintained in the dissolution process. This concentration gradient approach, inspired by Fick's first law [149],[151],[152]. The surface area of solid phase does not remain constant in our modelling as the surface area of dissolving particles changes as mass is removed. Thus,

the following modified Nernst-Brunner equation will be used as the governing mass transfer equation for filter cake dissolution as it addresses the dynamic nature of surface area during the dissolution process [152].

$$\frac{dm}{dt} = \frac{DA(t)\,(C_s - C_b)}{L} = k_c\,A(t)(C_s - C_b) \tag{6.1}$$

Where: m is the total dissolved mass, A is the total exposed surface area of the dissolving particle at time t, D is the diffusion coefficient of the solute in the solvent, L is the thickness of the boundary layer of unstirred solvent surrounding the particle, C_s is the solubility of the solvent in the solute (the highest possible solute mass concentration in the solvent at present conditions), and C_b is the mass concentration of the dissolved species in the entire solvent volume under consideration.

6.3.2 Ansys Fluent Interphase Mass Transfer Multiphase Mixture Model

Ansys Fluent will be used to solve the interphase species mass transfer using the multiphase mixture model. The mixture model, like the volume of fluid (VOF) model, uses a single fluid approach. It differs from the volume of fluid (VOF) model in two respects [153]:

1) The mixture model allows the phases to be interpenetrating. The volume fractions α_l and α_s for a control volume can therefore be equal to any value between 0 and 1, depending on the space occupied by phase *l* and phase *s*.
2) The mixture model allows the phases to move at different velocities using the concept of slip (or drift) velocities.

6.4 Model Formulation

To model interphase species mass transfer, phase species transport partial differential equations are solved along with the phase mass, momentum, and energy equations. Since the model is isothermal the energy conservation equation is not applicable. The governing partial differential equations describing mass conservation and momentum are presented in equations given below. We let the subscripts '*S*' and '*l*' denote the solid and liquid phases, respectively. The continuity equation then takes the form [154]:

Liquid phase:

$$\frac{\partial}{\partial t}(\rho_l \alpha_l) + \nabla(\alpha_l \rho_l \mathbf{U}_l) = \dot{m}_{ls} - \dot{m}_{sl} \tag{6.2}$$

Solid phase:

$$\frac{\partial}{\partial t}(\rho_s \alpha_s) + \nabla(\alpha_s \rho_s \mathbf{U}_s) = \dot{m}_{sl} - \dot{m}_{ls} \tag{6.3}$$

where **U** denotes the velocity, while ρ, α and t, denote the density, volume fraction and time, respectively. $\dot{m}_{ls}$ and $\dot{m}_{sl}$ represents the mass flow rate from the solid phase into the liquid, and from the liquid phase to the solid phase per unit volume, respectively. In three dimensional cartesian coordinates, ∇ which vector differential operator can be written as:

$$\nabla = \vec{e}_x \frac{\partial}{\partial x} + \vec{e}_y \frac{\partial}{\partial y} + \vec{e}_z \frac{\partial}{\partial z} \tag{6.4}$$

The momentum equations can be written as:

Liquid phase:

$$\frac{\partial}{\partial t}(\alpha_l \rho_l \mathbf{U}_l) + \nabla(\alpha_l \rho_l \mathbf{U}_l \mathbf{U}_l) = \nabla(\alpha_l \tau_l) - \alpha_l \nabla P + \alpha_l \rho_l \mathbf{g} - \mathbf{F} \tag{6.5}$$

Solid phase:

$$\frac{\partial}{\partial t}(\alpha_s \rho_s \mathbf{U}_s) + \nabla(\alpha_s \rho_s \mathbf{U}_s \mathbf{U}_s) = -\alpha_s \nabla P + \alpha_s \rho_s \mathbf{g} + \mathbf{F} \tag{6.6}$$

Where here *P*, and **g** represent the pressure and gravity. **F** represents the interfacial momentum transfer due to mass transfer. The momentum transfer per unit volume due to mass transfer can be represented as below [154].

$$\mathbf{F} = \dot{m}_{sl} \mathbf{U}_l - \dot{m}_{ls} \mathbf{U}_s \tag{6.7}$$

The liquid stress term τ_l is given by the following equation [155].

$$\tau_l = \mu_l [(\nabla \mathbf{U}_l) + (\nabla \mathbf{U}_l)^{\mathrm{T}} + \left[\zeta - \frac{2}{3} \mu_l\right] \nabla \mathbf{U}_l I] \tag{6.8}$$

Where μ_l , ζ ,T and I represents liquid molecular viscosity, bulk viscosity, temperature and Prandtl's mixing length, respectively.

The compositional transport equation that calculates mass transport of solute (oil solid phase) is expressed as below [156]:

$$\frac{\partial}{\partial t}(\rho m_s) + \nabla . (\rho m_s \mathbf{U}) = D_s \nabla^2 . \rho m_s \tag{6.9}$$

where m_s is the mass fraction of oil, and D_s (m·s-2) is the diffusivity of oil in nanofluids.

6.5 Method

ANSYS Fluent 15.0 were used for the filter cake dissolution problem simulations. The solution method goes through the principal steps of geometry and mesh generation, problem setup, solution solver and finally post processing of the results [157],[158].

6.5.1 Geometry and Mesh Generation

Model geometry creation was the first step towards solving the filter cake dissolution flow problem. The specifications for the two-dimensional geometry were developed based on the dimension of the high temperature high pressure (HTHP) filter press cell used in the experiment in **chapter 5**. The dimensions of the domain used in the model are 63.5mm × 95 mm as shown in Fig. 6.4. The domain was further split into two domains to represents the nanofluids and oil solid phase.

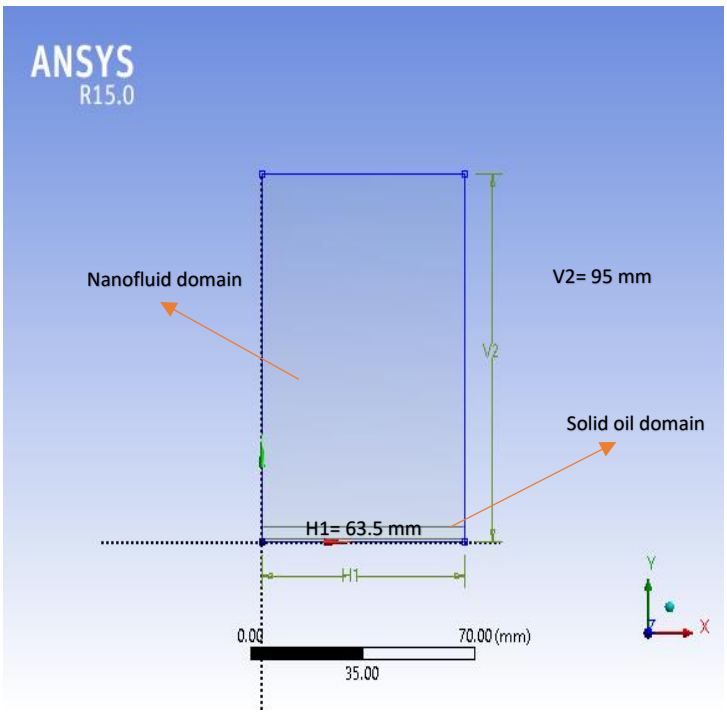

Figure 6.4: Dimension of the domain representing the filter cake (oil solid) and nano fluids inside HTHP cell.

After the geometry has been defined, it needs to be transformed into surface body from the sketch by applying sketch to surface function button of the Ansys geometry module. The meshing module was then deployed and generate mesh function was applied to generate a computational mesh, which is the representation of the volume of the geometry the solver can use to solve the flow problem with sets of boundary conditions defined. A mesh can be described as a volume which has been discretized into a series of smaller volumes or elements. A computational mesh consists of mesh elements and nodes that connect the edges of the elements. Generally, we start choosing the default meshing with unstructured grids and select the fine meshing. Few iterative of refining the mesh by selecting the appropriate elements size, which will influence the number of elements and nodes. The higher the number of nodes and elements, the higher the precision of the simulation results, however it will take longer simulation time and greater computing power depending on the complexity of the problem. Thus, selecting the optimum element type and size are paramount for the best acceptable quality results for this flow problem simulation. Generally, Ansys Fluent is capable of handling triangular and quadrilateral elements or the combination of these for the two-dimensional geometry. We will use mesh refinement method to generate the appropriate mesh and the mesh quality check was done using the mesh metric function by adjusting the skewness of the mesh as shown in Fig.6.5. Skewness is described as deviation from the perfect elements. The guidelines

for the skewness scale are to be between 0 and 1. The closer the average skewness value to 0 is the best option and 0.9 as the maximum acceptable value [159]. We have optimised the average skewness for our mesh generation to be 0.14.

The quality of a mesh can be defined in many ways, but a good mesh is generally characterized by compact elements with relatively large angles between its edges, and that neighbouring elements have approximately the same volume and elements type [158]. The mesh generation was done by applying the interconnection function between the nanofluid domain and oil solid phase domain as shown in Fig. 6.6 defining as one body with two parts. The accuracy of our solution converging very much depended on the quality of the mesh generated.

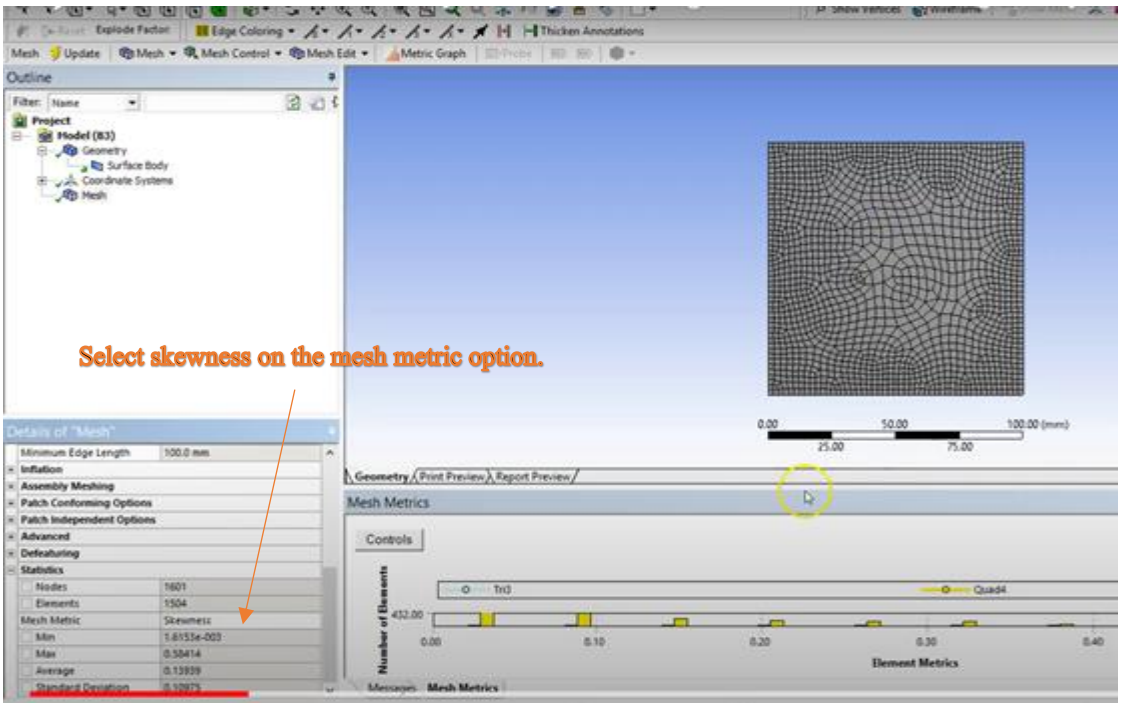

Figure 6.5: Method of checking mesh quality by adjusting the skewness average scale closer to 0 and below 0.9 value.

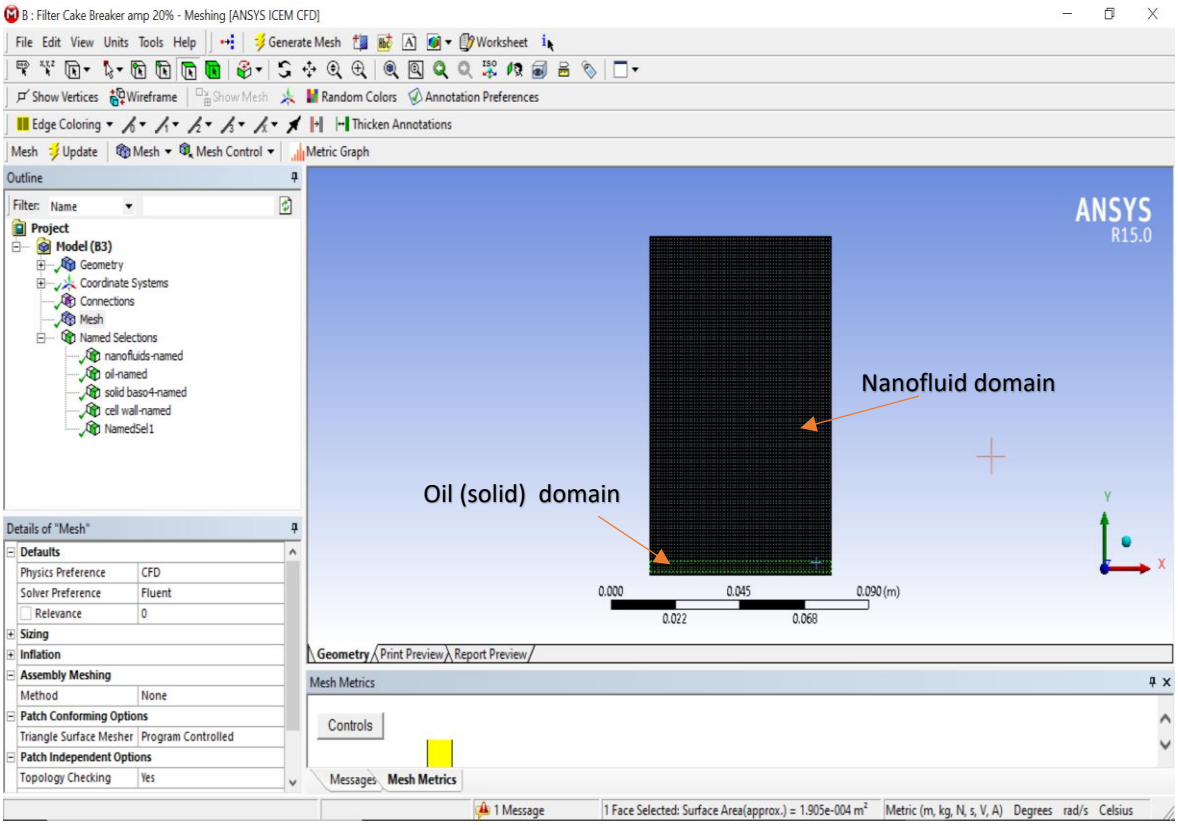

Figure 6.6: Mesh generation interconnecting between nanofluids and oil solid phase.

6.5.2 Solution Setup

After the mesh generating step completed, the solver setup module will be deployed to provide input for the problem solution. The simulation of the filter cake dissolution was designed based on the steps shown in Fig.6.7. The simulation provides results by solving the governing equations described in earlier section 6.3 and 6.4 that describe the interphase mass transfer mechanism between the solid oil phase and liquid nanofluid phase that happening during filter cake dissolution. The computational model for this flow problem is constructed using a pseudo-2-dimensional, 2-phase, Eulerian/Eulerian [160],[161],[162] finite-volume approach referred as mixture model incorporated in Ansys Fluent version 15 as shown in Fig.6.8. In this study, it was assumed that there are no chemical reactions taking place hence a species transport model without reaction was included in the simulation. It is also assumed that the secondary species or oil phase diffuse in the primary species or nanofluids phase at a constant mass transfer rate. The effect of interfacial tension (IFT) between the phases is taken care of by the surface tension coefficients and IFT value obtained from the experiments in Chapter 4. In this simulation, the two phases are modelled as continuous, interpenetrating, and incompressible media.

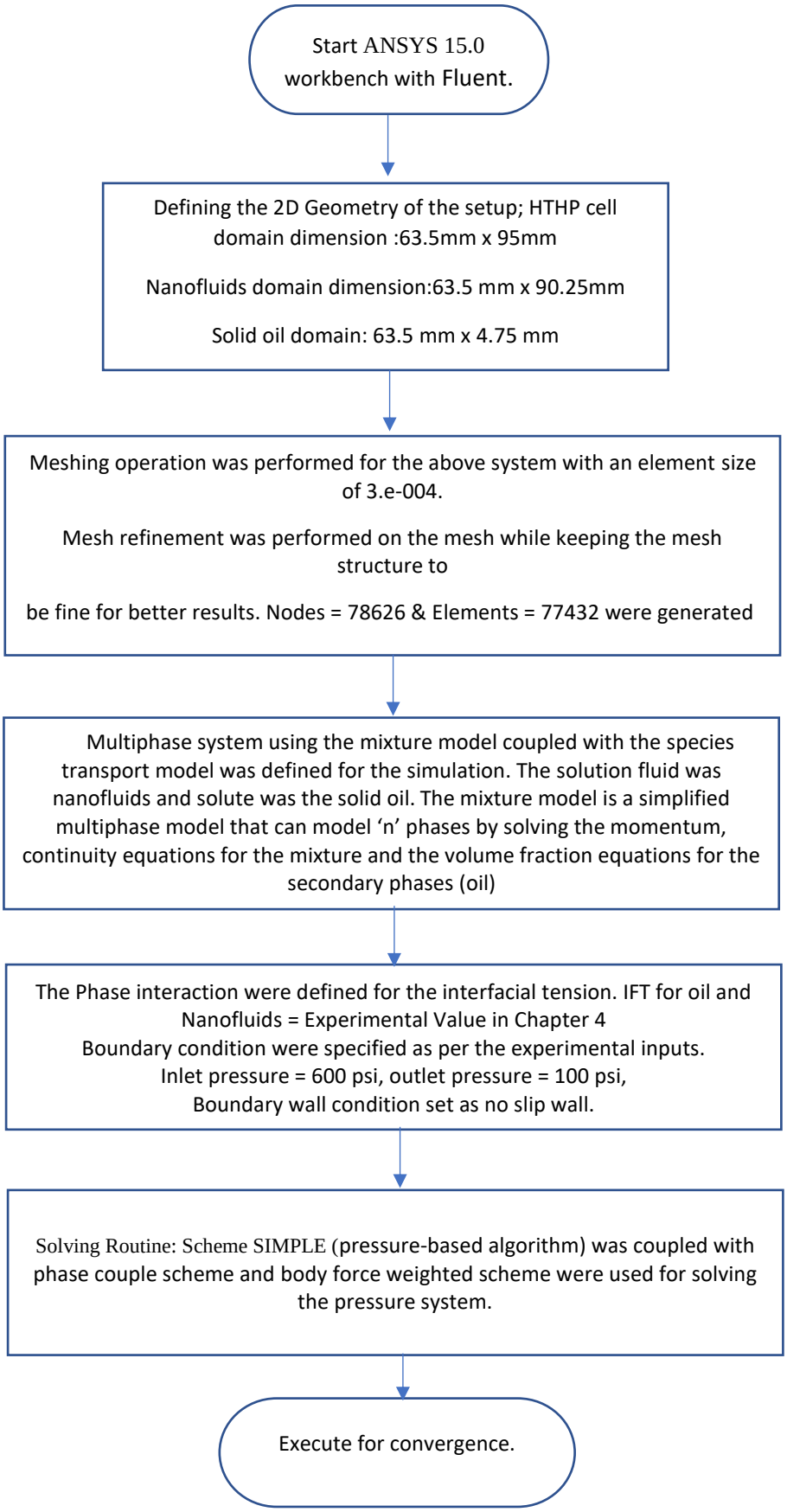

Figure 6.7: Flowchart describing the steps for the designing of simulation study.

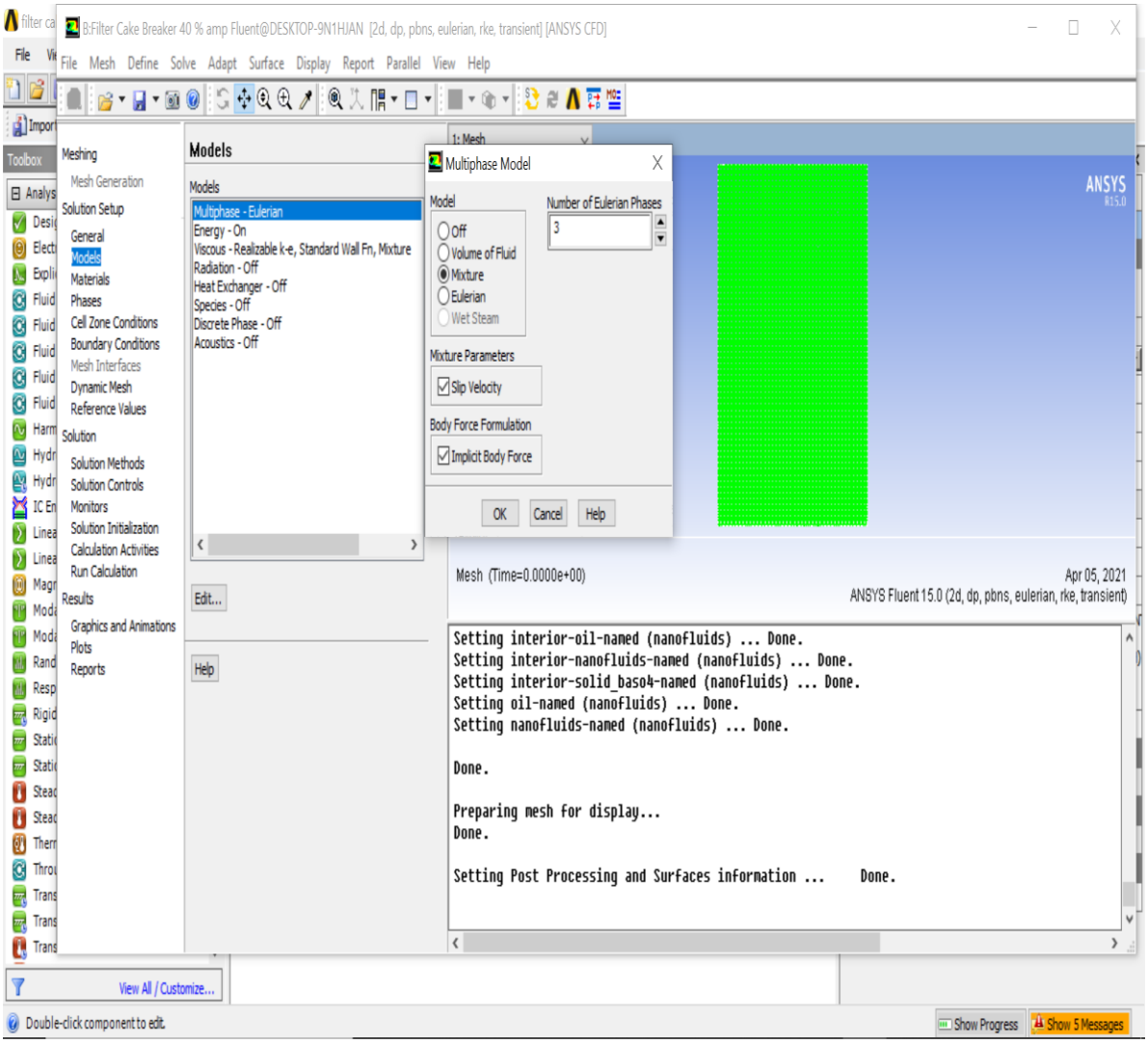

Figure 6.8: Multi Phase mixture model for solution setup.

The material parameters will be chosen from the Fluent data base and edited to match the viscosity, density, and the interfacial surface tension of the nanofluids, and oil solid phase as shown in Fig. 6.9 and Fig.6.10. Multiphase flow also required that a primary and secondary phase be indicated for the system. The secondary phase is the phase dispersed throughout the continuous primary phase. For this problem nanofluids was considered the primary phase and oil solid was considered the secondary phase as shown in Fig. 6.10. The bulk nano fluid is assumed to initially contain no oil. Thus, the following assumptions were used for the simulation study.

- The initial volume fraction of the nano fluid is 1 and oil solid volume fraction is 0.
- At the inlet boundary, the fluid velocity is set equal to the slip velocity of the particle.

- A non-slip wall boundary condition is applied to all the other surfaces of the domain.
- The maximum final volume fraction will be defined as 0.95 for the nanofluid and 0.05 as for the solid oil component in the bulk liquid phase.
- For a transient simulation flow phenomenon over time, a time-step size must then also be defined, as well as a simulation end time, the simulation end time is when all the oil solid particles dissolve.
- The boundary conditions for inlet pressure is set at 600 psi and outlet pressure is 100 psi,
- Operation condition of 500 psi and 250 ºC were set for the nanofluid and oil solid domain.
- Domain naming setup are as shown in Fig. 6.11.
- Nanofluids properties input such as viscosity, density, interfacial tension used for five amplitudes % scenario for the non-isothermal sonication simulations are based on the experiment data in **Chapter 4.**

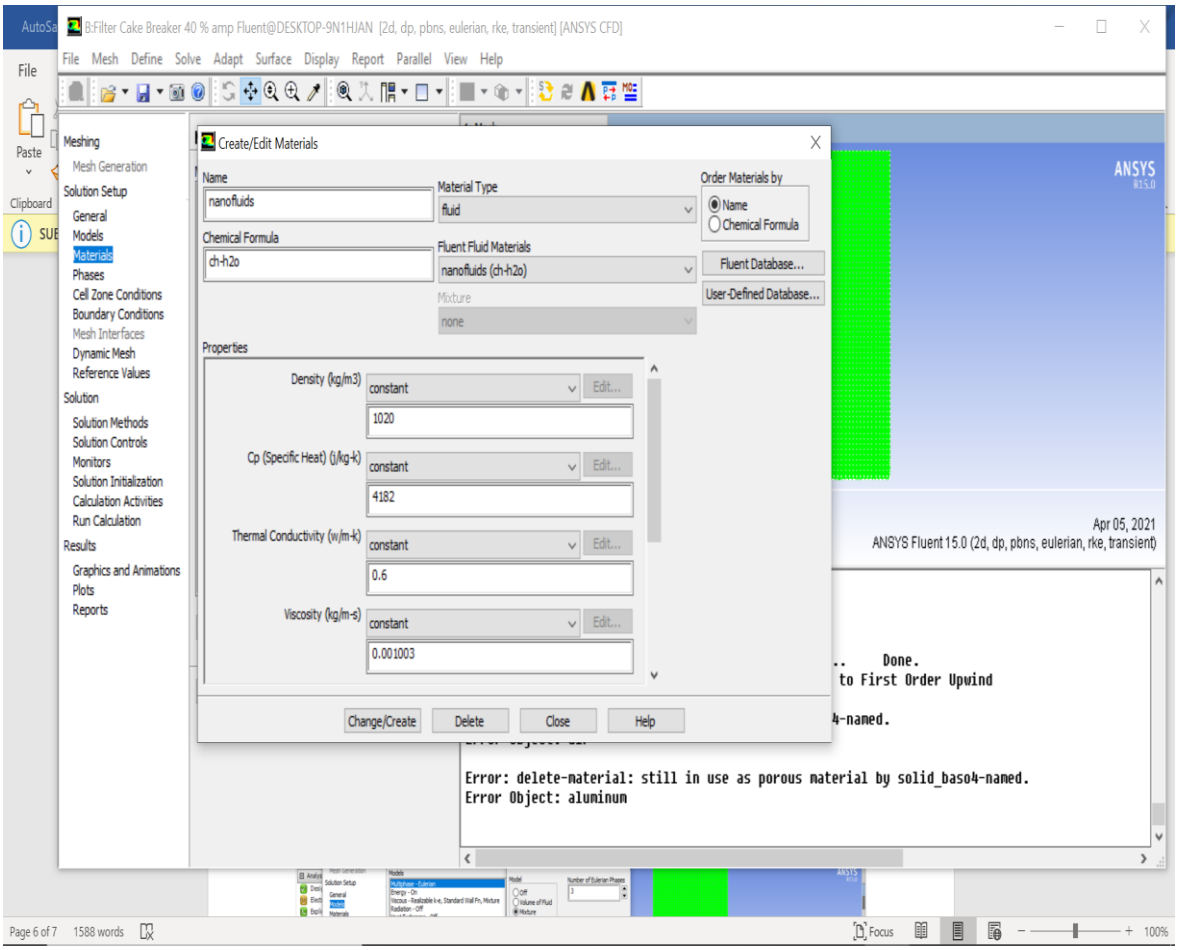

Figure 6.9: Material properties of nanofluid phases are defined by copy and editing from the fluent database.

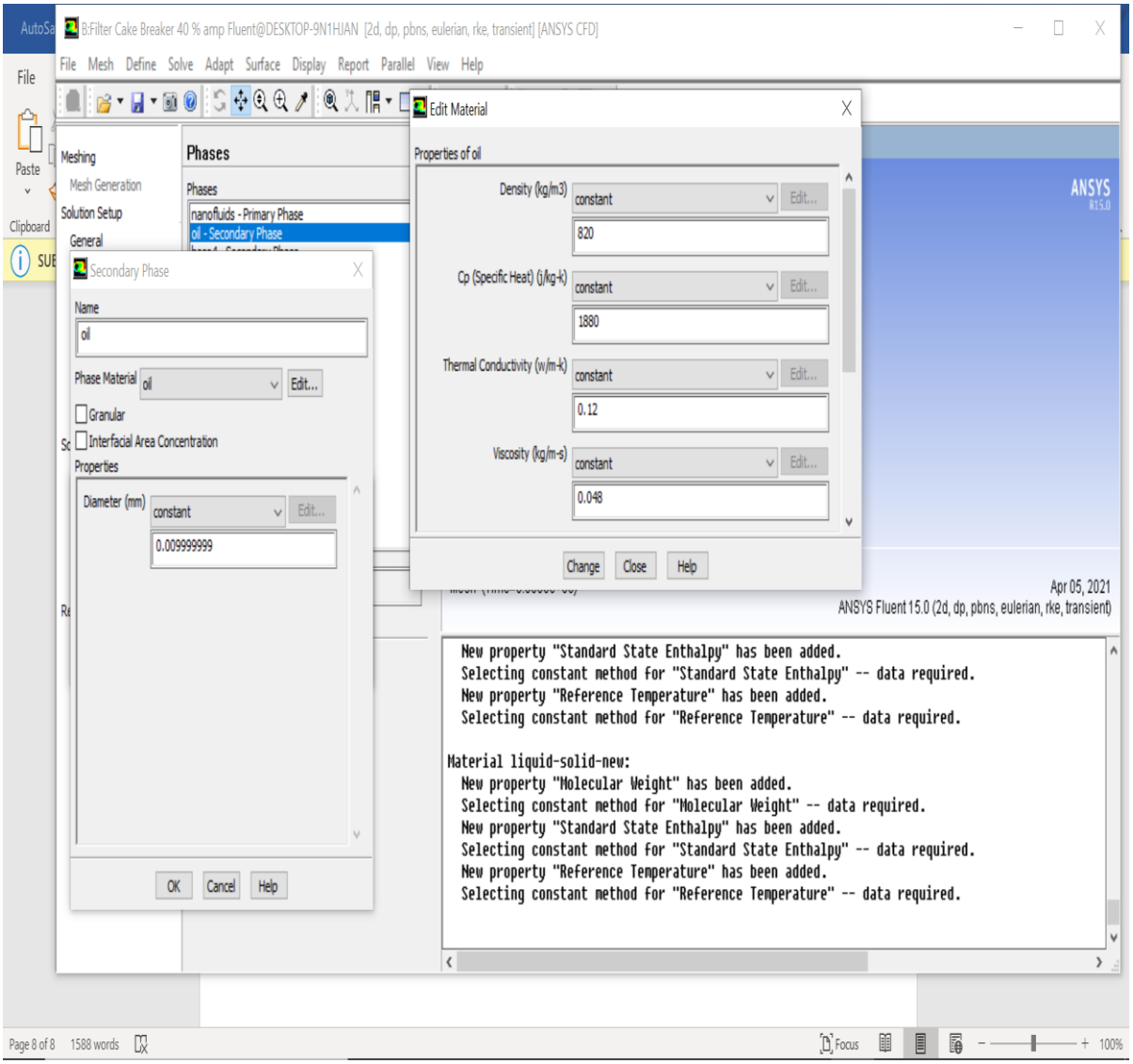

Figure 6.10: Material properties of oil solid phases are defined by copy and editing from the fluent database.

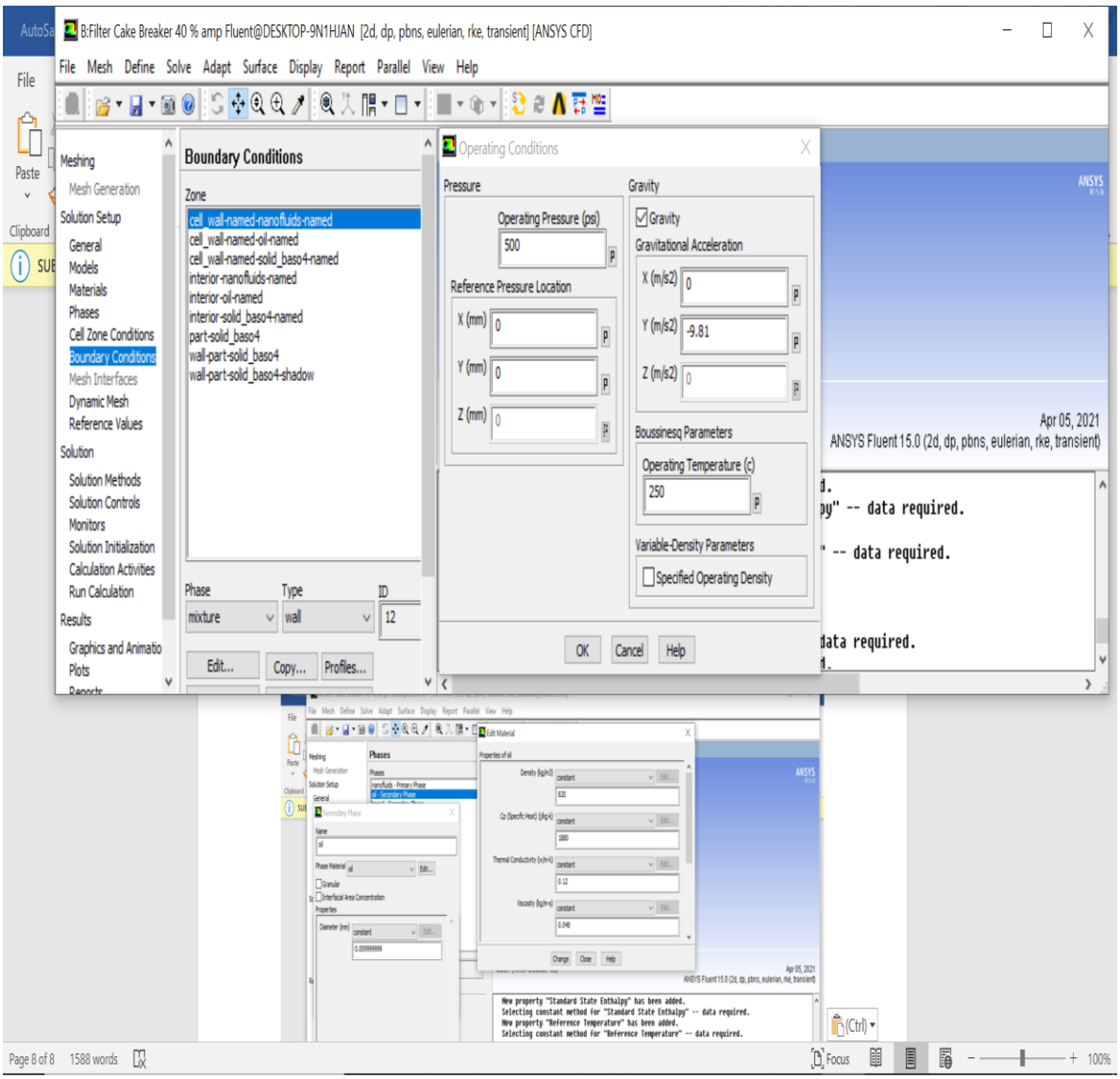

Figure 6.11: Boundary condition, naming and operation parameters setup.

6.5.3 Running Solution Solver

Running actual solution solver using the numerical methods to the mesh to find solutions to the selected equation systems is one of the important steps and it is also the step that can require the most time in a CFD project for converging solution [158]. Duration for a simulation is highly dependent on the complexity of the problem (e.g. the number of equations to be solved), the number of nodes in the mesh and the computer power available for the task [158]. We will use following set -up as shown in Fig. 6.12 and Fig. 6.13.

- The pressure-velocity coupling and phase coupled scheme solution method.

- First order upwind and first order implicit were defined for the discretization scheme and transition formulation respectively for reducing numerical smearing at phase boundaries.
- We also will define the time step (s) and number of time steps as shown in Fig. 6.13. We will start with 0.01 s and 500 for time steps and number of time steps respectively for our solution initially run. These two parameters can be varied to get an accurate converging result.

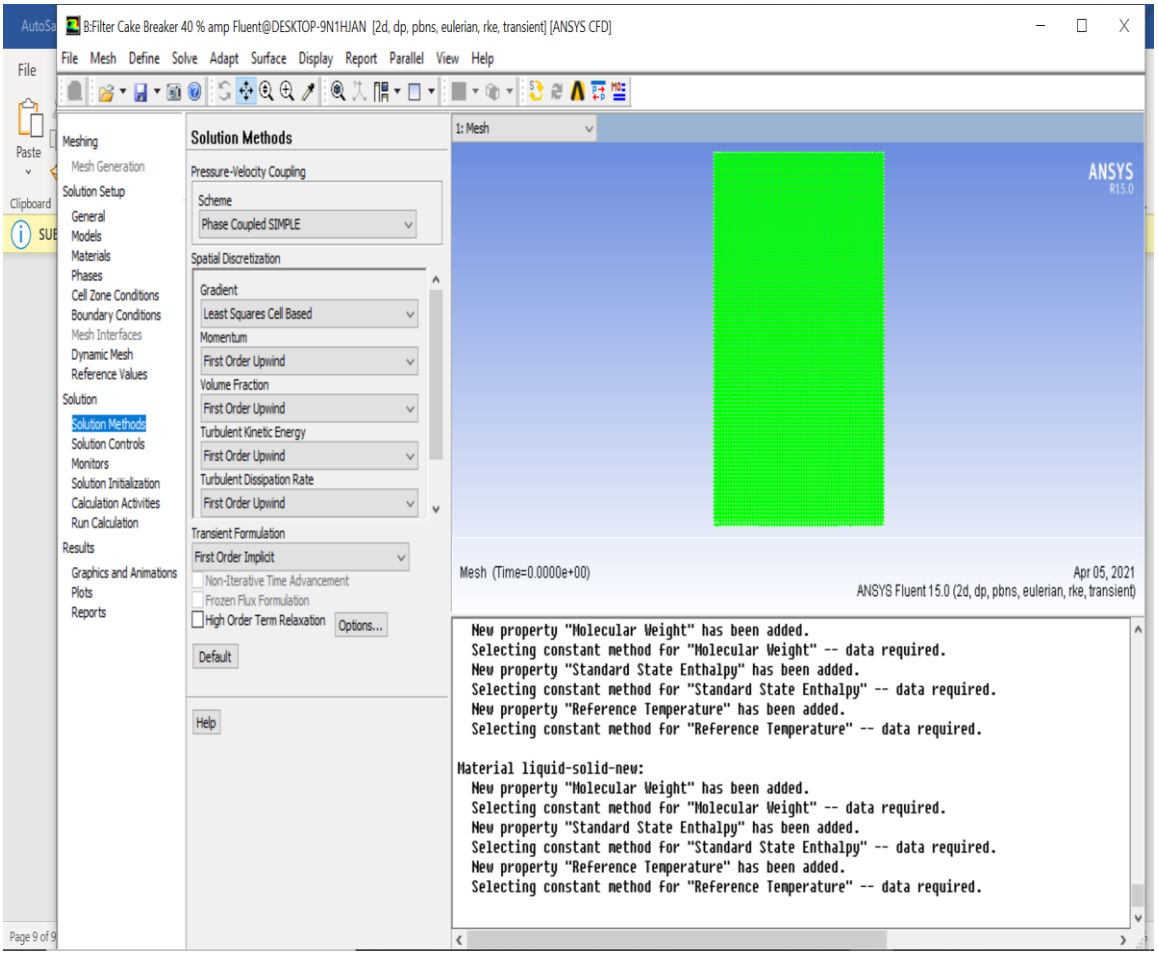

Figure 6.12: Solution method defined for running the problem solver.

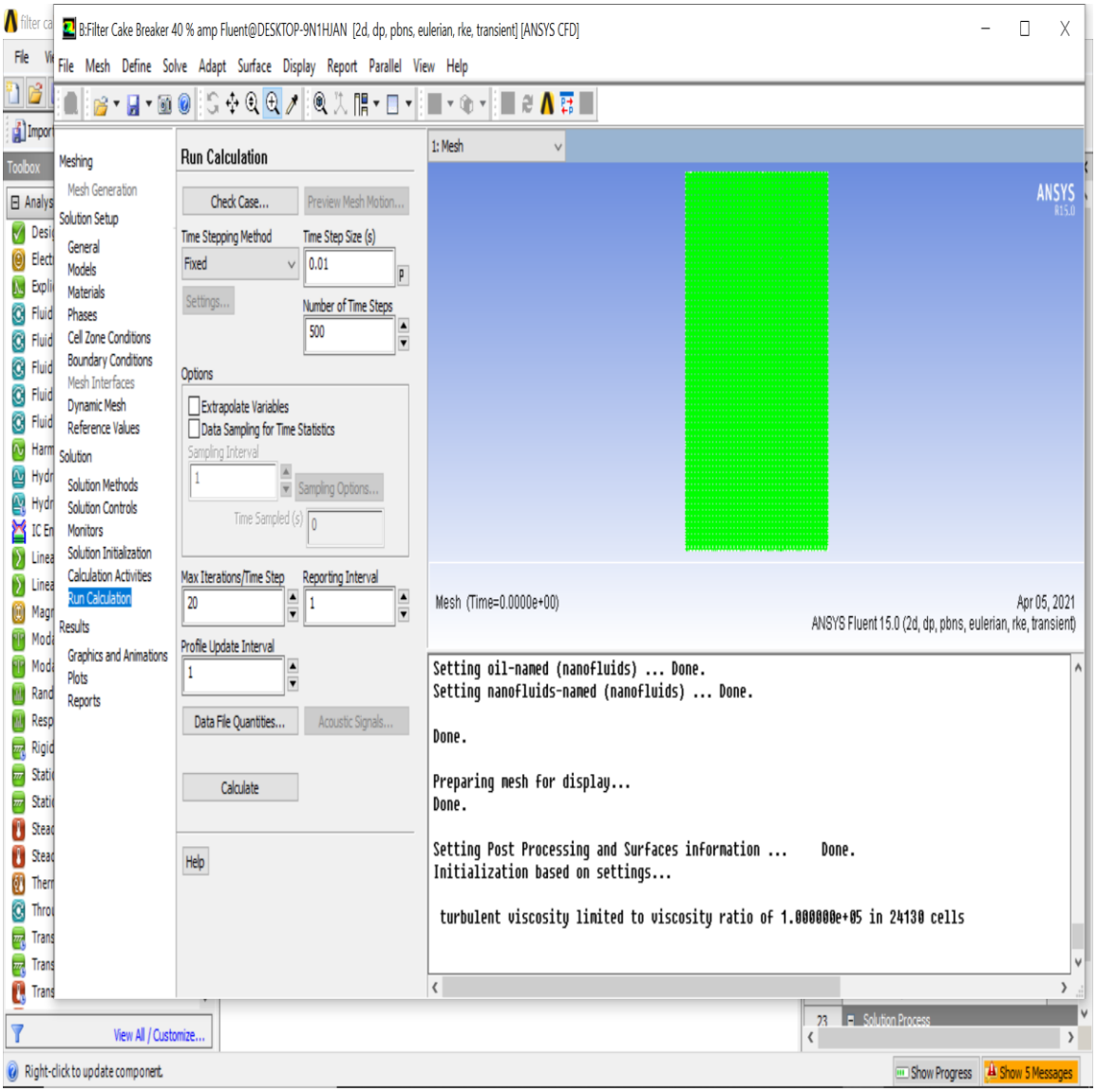

Figure 6.13: Example of time step and number of time steps defined for running the problem solver.

While the solver is running, it is possible to see how the solution is developing by tracking the residuals from the solution iterations. One residual is available per modelled variable (e.g. velocity in the x-direction, pressure, volume fraction) and node as shown in Fig. 6.14. The residual is a measurement of the imbalances for that variable in the current solution step. The smaller the imbalance, the better does a variable value match the differential equations the solver is trying to fit it to [158].

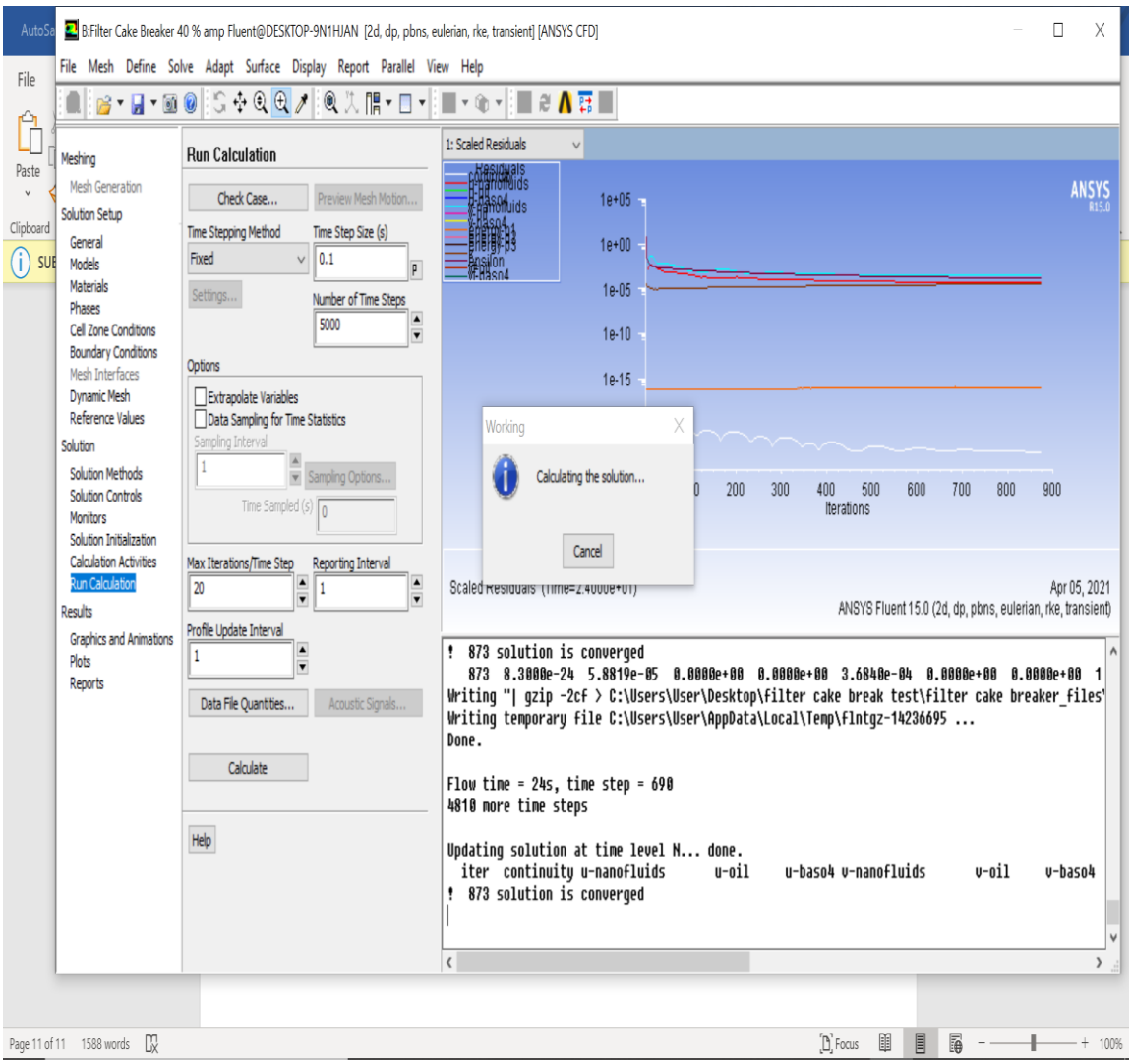

Figure 6.14: Residual iterations tracking for running the problem solver for convergence.

6.5.4 Post Processing and Reports

Once the solver completed the calculation, it creates a result file containing all the values of the system variables in each node. These results can then be used as an initial guess for later simulations, or post-processed and interpreted for discussion. In the post-processing module available in ANSYS Fluent 15.0, it is for example possible to visualise the value of all system variables on user-defined lines, planes, and volumes. The post processing also allows several calculations on the system variables, such as computing their mean values. For our simulation we will run simulation for the 5 scenarios of fluids properties that changes based on the ultrasound amplitude % variation. The volume fraction of oil in nanofluids will be tabulated and plotted. The oil volume fraction of the filter cake contour over time will be plotted from the graphical animation. An example of the oil and

nanofluid volume calculation at step time of 5 s is shown in Fig.6.15. These values will be converted in volume fraction and tabulated for plotting the graph of oil fraction over time.

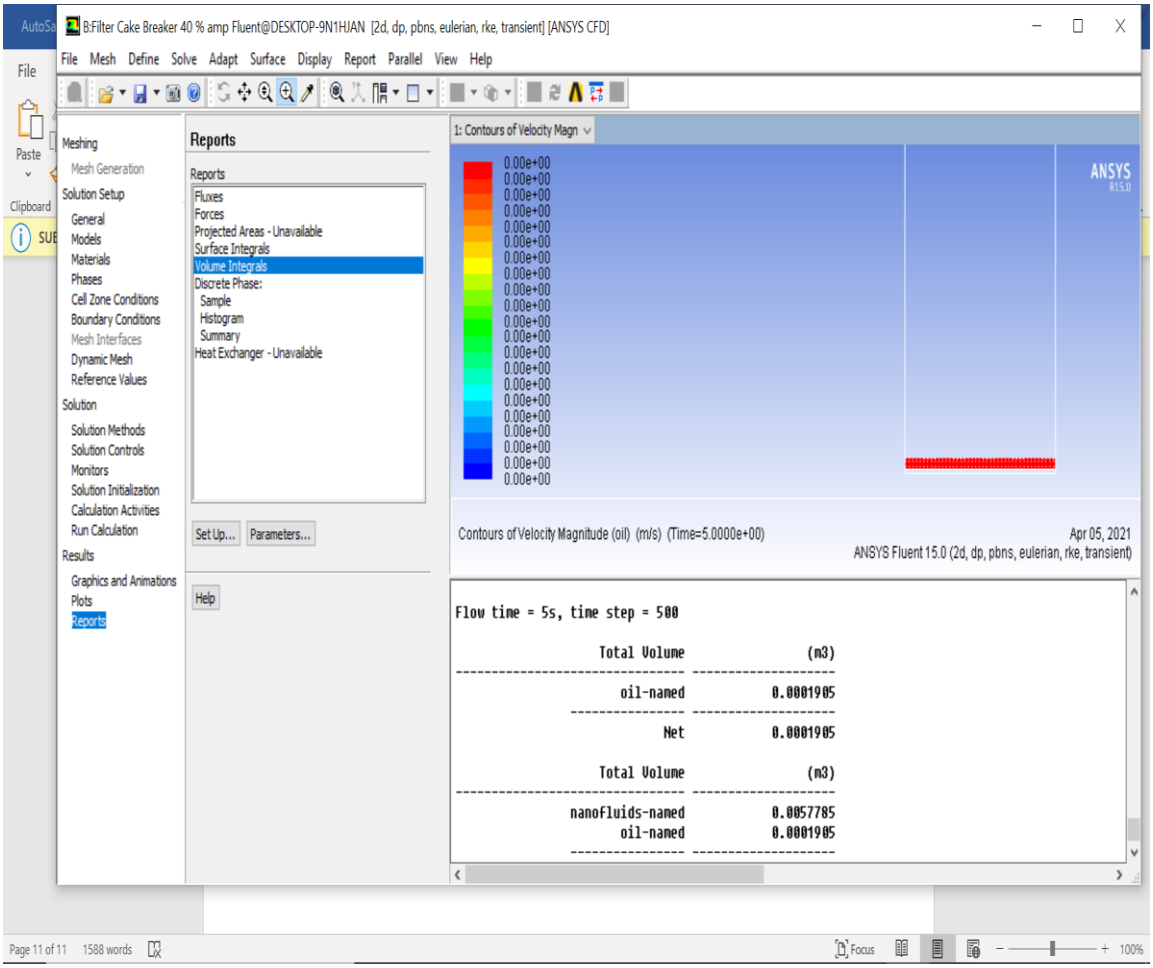

Figure 6.15: Volume calculation display for oil and nanofluid phase.

The animation of oil volume fraction of the solid filter cake contour profile was recorded and the images of the oil volume fraction at various time of dissolution of filter cake with nanofluids sonicated at 20 % amplitude been shown in Fig.6.16. The CFD simulation will be repeated for the other four scenarios ie, nanofluids sonicated under non isothermal condition at 40%, 60%, 80% and 100% amplitude. The input parameters, such as viscosity, interfacial tension, and density of the nanofluids will be varied accordingly from the experimental data obtained in chapter 4. The oil volume fraction results will be tabulated for comparison plot against the experimental results from **chapter 5.**

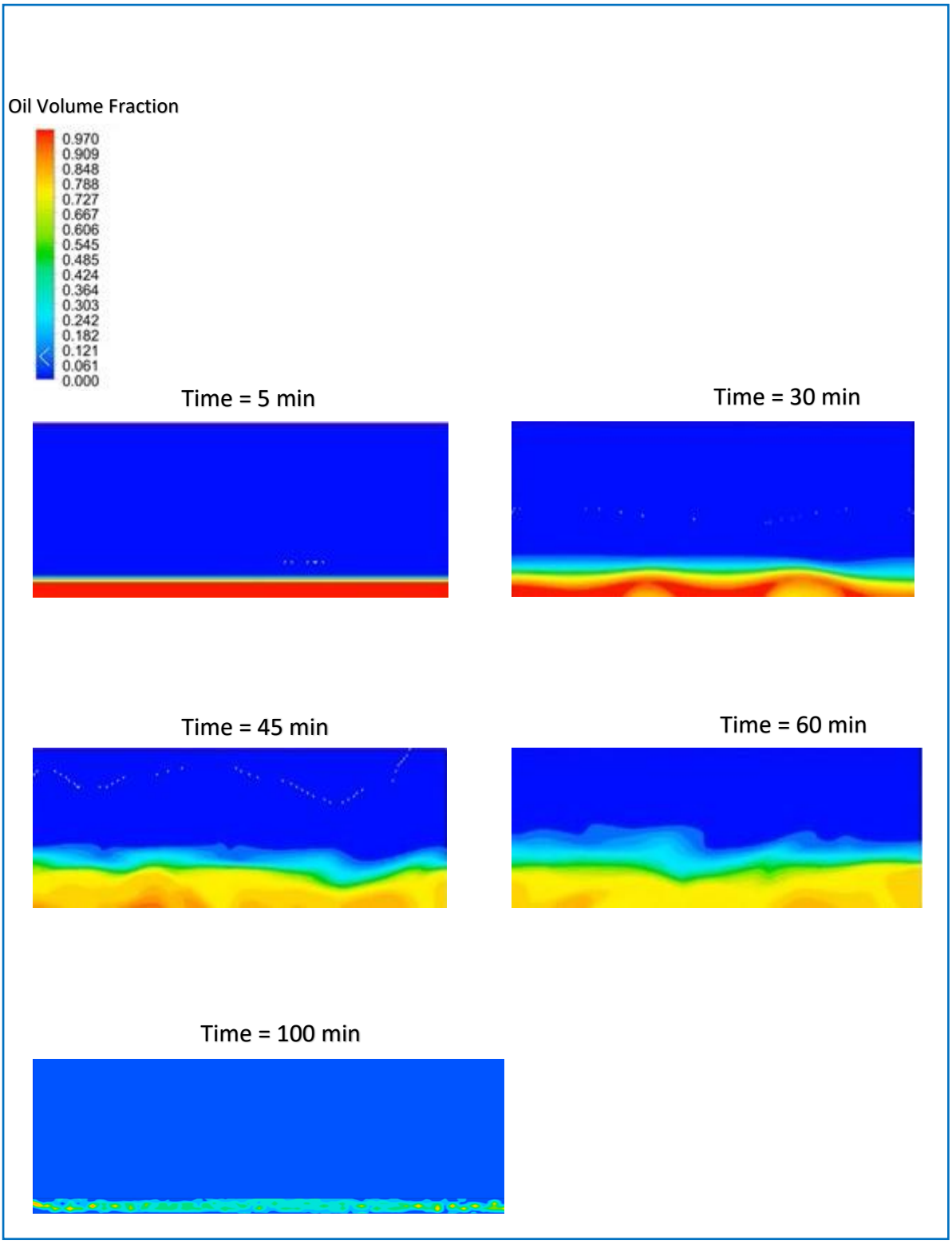

Figure 6.16: Oil volume fraction contour profile of the filter cake(oil solid phase) at various time of filter cake dissolution.

6.6 Observation and Remarks

The oil volume % over dissolution time for 5 scenarios of nanofluids sonicated at various amplitude at non isothermal condition was simulated and data were calculated for the plot as shown in Fig. 6.17. The comparison between the experiment plot and Ansys Fluent simulation plot indicate similar trend that the maximum oil diffusion from the filter cake into nanofluids achieved at 60% amplitude followed by amplitude 20%. The lowest amplitude was observed at 100% amplitude. The data for the 60% amplitude for both experiment and simulation results was plotted for comparison analysis as shown in Fig. 6.18.

.

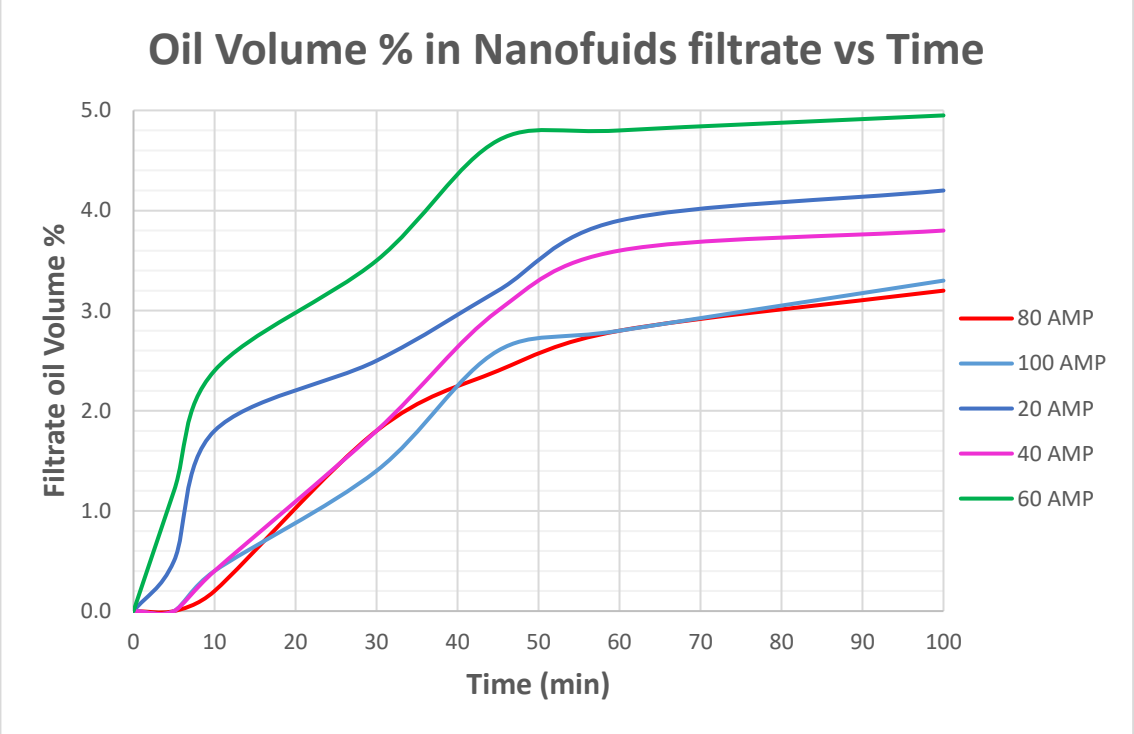

Figure 6.17: Graph plot of Oil volume % of the nanofluids filtrate at various amplitude % under non-isothermal condition over filter cake dissolution time simulated with Fluent.

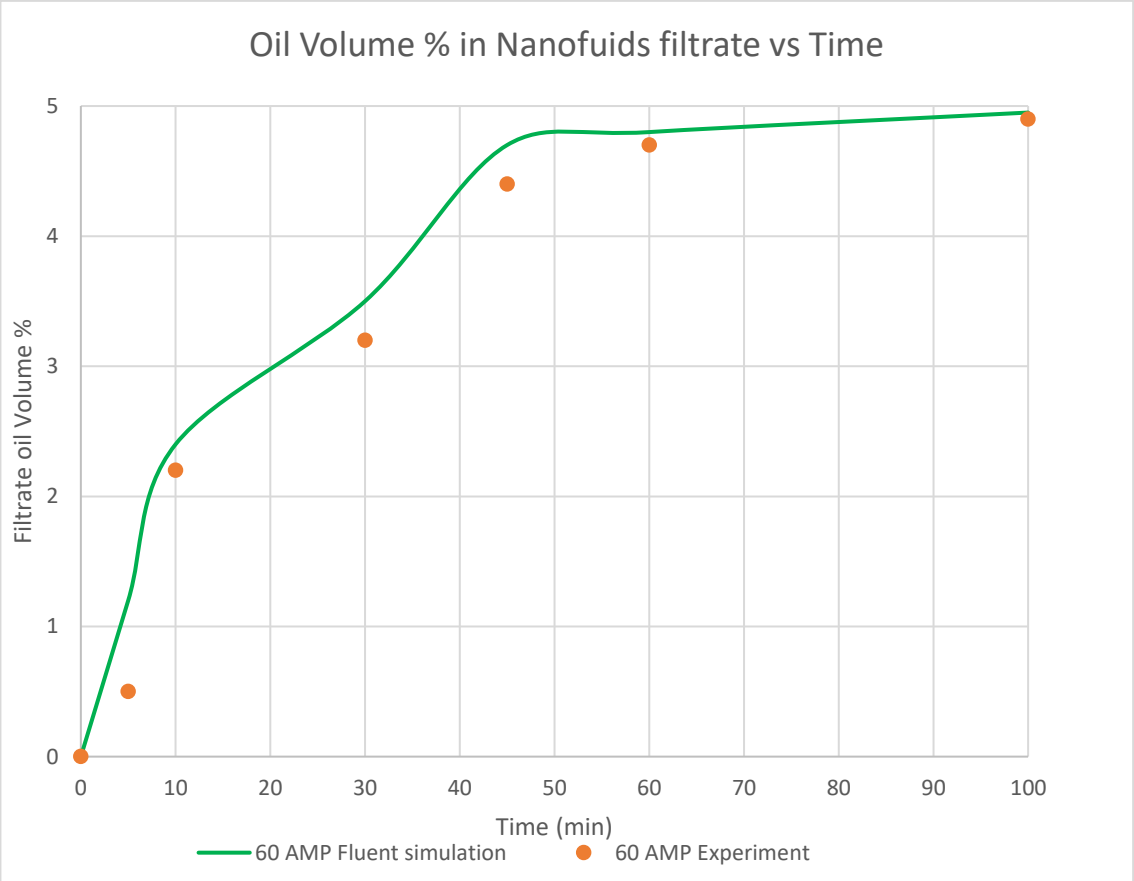

Figure 6.18: Oil volume % of the nanofluids filtrate at 60 % under non-isothermal condition over filter cake dissolution time comparison plot of experiment and simulation with fluent

Remarks

The observation derived from the plots shown in Fig.6.18 indicate that at any given time the filter cake dissolution rate was higher for theoretical simulation compared to experimental value. However, both the experiment and simulation show a similar correlation of oil diffusion into nanofluids during the filter cake dissolution. Thus, validating the model selected from the Ansys Fluent in agreement with experimental results.

6.7 Closure

The comparison between the experimental and Fluent simulation of the filter cake dissolution indicates that the key important fluids parameters that have major influence on mass transfer kinetics during well remediation process are viscosity, interfacial tension, and density. We can manipulate the diffusion rate of the oil into nanofluids by altering the amplitude % of the ultrasonic perturbation. The changes in intensity of the ultrasonication cause the physio-chemical properties to change which results in variation of the filter cake dissolution rate. Thus, based on the observations of both the experiment and stimulation, we can generalize that by identifying the optimum amplitude % of ultrasonication under non-isothermal condition of this study, we can enhance the well remediation process without the need to change the fluids formulation with higher surfactant concentration.

CHAPTER 7 Discussion and Conclusions

7.1 Introduction

This chapter provides overall discussion and summary of the experimental work and theoretical simulation carried out for the investigation of nanofluids physio-chemical properties due to the ultrasonic amplitude changes for near wellbore remediation application. The discussion will be focused on key aspect of nanofluid formulation, physio-chemical properties changes that effects the mass transfer kinetics during the near wellbore remediation process. The discussion will also cover the comparison of experimental observation with Ansys fluent simulation. Finally, we will outline the summary of the study findings, conclusions and future work recommendations.

7.2 Discussions

The following section discuss about the influence of surfactant selection on nanofluids properties and how the ultrasonic amplitude variations alter these properties under both condition, isothermal and non-isothermal. It also will cover the mass transfer kinetics evaluation comparison between the experiment and simulation.

7.2.1 Surfactant Influence on Nanofluids Viscosity

Surfactant selections play a key role in micellar based nanofluids synthesis process. The nanofluids functionality and its physio-chemical properties influenced by the size and the structure of micelles generated at nano scale. Thus, understanding the surfactant system behaviour as a function of concentration, temperature, and the presence of other additives in the system is important for the nanofluids formulation and their functionality effectiveness. It was reported in one of the research papers [163] that for low concentrations surfactant system with longer alky chain length similar to the surfactant used in this study, large difference in viscosity changes observed in small increases in concentration resulting from changes of micellar structure from spherical to prolate ellipsoids and cylinder. Viscosity characterisation experiment in chapter 4 observed changes in viscosity of the nanofluids system for both process conditions, isothermal and non-isothermal despite we have not changed concentration of surfactant. Thus, we can assume that micellar structural changes can be achieved by altering the sonication amplitude % and the process conditions that control the temperature of the system. The

fluctuation of viscosity of the nanofluids from the external perturbation of ultrasonic under various amplitude % and process condition support the viscoelastic behaviour of the nanofluids owing to their ability to break and make agglomeration, i.e. flexible and reversible structure under the external stimuli. The viscosity decreases when the nanofluids sonicated at lower amplitude % and show viscosity build up at higher amplitude % for both isothermal and non-isothermal conditions. The viscosity incremental for isothermal condition was greater compared to non-isothermal due to the temperature effect. These observations are valid for this particular type of surfactant system. We may observe different behaviour with other type of surfactants.

7.2.2 Density Changes and Correlation to Particle Size

The nanofluids density changes due to variations of sonication amplitude % as observed in our study, can be explained by the temperature effect on the volume expansion or contraction of the system. Under the non-isothermal conditions, temperature increase from ultrasonication have caused volume expansion as a result of more spacing between the molecules of nanofluids. This has resulted a relax or less ordered micellar structure as the cohesive force between the molecules of the nanofluids decrease. The opposite observed for the isothermal sonication conditions. This observation can be correlated to the mean average particle size gradual incremental for isothermal condition as the amplitude % increased. In other word it supported the volume contraction theory where the agglomeration of micellar causes less spacing between molecules and more orderly micellar structure resulting in density increase. The non-isothermal condition, amplitude % changes cause the mean average particle size to fluctuate and correlate to the viscoelastic behaviour owing to their ability to break and make agglomeration of the nanofluids structure. In this scenario after the 60% amplitude, higher amplitude led to bigger mean particle size due to coalescence.

7.2.3 Wettability

The wettability propensity of the nanofluids which are characterised by surface tension, interfacial tension and contacts angles properties changed when we varied the amplitude % of the sonication. These properties are influenced by the intermolecular surface activities and temperature. The surface activities have correlation to the properties that we have discussed earlier. Generally, surface activities of a fluids are higher when it has lower viscosity, density, and particle size, which mean the fluids has high wettability. In another

word, it has higher ability to disperse and dissolve another medium that come in contact. Hence, enhancing interfacial mass transfer kinetics. The study conclude that we achieve the desired physio-chemical properties for the near wellbore interface mass transfer kinetics when we induced the nanofluids at 60% amplitude under non-isothermal condition.

7.2.4 Experiment and Simulation Comparison of Filter Cake Dissolution Rate

The key physio-chemical properties of nanofluids such as density, viscosity and interfacial tension that obtained from experiment for various amplitude were used as nanofluids properties input for the Ansys Fluent filter cake dissolution simulation studies and the findings converged with experimental findings. We observed similar filter cake dissolution rate trend when we compared the plot for both the experiment and simulation. Nanofluids sonicated at 60% amplitude under non-isothermal condition provide the maximum dissolution rate for both the cases. Thus, we could generalise the correlation that the three physio-chemical properties mentioned above have the most influence in mass transfer kinetics during the near wellbore remediation process.

7.2.4 Delivery of The Objectives

The methodology adopted to conduct the study has delivered the following objectives.

1) Developed a protocol for stable nanofluids synthesis for field implementation.
2) The limiting mass transfer mechanism for near wellbore damage media was determined.
3) The effects of various ultrasonic amplitude, under both conditions isothermal and non-isothermal on nanofluids physio-chemical properties and mass transfer kinetics during well remediation was determined.
4) Developed the correlation between the ultrasonic amplitude %, nanofluids physio-chemical properties and mass transfer kinetics during well remediation.
5) Validated the effect of coupling near well remediation in EOR process.

7.3 Summary

This thesis study emphasized on understanding the fundamental effect of external perturbation such as ultrasonic on physio-chemical properties of nanofluids that influence the mass transfer kinetics of near wellbore remediation process. The nanofluids were synthesized using single step, Chemical Solution Method under the induction of a fixed 500 watt and 20 kH frequency ultrasonic laboratory machine. The formulation of nanofluids was optimised using the phase behavior studies to achieve the desired single phase nano emulsion formation. The optimised nanofluids were sonicated at five different amplitudes % at fixed 500 watt and 20 kH frequency for two different process condition, isothermal and non-isothermal. The physio-chemical properties characterisation of the nanofluids experiments were carried out to study the effect of amplitude % variations on those properties under isothermal and non-isothermal conditions. The physio-chemical properties of the nanofluids include viscosity, particle size, zeta potential, surface tension, interfacial tension, contact angles, pH and density. The characterisation technique for those physio-chemical properties were explained in detailed in chapter 4. The nanofluids sonicated at five different amplitudes % were further evaluated for mass transfer kinetics for near wellbore remediation using the filter cake dissolution and sand packed column flow tests. The mass transfer kinetics evaluation tests indicate that sonication of nanofluids at 60% amplitude under non-isothermal process condition provide the most favourable physio-chemical properties for near wellbore remediation, particularly interfacial tension and viscosity that influence the most on the mechanism of mass transfer during the remediation process. Ansys Fluent computational fluids dynamic software was used to perform theoretical simulation of the filter cake dissolution process. The results of filter cake dissolution from experimental and simulation were compared for generalizing the correlation between the ultrasonic external perturbation and physio-chemical properties and their effect to mass transfer kinetics during wellbore remediation process. Some of the key findings of this thesis work can be summarised in the following points.

1) The ultrasonic external perturbation intensity or amplitude does affect the physio-chemical properties of this nanofluids. Thus, we can manipulate the amplitude to achieve our desired properties of the fluids.
2) The optimum amplitude % and synthesizing condition of the nanofluids are dependent on the optimised nanofluids formulation and for the scope of this thesis work, we have discovered that 60 % amplitude sonication under non-isothermal

conditions provided the best-case scenario of mass transfer kinetics enhancement during the near wellbore remediation process.

3) The mass transfer kinetics of near wellbore remediation can be enhanced or delayed by changing the amplitude or intensity of sonication induced on nanofluids without the need to modify the fluids formulation. Thus, reduce the costly process of fluids formulation modification at wellsite.

4) Interfacial tension and contact angles properties which directly indicate the wetting nature of the nanofluids are one of the main properties influence the mass transfer diffusion mechanism during the near wellbore remediation. The lower the value of both properties, the mass transfer diffusion kinetics during the near wellbore remediation was higher. The other two properties that have significant influence on mass transfer kinetics are particle size and viscosity of the fluids.

5) The 60 % amplitude under non-isothermal conditions sonication provided the lowest value on the four key properties mentioned earlier resulting in the highest mass transfer kinetics rate. Thus, we can establish a generalised correlation that the smaller the particle size, viscosity, interfacial tension, and contact angles of nanofluids, the higher the mass transfer kinetics mechanism during the near wellbore remediation process.

6) The experimental findings of the above generalised correlation are also valid for the Ansys fluent theoretical simulation. Thus, validating the generalised correlation.

7) The sand packed column flow test indicate that the near wellbore remediation enhancement has direct influence on the success of Enhanced oil recovery. The near wellbore remediation generates an improved pathway for hydrocarbon flow enhancement.

7.4 Conclusions

This is the first study that integrate the various aspect of nanofluids design for near wellbore remediation. The study provides us the protocol for nanofluid formulation and synthesis, the effects of amplitude on physio-chemical properties and their correction to mass transfer kinetics during the near wellbore remediation. Furthermore, we have

demonstrated the importance of near wellbore remediation for enhance oil recovery process by conducting the sand packed column flow test. Thus, the structured nanofluids design and optimisation for wellbore remediation with appropriate perturbation of ultrasonic amplitude can be achieved with minimal laboratory test hours and eliminate the trial-and-error laboratory testing process.

7.5 Future Work Recommendation

This study was focused on the effects of variations of amplitude % of ultrasonication on nanofluids physio-chemical properties for near wellbore remediation under both isothermal and non-isothermal conditions with a fixed 500-watt power and 20 kHz frequency for a duration of 30 minutes. The study was carried on nanofluids designed using a specific type of alkyl polyglucoside surfactant, Triton CG-425. It is observed that mass transfer kinetics enhanced with increase of ultrasonic intensity or amplitude, except for certain condition which reported that further increase in amplitude leads to reduction in mass transfer kinetics. This highlighted to us that an optimum amplitude % or intensity point of sonication provide the highest mass transfer enhancement for this study. However, several pass research [91],[164],[165] have indicated that, different nanofluids will react differently to the ultrasonication parameters such as power, frequency, intensity or amplitude and sonication time. Thus, the optimum point can be different for nanofluids designed with different surfactant type selection, ultrasonic operating parameters, and process conditions. The non-availability of such study for variety of surfactant selection, ultrasonic operating parameters and process conditions could provide the pathway for future research works. Such broader research works not only will further enhance the current application of nanofluids for oil and gas but could extend to other industries such as medical and food.

REFERENCES.

1. De, A., et al., *A brief overview of nanotechnology.* Targeted delivery of pesticides using biodegradable polymeric nanoparticles, 2014: p. 35-36.
2. Jampílek, J. and K. Kráľová, *Application of nanotechnology in agriculture and food industry, its prospects and risks.* Ecological Chemistry and Engineering S, 2015. **22**(3): p. 321-361.
3. Mamo, T., et al., *Emerging nanotechnology approaches for HIV/AIDS treatment and prevention.* Nanomedicine, 2010. **5**(2): p. 269-285.
4. Cheng, H., et al., *Nanotechnology overview: Opportunities and challenges*, in *Nanotechnology: Delivering on the Promise Volume 1*. 2016, ACS Publications. p. 1-12.
5. Haderer, M., *I need to know: An introduction to the oil industry and OPEC*. 2013, Vienna: Ueberreuter Print GmbH.
6. Chegenizadeh, N., A. Saeedi, and Q. Xie, *Application of nanotechnology for enhancing oil recovery–A review.* Petroleum, 2016. **2**(4): p. 324-333.
7. Bera, A. and H. Belhaj, *Application of nanotechnology by means of nanoparticles and nanodispersions in oil recovery-A comprehensive review.* Journal of Natural Gas Science and Engineering, 2016. **34**: p. 1284-1309.
8. Yang, J., et al., *Advances of nanotechnologies in oil and gas industries.* Energy Exploration & Exploitation, 2015. **33**(5): p. 639-657.
9. Nwidee, L.N., *Nanoparticles for Enhanced Oil Recovery Processes*. 2017, Curtin University.
10. Agi, A., et al., *Comparative study of ultrasound assisted water and surfactant flooding.* Journal of King Saud University-Engineering Sciences, 2019. **31**(3): p. 296-303.
11. Xu, H. and C. Pu, *Removal of near-wellbore formation damage by ultrasonic stimulation.* Petroleum science and technology, 2013. **31**(6): p. 563-571.
12. Dehshibi, R.R., et al., *Experimental investigation on the effect of ultrasonic waves on reducing asphaltene deposition and improving oil recovery under temperature control.* Ultrasonics sonochemistry, 2018. **45**: p. 204-212.
13. Caicedo, S.A. *Feasibility Study of Ultrasound for Oilwell Stimulation Based on Wave Properties Considerations*. in *Latin American & Caribbean Petroleum Engineering Conference*. 2007. OnePetro.
14. Mandal, A. and A. Bera, *Surfactant stabilized nanoemulsion: characterization and application in enhanced oil recovery.* International Journal of Chemical and Molecular Engineering, 2012. **6**(7): p. 537-542.
15. Houseworth, J., *Advanced Well Stimulation Technologies.*
16. Abramova, A., et al., *Ultrasonic technology for enhanced oil recovery.* Engineering, 2014. **2014**.
17. Mullakaev, M., V. Abramov, and A. Abramova, *Development of ultrasonic equipment and technology for well stimulation and enhanced oil recovery.* Journal of petroleum science and engineering, 2015. **125**: p. 201-208.
18. Bekbauov, B., A. Berdyshev, and Z. Baishemirov. *Numerical Simulation of Chemical Enhanced Oil Recovery Processes*. in *DOOR (Supplement)*. 2016. Citeseer.
19. Agista, M.N., K. Guo, and Z. Yu, *A state-of-the-art review of nanoparticles application in petroleum with a focus on enhanced oil recovery.* Applied sciences, 2018. **8**(6): p. 871.
20. Nitters, G., et al. *Structured approach to advanced candidate selection and treatment design of stimulation treatments*. in *SPE Annual Technical Conference and Exhibition*. 2000. OnePetro.
21. Terry, R.E., *Enhanced oil recovery.* Encyclopedia of physical science and technology, 2001. **18**: p. 503-518.
22. Muggeridge, A., et al., *Recovery rates, enhanced oil recovery and technological limits.* Philosophical Transactions of the Royal Society A: Mathematical, Physical and Engineering Sciences, 2014. **372**(2006): p. 20120320.

23. Andreassen, L., *Nanoparticle effect on interfacial properties related to Enhanced Oil Recovery*. 2015, NTNU.
24. Priskila, L.M., *Evaluation of Fishbone Lateral Stimulation: A Simulation Study*. 2014, Institutt for petroleumsteknologi og anvendt geofysikk.
25. Fredd, C. and H.S. Fogler. *Alternative stimulation fluids and their impact on carbonate acidizing*. in *SPE Formation Damage Control Symposium*. 1996. OnePetro.
26. Qiu, X. and F.F. Chang, *Estimating diffusion coefficient for a reservoir stimulation fluid*. 2015, Google Patents.
27. Suleimanov, B.A., F. Ismailov, and E. Veliyev, *Nanofluid for enhanced oil recovery.* Journal of Petroleum science and Engineering, 2011. **78**(2): p. 431-437.
28. Peng, B., et al., *A review of nanomaterials for nanofluid enhanced oil recovery.* RSC advances, 2017. **7**(51): p. 32246-32254.
29. Uddin, M., et al., *Fundamentals of nanofluids: evolution, applications and new theory.* 2016.
30. Choi, S.U., *Nanofluids: from vision to reality through research.* Journal of Heat transfer, 2009. **131**(3).
31. Krishnamurthy, S., et al., *Enhanced mass transport in nanofluids.* Nano letters, 2006. **6**(3): p. 419-423.
32. Kutty, S.M., et al. *Well Performance Improvement Using Complex Nano Fluids*. in *Abu Dhabi International Petroleum Exhibition and Conference*. 2015. OnePetro.
33. Mahmoudkhani, A., et al. *Microemulsions as flowback aids for enhanced oil and gas recovery after fracturing, myth or reality: A Turnkey study to determine the features and benefits*. in *SPE International Symposium on Oilfield Chemistry*. 2015. OnePetro.
34. Kale, S.N. and S.L. Deore, *Emulsion micro emulsion and nano emulsion: a review.* Systematic Reviews in Pharmacy, 2017. **8**(1): p. 39.
35. Anton, N. and T.F. Vandamme, *Nano-emulsions and micro-emulsions: clarifications of the critical differences.* Pharmaceutical research, 2011. **28**(5): p. 978-985.
36. Quintero, L., J. Mckellar, and D. Clark, *Nanoemulsion.* Patent no. US8822385B2, 2014.
37. Solans, C., et al., *Nano-emulsions.* Current opinion in colloid & interface science, 2005. **10**(3-4): p. 102-110.
38. Gupta, A., et al., *Nanoemulsions: formation, properties and applications.* Soft matter, 2016. **12**(11): p. 2826-2841.
39. Sugumar, S., A. Mukherjee, and N. Chandrasekaran, *Nanoemulsion formation and characterization by spontaneous emulsification: Investigation of its antibacterial effects on Listeria monocytogenes.* Asian Journal of Pharmaceutics, 2015: p. 23.
40. Wang, C., et al., *Use of nanoemulsion for effective removal of both oil-based drilling fluid and filter cake.* Journal of Natural Gas Science and Engineering, 2016. **36**: p. 328-338.
41. Quintero, L., et al., *Microemulsion and nanoemulsion breaker fluids with organic peroxides*. 2016, Google Patents.
42. Mason, T.G., et al., *Nanoemulsions: formation, structure, and physical properties.* Journal of Physics: condensed matter, 2006. **18**(41): p. R635.
43. Saidur, R., K. Leong, and H.A. Mohammed, *A review on applications and challenges of nanofluids.* Renewable and sustainable energy reviews, 2011. **15**(3): p. 1646-1668.
44. Yu, W. and H. Xie, *A review on nanofluids: preparation, stability mechanisms, and applications.* Journal of nanomaterials, 2012. **2012**.
45. Yusof, N.S.M. and M. Ashokkumar, *Ultrasound-induced formation of high and low viscoelastic nanostructures of micelles.* Soft Matter, 2013. **9**(6): p. 1997-2002.
46. Wang, L. and J. Fan, *Nanofluids research: key issues.* Nanoscale research letters, 2010. **5**(8): p. 1241-1252.
47. David, J. and N. Cheeke, *Fundamentals and applications of ultrasonic waves.* 2017.
48. Yusof, N.S.M. and M. Ashokkumar, *Ultrasonic transformation of micelle structures: Effect of frequency and power.* Ultrasonics sonochemistry, 2015. **24**: p. 8-12.

49. Mirzaei-Paiaman, A. and M. Nourani, *Positive effect of earthquake waves on well productivity: Case study: Iranian carbonate gas condensate reservoir.* Scientia Iranica, 2012. **19**(6): p. 1601-1607.
50. Beresnev, I.A. and P.A. Johnson, *Elastic-wave stimulation of oil production: A review of methods and results.* Geophysics, 1994. **59**(6): p. 1000-1017.
51. Aarts, A. and G. Ooms, *Net flow of compressible viscous liquids induced by travelling waves in porous media.* Journal of engineering mathematics, 1998. **34**(4): p. 435-450.
52. Graham, D. and J.J. Higdon, *Oscillatory flow of droplets in capillary tubes. Part 1. Straight tubes.* Journal of Fluid Mechanics, 2000. **425**: p. 31-53.
53. Wong, S.-W., et al. *Near wellbore stimulation by acoustic waves*. in *SPE European Formation Damage Conference*. 2003. OnePetro.
54. Wong, S.-W., et al., *High-power/high-frequency acoustic stimulation: a novel and effective wellbore stimulation technology.* SPE Production & Facilities, 2004. **19**(04): p. 183-188.
55. Abdallah, W., et al., *Fundamentals of wettability.* Technology, 1986. **38**(1125-1144): p. 268.
56. Bosiljkov, T., et al., *Influence of high intensity ultrasound treatments on physical properties of sheep milk.* Hrvatski časopis za prehrambenu tehnologiju, biotehnologiju i nutricionizam, 2012. **7**(SPECIAL ISSUE-7th): p. 44-48.
57. Iwunze, M.O., *The Determination of the Physico-Chemical Properties of Nanoemulsion.* Journal of Materials Science and Engineering A, 2017. **7**(1-2): p. 19-24.
58. Miller, C.A. and P. Neogi, *Interfacial phenomena: equilibrium and dynamic effects*. Vol. 139. 2007: CRC Press.
59. Hartland, S., *Surface and interfacial tension: measurement, theory, and applications*. 2004: CRC Press.
60. von Fraunhofer, J.A., *Adhesion and cohesion.* International journal of dentistry, 2012. **2012**.
61. Ghosh, P., *Interfacial Tension.* NPTEL—Chem. Eng.—Interfacial Eng, 2009: p. 1-22.
62. Glover, P.W., *Petrophysics.* University of Aberdeen, UK, 2000.
63. Yuan, Y. and T.R. Lee, *Contact angle and wetting properties*, in *Surface science techniques*. 2013, Springer. p. 3-34.
64. Brege, J., et al. *Using microemulsion technology to remove oil-based mud in wellbore displacement and remediation applications*. in *North Africa technical conference and exhibition*. 2012. OnePetro.
65. Quintero, L., T.A. Jones, and G. Pietrangeli. *Phase boundaries of microemulsion systems help to increase productivity*. in *SPE European Formation Damage Conference*. 2011. OnePetro.
66. Darugar, Q.A., et al. *Wellbore remediation using microemulsion technology to increase hydrocarbon productivity*. in *SPE Saudi Arabia Section Technical Symposium and Exhibition*. 2012. OnePetro.
67. Mandavi, R., S.K. Sar, and N. Rathore, *Critical micelle concentration of surfactant, mixed–surfactant and polymer by different method at room temperature and its importance.* Oriental Journal of Chemistry, 2008. **24**(2): p. 559.
68. Yu, D., F. Huang, and H. Xu, *Determination of critical concentrations by synchronous fluorescence spectrometry.* Analytical Methods, 2012. **4**(1): p. 47-49.
69. Wilhelm, E., et al., *Developments and applications in solubility*. 2007: Royal Society of Chemistry.
70. Eisen, L., N. Marano, and S. Glazier, *Activity-based approach for teaching aqueous solubility, energy, and entropy.* Journal of chemical education, 2014. **91**(4): p. 484-491.
71. Smith, B.T., *Remington education: physical pharmacy*. 2015: Pharmaceutical Press.
72. Sharma, N., et al., *Nanoemulsion: A new concept of delivery system.* Chronicles of Young Scientists, 2010. **1**(2): p. 2-6.

73. Bergman, T.L., et al., *Fundamentals of heat and mass transfer*. 2011: John Wiley & Sons.
74. Chisti, Y., *Mass transfer.* Kirk‐Othmer Encyclopedia of Chemical Technology, 2000: p. 1-70.
75. Cussler, E.L. and E.L. Cussler, *Diffusion: mass transfer in fluid systems*. 2009: Cambridge university press.
76. Wesselingh, J. and R. Krishna, *Mass transfer in multicomponent mixtures*. 2000: Delft University Press Delft.
77. Bird, R.B., *Transport phenomena.* Appl. Mech. Rev., 2002. **55**(1): p. R1-R4.
78. Fowler, K., et al., *Maxwell–Stefan diffusion: a framework for predicting condensed phase diffusion and phase separation in atmospheric aerosol.* Atmospheric Chemistry and Physics, 2018. **18**(3): p. 1629-1642.
79. Allen, M.P., *Introduction to molecular dynamics simulation.* Computational soft matter: from synthetic polymers to proteins, 2004. **23**(1): p. 1-28.
80. Tang, Y., et al., *Numerical simulation and optimization of enhanced oil recovery by the in situ generated CO2 Huff-n-puff process with compound surfactant.* Journal of Chemistry, 2016. **2016**.
81. Abadli, F., *Simulation study of enhanced oil recovery by ASP (alkaline, surfactant and polymer) flooding for Norne field C-segment*. 2012, Institutt for petroleumsteknologi og anvendt geofysikk.
82. Daripa, P. *Fluid dynamical and modeling issues of chemical flooding for enhanced oil recovery*. in *International Conference on Offshore Mechanics and Arctic Engineering*. 2013. American Society of Mechanical Engineers.
83. Veilleux, J., *The hydrodynamics of mass diffusion enhancement in nanofluids.* 2011.
84. Naderi, K. and T. Babadagli, *Pore-scale investigation of immiscible displacement process in porous media under high-frequency sound waves.* Journal of fluid mechanics, 2011. **680**: p. 336-360.
85. Permsukarome, P., C. Chang, and H.S. Fogler, *Kinetic study of asphaltene dissolution in amphiphile/alkane solutions.* Industrial & engineering chemistry research, 1997. **36**(9): p. 3960-3967.
86. Pursley, J.T., D.L. Holcomb, and G.S. Penny, *Composition and process for well cleaning*. 2008, Google Patents.
87. Quintero, L., et al. *Optimization of microemulsion formulations with linker molecules*. in *SPE European Formation Damage Conference & Exhibition*. 2013. OnePetro.
88. Oliveira, V.S., S. Rodrigues, and F.A. Fernandes, *Effect of high power low frequency ultrasound processing on the stability of lycopene.* Ultrasonics sonochemistry, 2015. **27**: p. 586-591.
89. Astráin-Redín, L., et al., *Application of high-power ultrasound in the food industry*, in *Sonochemical Reactions*. 2019, IntechOpen.
90. Shahavi, M.H., et al., *Evaluation of critical parameters for preparation of stable clove oil nanoemulsion.* Arabian Journal of Chemistry, 2019. **12**(8): p. 3225-3230.
91. Keck, C.M., et al., *Formulation of solid lipid nanoparticles (SLN): The value of different alkyl polyglucoside surfactants.* International journal of pharmaceutics, 2014. **474**(1-2): p. 33-41.
92. Kumar, N. and A. Mandal, *Surfactant stabilized oil-in-water nanoemulsion: stability, interfacial tension, and rheology study for enhanced oil recovery application.* Energy & Fuels, 2018. **32**(6): p. 6452-6466.
93. Lekkerkerker, H., W. Kegel, and J.T.G. Overbeek, *Phase behavior of ionic microemulsions.* Berichte der Bunsengesellschaft für physikalische Chemie, 1996. **100**(3): p. 206-217.
94. Barnes, J.R., et al. *Phase behaviour methods for the evaluation of surfactants for chemical flooding at higher temperature reservoir conditions*. in *SPE Symposium on Improved Oil Recovery*. 2008. OnePetro.

95. Yang, J., et al., *Preparation of d-limonene oil-in-water nanoemulsion from an optimum formulation.* Journal of oleo science, 2014. **63**(11): p. 1133-1140.
96. Mahbubul, I., et al., *Effective ultrasonication process for better colloidal dispersion of nanofluid.* Ultrasonics sonochemistry, 2015. **26**: p. 361-369.
97. Hu, H., et al., *Effects of ultrasound on structural and physical properties of soy protein isolate (SPI) dispersions.* Food Hydrocolloids, 2013. **30**(2): p. 647-655.
98. Jambrak, A.R., et al., *Ultrasonic effect on physicochemical and functional properties of α-lactalbumin.* LWT-Food science and Technology, 2010. **43**(2): p. 254-262.
99. Hashtjin, A.M. and S. Abbasi, *Optimization of ultrasonic emulsification conditions for the production of orange peel essential oil nanoemulsions.* Journal of food science and technology, 2015. **52**(5): p. 2679-2689.
100. McBryde, W., *The pH meter as a hydrogen-ion concentration probe.* Analyst, 1969. **94**(1118): p. 337-346.
101. Sirichote, W. and W. Praditviengkum, *Development of Digital pH Meter.* 2012.
102. Esteves, R., N. Onukwuba, and B. Dikici Ph D, *Determination of surfactant solution viscosities with a rotational viscometer.* Beyond: Undergraduate Research Journal, 2016. **1**(1): p. 2.
103. Managemenat, E.P., *Theory and Application of Conductivity.(2010). Application Data Sheet ADS 43-018/rev. D January 2010*. 2014.
104. Wu, Y. and W. Koch, *Absolute determination of electrolytic conductivity for primary standard KCl solutions from 0 to 50 C.* Journal of solution chemistry, 1991. **20**(4): p. 391-401.
105. Ge-hua, C. *The development of a new type of conductivity meter*. in *2010 International Conference on Computer, Mechatronics, Control and Electronic Engineering*. 2010. IEEE.
106. Marsalek, R., *Particle size and zeta potential of ZnO.* APCBEE procedia, 2014. **9**: p. 13-17.
107. Pecora, R., *Dynamic light scattering measurement of nanometer particles in liquids.* Journal of nanoparticle research, 2000. **2**(2): p. 123-131.
108. Kaszuba, M., et al., *Measuring sub nanometre sizes using dynamic light scattering.* Journal of nanoparticle research, 2008. **10**(5): p. 823-829.
109. Stetefeld, J., S.A. McKenna, and T.R. Patel, *Dynamic light scattering: a practical guide and applications in biomedical sciences.* Biophysical reviews, 2016. **8**(4): p. 409-427.
110. Babick, F., *Dynamic light scattering (DLS)*, in *Characterization of Nanoparticles*. 2020, Elsevier. p. 137-172.
111. Kaszuba, M., et al., *High-concentration zeta potential measurements using light-scattering techniques.* Philosophical transactions of the royal society a: mathematical, physical and engineering sciences, 2010. **368**(1927): p. 4439-4451.
112. Olson, E., *Zeta potential and colloid chemistry.* Journal of GXP Compliance, 2012. **16**(1): p. 81.
113. Ghadimi, A., R. Saidur, and H. Metselaar, *A review of nanofluid stability properties and characterization in stationary conditions.* International journal of heat and mass transfer, 2011. **54**(17-18): p. 4051-4068.
114. Hunter, R.J., *Zeta potential in colloid science: principles and applications*. Vol. 2. 2013: Academic press.
115. Berry, J.D., et al., *Measurement of surface and interfacial tension using pendant drop tensiometry.* Journal of colloid and interface science, 2015. **454**: p. 226-237.
116. Saad, S.M., Z. Policova, and A.W. Neumann, *Design and accuracy of pendant drop methods for surface tension measurement.* Colloids and Surfaces A: Physicochemical and Engineering Aspects, 2011. **384**(1-3): p. 442-452.
117. Szymczyk, K. and A. Taraba, *Aggregation behavior of Triton X-114 and Tween 80 at various temperatures and concentrations studied by density and viscosity measurements.* Journal of Thermal Analysis and Calorimetry, 2016. **126**(1): p. 315-326.

118. Thomas, S., et al., *Transport properties of polymeric membranes*. 2017: Elsevier.
119. BUBIĆ PAJIĆ, N.Z., et al., *Alkyl polyglucoside vs. ethoxylated surfactant-based microemulsions as vehicles for two poorly water-soluble drugs: Physicochemical characterization and in vivo skin performance.* Acta Pharmaceutica, 2017. **67**(4): p. 415-439.
120. Arps, J., *The effect of temperature on the density and electrical resistivity of sodium chloride solutions.* Journal of Petroleum Technology, 1953. **5**(10): p. 17-20.
121. Yusof, N.S.M., et al., *Physical and chemical effects of acoustic cavitation in selected ultrasonic cleaning applications.* Ultrasonics sonochemistry, 2016. **29**: p. 568-576.
122. Kochurova, N., et al., *Viscosity of aqueous micellar solutions of surfactants.* Colloid Journal, 2012. **74**(5): p. 564-568.
123. Asadi, A., et al., *Effect of sonication characteristics on stability, thermophysical properties, and heat transfer of nanofluids: A comprehensive review.* Ultrasonics sonochemistry, 2019. **58**: p. 104701.
124. Saeed, R., S. Masood, and S. Rehanullah, *Electrical conductivity of sodium chloride and potassium chloride in water soluble polymers at different temperatures.* Int J Pharm Chem Sci, 2011. **1**: p. 1591-1605.
125. Xu, R., *Progress in nanoparticles characterization: Sizing and zeta potential measurement.* Particuology, 2008. **6**(2): p. 112-115.
126. Kim, J.-Y., M.-G. Song, and J.-D. Kim, *Zeta potential of nanobubbles generated by ultrasonication in aqueous alkyl polyglycoside solutions.* Journal of colloid and interface science, 2000. **223**(2): p. 285-291.
127. Raso, J., et al., *Influence of different factors on the output power transferred into medium by ultrasound.* Ultrasonics sonochemistry, 1999. **5**(4): p. 157-162.
128. Silva, M., B. Zisu, and J. Chandrapala, *Influence of low-frequency ultrasound on the physico-chemical and structural characteristics of milk systems with varying casein to whey protein ratios.* Ultrasonics sonochemistry, 2018. **49**: p. 268-276.
129. Cho, S.-H., et al., *Ultrasonic formation of nanobubbles and their zeta-potentials in aqueous electrolyte and surfactant solutions.* Colloids and Surfaces A: Physicochemical and Engineering Aspects, 2005. **269**(1-3): p. 28-34.
130. Siddig, O., et al., *Novel Cake Washer for Removing Oil-Based Calcium Carbonate Filter Cake in Horizontal Wells.* Sustainability, 2020. **12**(8): p. 3427.
131. Quintero, L., et al. *NAF filter cake removal using microemulsion technology*. in *European Formation Damage Conference*. 2007. OnePetro.
132. Zhong, H., et al., *Minimizing the HTHP filtration loss of oil-based drilling fluid with swellable polymer microspheres.* Journal of Petroleum Science and Engineering, 2019. **172**: p. 411-424.
133. Zubail, M., et al. *Improved Producibility after Delayed Filter Cake Breaker Treatment in the Safaniya Offshore Field in Saudi Arabia*. in *SPE Kuwait International Petroleum Conference and Exhibition*. 2012. OnePetro.
134. Penny, G., et al. *Nanofluid System Improves Post Frac Oil and Gas Recovery in Hydrocarbon Rich Gas Reservoirs*. in *SPE Improved Oil Recovery Symposium*. 2012. OnePetro.
135. Sharma, P., K. Kostarelos, and S.S. Palayangoda, *Hydrocarbon recovery from oil sands by cyclic surfactant solubilization in single-phase microemulsions.* Journal of Energy Resources Technology, 2019. **141**(8).
136. Mayer, A.S., L. Zhong, and G.A. Pope, *Measurement of mass-transfer rates for surfactant-enhanced solubilization of nonaqueous phase liquids.* Environmental science & technology, 1999. **33**(17): p. 2965-2972.
137. Burnett, D., F. Gutierres, and G. Serrano. *Improved Filtercake Cleanup Practices for Horizontal Well Completions in Unconsolidated Sands: Correlation Models for Filter-Cake Removal*. in *SPE Annual Technical Conference and Exhibition*. 2002. OnePetro.

138. Nasr-El-Din, H.A. and A.M. Al Moajil. *Evaluation of in-situ generated acids for filter cake clean up*. in *European Formation Damage Conference*. 2007. OnePetro.
139. da Silva, V.L., et al., *Application of SDS surfactant microemulsion for removal of filter cake of oil-based drilling fluid: influence of cosurfactant.* Journal of Petroleum Exploration and Production Technology, 2020. **10**(7): p. 2845-2856.
140. Meziane, S. and H. Kadi, *Kinetics and thermodynamics of oil extraction from olive cake.* Journal of the American oil Chemists' society, 2008. **85**(4): p. 391-396.
141. Medjor, W., V. Akpoveta, and F. Egharevba, *Kinetics and physicochemical studies of surfactant enhanced remediation of hydrocarbons contaminated groundwater.* Egyptian Journal of Petroleum, 2018. **27**(2): p. 169-176.
142. Richardson, J., J. Harker, and J. Backhurst, *Flow of fluids through granular beds and packed columns.* Chemical Engineering, 2002. **2**: p. 191-236.
143. Kuang, X., et al., *Air and water flows in a vertical sand column.* Water resources research, 2011. **47**(4).
144. Lucas, C.R.d.S., et al., *Investigating the fluid–solid interaction of acid nonionic nanoemulsion with carbonate porous media.* Molecules, 2020. **25**(6): p. 1475.
145. Dhanarajan, G., et al., *Performance evaluation of biosurfactant stabilized microbubbles in enhanced oil recovery.* bioRxiv, 2018: p. 504431.
146. Mandal, A. and A. Bera, *Modeling of flow of oil-in-water emulsions through porous media.* Petroleum Science, 2015. **12**(2): p. 273-281.
147. Nasr-El-Din, H.A., et al. *Filter-cake cleanup in MRC wells using enzyme/surfactant solutions*. in *SPE International Symposium and Exhibition on Formation Damage Control*. 2006. OnePetro.
148. Berry, S.L. and B.B. Beall. *Laboratory development and application of a synthetic oil/surfactant system for cleanup of OB and SBM filter cakes*. in *SPE International Symposium and Exhibition on Formation Damage Control*. 2006. OnePetro.
149. Gao, J.Y., *Studying dissolution with a model integrating solid–liquid interface kinetics and diffusion kinetics.* Analytical chemistry, 2012. **84**(24): p. 10671-10678.
150. Niessner, J. and S.M. Hassanizadeh, *Mass and heat transfer during two-phase flow in porous media-theory and modeling*, in *Mass Transfer in Multiphase Systems and its Applications*. 2011, InTechOpen.
151. Turlo, V., O. Politano, and F. Baras, *Dissolution process at solid/liquid interface in nanometric metallic multilayers: Molecular dynamics simulations versus diffusion modeling.* Acta Materialia, 2015. **99**: p. 363-372.
152. Seager, R., et al., *Solid dissolution in a fluid solvent is characterized by the interplay of surface area-dependent diffusion and physical fragmentation.* Scientific reports, 2018. **8**(1): p. 1-17.
153. Smith, C. *A Solution for Every Multiphase Challenge*. in *Slides presented at CAE Support and Training Conference, Phoenix, AZ*. 2012.
154. Holbeach, J.W. and M.R. Davidson, *Modelling the dispersion of dissolving spherical particles.* Progress in Computational Fluid Dynamics, an International Journal, 2004. **4**(2): p. 78-91.
155. Williams, P. and A. Baker, *Incompressible computational fluid dynamics and the continuity constraint method for the three-dimensional Navier-Stokes equations.* Numerical Heat Transfer, 1996. **29**(2): p. 137-273.
156. Yao, L., S. Cockcroft, and D. Maijer. *A Study of the Mass Transfer Kinetics during the Dissolution of Ti-N Particles in Liquid Titanium*. in *IOP Conference Series: Materials Science and Engineering*. 2019. IOP Publishing.
157. Sparrell, C.L., M.P. Hesler, and H.M. Duscha, *Computational Fluid Dynamics Analysis of Two-Phase Flow in a Packed Bed Reactor.* 2012.
158. Larsson, H.K., et al., *Modelling of Mass Transfer Phenomena in Chemical and Biochemical Reactor Systems using Computational Fluid Dynamics.* Danmarks Tekniske Universitet (DTU), 2015.

159. Baker, M.J., *CFD simulation of flow through packed beds using the finite volume technique.* 2011.
160. HOLBEACH, J.W. and M.R. DAVIDSON. *Eulerian model for dissolution and dispersion of particles entering a liquid*. in *Third International Conference on CFD in the Minerals and Process Industries, CSIRO, Melbourne, Australia*. 2003.
161. Cao, H., *Simulations of Dissolution of Structured Particles*. 2015, University of Leeds.
162. Özkan, F., et al., *Numerical investigation of interfacial mass transfer in two phase flows using the VOF method.* Engineering Applications of Computational Fluid Mechanics, 2016. **10**(1): p. 100-110.
163. Rafique, A.S., et al., *Micellar structure and transformations in sodium alkylbenzenesulfonate (NaLAS) aqueous solutions: effects of concentration, temperature, and salt.* Soft Matter, 2020. **16**(33): p. 7835-7844.
164. Somasundaran, P.P., *Optimization of Surfactant Mixtures and Their Interfacial Behavior for Advanced Oil Recovery*. 2002, National Petroleum Technology Office, Tulsa, OK (US).
165. Afzal, A., et al., *An overview on the effect of ultrasonication duration on different properties of nanofluids.* Journal of Thermal Analysis and Calorimetry, 2019. **135**(1): p. 393-418.